Influence of Amyloid Aggregates on the Trafficking and Signaling of GPCRs

---

Arthur Gibert

Univ.-Diss.

**zur Erlangung des akademischen Grades
"doctor rerum naturalium"
(Dr. rer. nat.)
in der Wissenschaftsdisziplin "Molekulare Biologie"**

**eingereicht an der
Mathematisch-Naturwissenschaftlichen Fakultät
Institut für Biochemie und Biologie
der Universität Potsdam**
und
außeruniversitäres Institut

Ort und Tag der Disputation: Berlin, 18. März 2021

Hauptbetreuer:
Prof. Ralf Schülein
Leibniz-Forschungsinstitut für Molekulare Pharmakologie im Forschungsverbund Berlin e.V. (FMP)

Betreuer:
Prof. Gerhard Püschel
Universität Potsdam

Gutachter:
PD Dr. Enno Klussmann
Max-Delbrück-Centrum für Molekulare Medizin (MDC)

Acknowledgements

I want to express my profound gratitude to Prof. Ralf Schülein who not only gave me the opportunity to first do my master thesis and then my doctoral work in his laboratory but also supported me during all these years. I want to especially thank Dr. Claudia Rutz for her continuous supervision, training, and advice on how to achieve the highest standard of work in the lab. I also want to thank Prof. Gehard Püschel for accepting to be my supervising professor at Potsdam University and allowing me to defend my doctoral work there.

I want to thank the people around me in the lab, Betina Kahlich for the constant technical support; the members of the Krause group, Dr. Katrin Hinz, Dr. Patrick Marcinkowski, Dr. Jonas Protz for the continuous collaboration, advice and making working in the lab such a nice environment; Jenny Eichhorst, Dr. Martin Lehmann for their constant help with the microscopy. The group of Prof. Janine Kirstein that adopted me and provided me with social life by inviting me to their lab outings, especially Dr. Diogo Feleciano, Lucia Pigazzini and Dr. Annika Scior whom I became quite close to.

I also want to thank lots of people on the campus, including many members of the MDC, Polina, Anthony, Phillip, Johannes, Olga, Thais, Kitty, Bastian, Ole that I meet at numerous Beer hours, and became close friends.

I want to thank my family, my father, my mother and sister that have always been a great support and a source of comfort and joy no matter the situation. They have always been there for me.

I want to thank Maryia, my amazing wife who is the smartest and most courageous woman I know, and I am extremely proud to share my life with such an amazing person. I want to thank my sister-in-law, Elena that has been through a PhD as well and has been teaching me how to not get too crazy during this time and always knew how to make me relax when I was losing track.

Abstract (English)

The prevalence of diseases associated with misfolded proteins increases with age. When cellular defense mechanisms become limited, misfolded proteins form aggregates and may also develop more stable cross-β structures ultimately forming amyloid aggregates. Amyloid aggregates are associated with neurodegenerative diseases such as Alzheimer's disease and Huntington's disease. The formation of amyloid deposits, their toxicity and cellular defense mechanisms have been intensively studied. However, surprisingly little is known about the effects of protein aggregates on cellular signal transduction. It is also not understood whether the presence of aggregation-prone, but still soluble proteins affect signal transduction.

In this study, the still soluble aggregation-prone HttExon1Q74 and its amyloid aggregates were used to analyze the effect of amyloid aggregates on internalization and receptor activation of G protein-coupled receptors (GPCRs), the largest protein family of mammalian cell surface receptors involved in signal transduction. The aggregated HttExon1Q74, but not its soluble form, could inhibit ligand-induced clathrin-mediated endocytosis (CME) of various GPCRs. Most likely this inhibitory effect is based on a terminal sequestration of the HSC70 chaperone to the aggregates which is necessary for CME. Using the vasopressinV1a receptor (V1aR) and the corticotropin-releasing factor receptor 1 (CRF1R) as a model, it could be shown that the presence of HttExon1Q74 aggregates and the inhibition of ligand-induced CME leads to an accumulation of desensitized receptors at the plasma membrane. In turn, this disrupts Gq-mediated Ca2+ signaling and Gs-mediated cAMP signaling of the V1aR and the CRF1R respectively. In contrast to HttExon1Q74 amyloid aggregates, soluble HttExon1Q74 as well as amorphous aggregates did not inhibit GPCR internalization and signaling demonstrating that cellular signal transduction mechanisms are specifically impaired in response to the formation of amyloid aggregates.

In addition, preliminary experiments could show that HttExon1Q74 aggregates provoke an increase in membrane expression of a protein from a structurally and functionally unrelated membrane protein family, namely the serotonin transporter SERT. As SERT is the main pharmacological target to treat depression this could shed light on this commonly occurring comorbidity in neurodegenerative diseases, in particular in early disease states.

Abstract (German)

Die Prävalenz von Krankheiten, die mit fehlgefalteten Proteinen assoziiert sind, nimmt mit dem Alter zu. Wenn die zellulären Abwehrmechanismen weniger effizient werden, können fehlgefaltete Proteine nicht nur einfache Aggregate bilden, sondern auch stabilere Cross-β-Strukturen, die am Ende zu sogenannten Amyloidaggregaten führen können. Amyloidaggregate sind mit neurodegenerativen Erkrankungen wie z. B. der Alzheimer Erkrankung und dem Huntington-Syndrom assoziiert. Die Bildung von Amyloidablagerungen, ihre Toxizität und die zellulären Abwehrmechanismen wurden in den letzten Jahren intensiv untersucht. Über die Auswirkungen von Proteinaggregaten auf die zelluläre Signaltransduktion ist jedoch überraschend wenig bekannt. Es ist auch nicht bekannt, ob bereits das Vorhandensein von löslichen Vorstadien dieser zur Aggregation neigenden Protein, die Signaltransduktion von Zellen beeinflusst.

In dieser Studie wurden Amyloidaggregate des auf dem Huntingtin-Protein basierenden Konstrukts HttExon1Q74 und seine noch löslichen Formen verwendet, um deren Wirkung auf die Internalisierung und Rezeptoraktivierung von G-Protein-gekoppelten Rezeptoren (GPCRs) zu analysieren. GPCR bilden die größte Proteinfamilie von Oberflächenrezeptoren in Säugerzellen und spielen eine entscheidende Rolle in der zellulären Signaltransduktion. Es konnte gezeigt werden, dass aggregiertes HttExon1Q74, aber nicht seine noch lösliche Form, die ligandeninduzierte Clathrin-vermittelte Endozytose (CME) verschiedener GPCRs hemmt. Höchstwahrscheinlich beruht dieser inhibitorische Effekt auf einer Sequestrierung des HSC70-Chaperons zu den HttExon1Q74-Aggregaten. In früheren Studien konnte bereits gezeigt werden, dass HSC70 die für CME notwendig ist. Unter Verwendung des VasopressinV1a-Rezeptors (V1aR) und des Corticotropin-Releasing-Faktor-Rezeptors 1 (CRF1R) als Modellproteine, konnte in dieser Arbeit ferner gezeigt werden, dass das Vorhandensein von HttExon1Q74-Aggregaten und die Hemmung der ligandeninduzierten CME zu einer Akkumulation desensibilisierter Rezeptoren in der Plasmamembran führt. Dies stört wiederum die Gq-vermittelte Ca^{2+}-Signalisierung und die Gs-vermittelte cAMP-Signalisierung des V1aR bzw. des CRF1R. Im Gegensatz zu HttExon1Q74-Amyloidaggregaten hemmten lösliches HttExon1Q74 sowie amorphe Proteinaggregate die GPCR-Internalisierung und –Signalisierung nicht. Dies zeigt, dass Amyloidaggregate zelluläre Signaltransduktionsmechanismen spezifisch beeinträchtigen können.

Darüber hinaus konnten vorläufige Experimente zeigen, dass HttExon1Q74-Aggregate eine Erhöhung der Membranexpression des Serotonintranporters SERT verursachen, eines Membranproteins das strukturell und funktionell nicht mit GPCR verwandt ist. Da SERT das wichtigste pharmakologische Zielmolekül bei der Behandlung von depressiven Syndromen ist, könnten diese Daten dazu beitragen, besser zu verstehen, warum Depressionen in sehr frühen Stadien von neurodegenerativen Erkrankungen gehäuft auftreten.

LIST OF FIGURES

I. Introduction

Proteins must fold into a specific structure to ensure their functional integrity and stability. During evolution, cells have developed complex defense mechanisms to cope with protein misfolding. Molecular chaperones are a vital component of the cellular proteostasis network as they prevent misfolding, aid in folding and refolding, target misfolded proteins to autophagy or proteasomal pathways or disaggregate protein aggregates (1–4).

Failing to limit the number of misfolded proteins leads to their accumulation and eventually to aggregate formation. Some misfolded proteins form more stable and toxic cross-β structures known as amyloid aggregates. The presence of these amyloid aggregates is associated with a number of late age of onset neurodegenerative diseases (5, 6) such as Huntington's disease (HD) (7), Alzheimer's disease (8), Parkinson's disease (8) and amyotrophic lateral sclerosis (ALS) (9, 10).

Intense research efforts were focused on explaining the formation of amyloid aggregates, their toxicity and cellular defense mechanisms. Surprisingly little is known about the effects of protein aggregates on cellular signal transduction mechanisms. However, it is known that aggregates composed of polyglutamine, ataxin-1 and pathological mutants of superoxide dismutase 1 (SOD1) sequester HSC70 to the aggregates, thereby limiting the available pool of HSC70. This chaperone protein is required for multiple steps of clathrin-mediated endocytosis (CME). Its sequestration to the aggregates consequently limits its availability for CME (11) (figure 1) and consequently impair CME in mammalian cells (11). An inhibition of CME by amyloids aggregates would challenge the function of many signal transduction processes, in particular those mediated by G Protein-coupled receptors (GPCRs), the largest family of cell surface receptors and the most important drug targets (12).

Activation of GPCRs by their ligands leads to signal transduction by G protein coupling and second messenger formation. Activated receptors are desensitized by phosphorylation through G protein-coupled receptor kinases (GRKs) (13). Following β-arrestin recruitment, the GPCRs are internalized predominantly by CME and either recycled to the plasma membrane or targeted to the lysosomal degradation pathway (14, 15). An inhibition of CME by amyloid aggregates should consequently lead to the
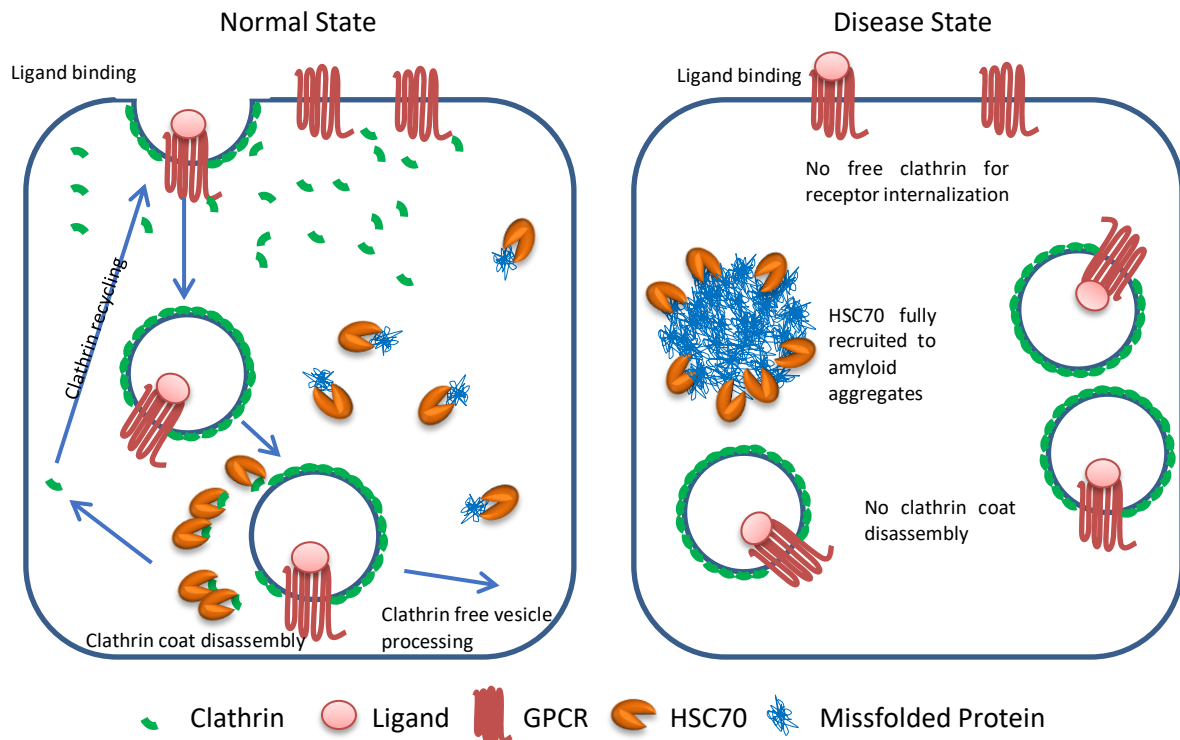
Figure 1. Effect of amyloid aggregates on clathrin mediated endocytosis (CME). HSC70 is required for both handling misfolded protein aggregates and clathrin mediated endocytosis. In diseases such as Huntington's disease, where amyloid aggregates are present, HSC70 is mainly recruited to the amyloid aggregates and clathrin coat disassembly is impaired. This leads to an accumulation of clathrin coated vesicles, a reduction of free clathrin molecules and a disruption of CME. Moreover, proteins to be internalized accumulate on the plasma membrane (adapted from (Yu et al. 2014)).

accumulation of desensitized GPCRs on the plasma membrane and thereby to a progressive breakdown of signal transduction.

It is very important to get a deeper insight into the effects of amyloid aggregates on signal transduction since defects in these processes may have a substantial influence on the pathophysiology and progression of amyloid aggregate diseases, in particular in their early stages. In Huntington's disease (HD), for example, it has been known for a long time that neuropsychiatric syndromes such as episodes of major depression may develop years before the appearance of the characteristic motor symptoms of the disease (16). The development of episodes of major depression in prodromal disease stages indicate that the CNS serotonergic system and/or the hypothalamic pituitary adrenal (HPA) stress axis may be affected in the patients. Recent *in vivo* studies indicate that the behavioral symptoms in pre-manifest HD also correlate with a reduced activity of the endocannabinoid system (17, 18). All three, the serotonergic system, the HPA axis and the endocannabinoid system depend predominantly on GPCRs and their functional signal transduction which may thus be severely influenced by the presence of amyloid aggregates.

In this study various GPCRs were employed to study the influence of amyloid and amorphous protein aggregates on GPCR trafficking and signal transduction. As a model for amyloid aggregate formation, the mutant huntingtin protein (HTT) was used (7, 19). HTT is the causative agent of HD, an incurable neurodegenerative disorder which typically manifests between 30 and 50 years of age (20–22). The neuropathology of HD is characterized by final neuronal death. The cortical projections to the striatum and the neurons of the striatum itself are mainly affected during disease progression. In affected patients, autosomal dominant inherited mutations in the first exon of the HTT gene, aberrantly expand the protein with a poly-glutamine stretch leading to amyloid aggregate formation when the number of glutamines exceeds a critical $\sim$35-37 repeat threshold (19, 22). In this study, exon 1-encoded HTT with 74 glutamine residues (HttExon1Q74) as a model for an amyloid aggregate-forming protein was used. As a negative control, exon 1-encoded HTT with only 23 glutamine residues (HttExon1Q23), which is below the critical repeat threshold, was used.

Our first goal was to analyze whether the still soluble, aggregation-prone HttExon1Q74 and/or its amyloid aggregates affect ligand-induced CME and activation of GPCRs, as these effects remain enigmatic.

As the prevalence of depression has been found to be highly increased in patients with neurodegenerative diseases (16, 19, 23–25), understanding the influence of amyloid aggregates on the activity and trafficking of the serotonin transporter (SERT) could provide basis for the understanding the etiology of this comorbidity. Low synaptic 5-HT concentration is associated with depression and therefore inhibiting the function of SERT has been found to be an effective treatment strategy against the symptoms of this disease. These days, SERT is the main target for treatment of depression with about 70 compounds developed in order to affect its function (DrugBank (26, 27)). Another aim of this work was, thus, to study whether the formation of HttExon1Q74 aggregates also influence SERT expression levels in the plasma membrane.

Subsequently, the influence of other amyloid aggregates such as α-Synuclein (α-Syn) and mutants of SOD1 on the CME of GPCRs and SERT should also be analyzed.

The following chapters of this introduction will summarize in more detail aspects of GPCRs, SERT, CME and amyloid aggregates which were relevant for this work.

1. G Protein-Coupled Receptors

Complex multicellular organisms evolved in such a way that their cells became able to communicate with each other and respond to external stimuli by using a complex system of receptors. The biggest family of receptors is the GPCR family (28) which are only found in eukaryotes and enable communication between the extracellular and intracellular space.

GPCRs are integral seven transmembrane helix proteins that resides primarily on the plasma membrane. GPCRs have an extracellular N-terminus and an intracellular C-terminus. Extracellular loops are generally glycosylated and contain a highly conserved disulfide bond required for the functional structure of the receptors.

GPCRs can be activated by a huge variety of ligands including but not limited to photon, hormones, neurotransmitters or mechanical stimuli. The size of these ligands ranges from small molecules, peptides to large proteins and even viruses (EG: CCR5 and HIV). They are involved in a very large number of physiological processes and are often the target of therapeutic strategies (12, 29, 30). It is worth noting that more than half of the receptors of the GPCR family are involved in sensory functions with about 400 olfactory receptors, 9 light perception receptors (31), 33 taste receptors, and 5 pheromone receptors (32).

In the drug market, GPCRs represent 27% of market share by target class, this reflects close to 890 US$ billion of sales between 2011 and 2015 (30). This is not surprising considering that GPCRs represent the biggest super family of protein in humans (12). With about 900 different members identified, a significant proportion (~4%) of the genetic material of humans is dedicated to these receptors (28, 33). GPCRs are classified in a 6 class system based on sequence identity. Only three of which are present in human (34–37).

Class A GPCRs are the largest class, containing 85% of all receptors. They share significant sequence homology to the light-activated GPCR rhodopsin and contain a DRY motif in the third transmembrane domain (rhodopsin-like GPCRs). They include neuropeptide, hormone and nucleotide binding receptors (37).

The receptors of the class B (secretin receptor family) have longer N-terminal domains and form a group structurally and functionally divergent from other GPCR classes (37).

Receptors belonging to class C (metabotropic glutamate receptor family) have N-terminal signal sequences and a large hydrophilic extracellular agonist-binding region containing several conserved cysteine residues which could be involved in the formation of disulfide bonds. They are known to form constitutive dimers (37).

To date, the crystal structures of at least 67 different GPCRs have been solved (GPCR-EXP https://zhanglab.ccmb.med.umich.edu/GPCR-EXP/). Most structures indicate that ligand binding happens at the extracellular side and causes TM5 and TM6 to create a cavity. The structure of the activated beta-2-adrenergic receptor together with Gs (PDB ID: 3sn6) showed that this cavity is the binding site for the α subunit of Gs (38). Binding for most small ligands has been suggested to happen in the cavity formed by the transmembrane domains on the extracellular side with TM2 then covering this cavity but other mechanisms have been described (39). Larger ligands interact with extracellular domains.

The activation of GPCRs by their ligands leads to signal transduction by G protein coupling and second messenger formation. G proteins are trimeric membrane interacting complexes formed of three subunits: G_α, G_β and G_γ. G protein complexes are classified according to their Gα subunit type and G_s, G_i, $G_{q/11}$ and $G_{12/13}$ complexes can be distinguished. While receptors have a higher affinity for one specific type of trimeric G protein, most receptors can also activate more than one type (40).

Whether, a GPCRs couples with the G protein before or after GPCR activation is still under debate (41). When activated, a GPCR acts as a guanine nucleotide exchange factor and the G protein's GDP is replaced by GTP. This causes a dissociation of the complex, G_α becomes cytosolic while the G beta-gamma complex ($G_{\beta\gamma}$) remains bound to the receptor at the plasma membrane.

Each activated Gα in turn activates the following secondary messenger pathway.

- $G_{\alpha s}$ activates adenylyl cyclase activity which in turn hydrolyses ATP into cAMP and increases cytosolic cAMP levels
- $G_{\alpha i}$ inhibits adenylyl cyclase thereby inhibiting cAMP production
- $G_{\alpha q/11}$ activates phospholipase C which hydrolyses PIP2 into IP3 and DAG. DAG then activates the protein kinase C (PKC) while IP3 binds to ER calcium channels and causes an increase of intracellular calcium in the cytoplasm.

- $G_{12/13}$ activates Rho GTPases which regulate actin dynamics and are important for organelle development, cytoskeletal dynamics, cell movement etc.

Signaling downregulation is triggered by the hydrolysis of GTP into GDP by the G_{α} enzymatic activity which is increased by regulators of G protein signaling (RGSs). G_{α} is then able to bind $G_{\beta\gamma}$. $G_{\beta\gamma}$ has an inhibitory effect on G_{α} but signaling functions of $G_{\beta\gamma}$ were also identified (42).

After activation, the receptors are tightly regulated. This regulation can either be homologous or heterologous. Homologous regulation targets a receptor which has bound its specific ligand. Heterologous regulation means that the GPCR is regulated irrespectively of ligand binding. Regulation of a GPCR includes phosphorylation of the intracellular domains, mostly in the C-terminus region. Phosphorylation is then followed by endocytosis which regulated by β-arrestin and clathrin.

G protein selectivity can be modulated by kinase activity. β2-adrenoceptors, for example, have been shown to be regulated through this process. cAMP-mediated PKA phosphorylation creates a shift in G protein selectivity from G_s to G_i (43). Another example is the PKA-mediated phosphorylation of the CRF1R at serine 301 which leads to a reduced $G_{q/11}$ signaling (44). The main GPCR regulator are the G protein-coupled receptor kinases (GRK) (13). These protein kinases perform phosphorylations that ultimately lead to the internalization of the receptors. Phosphorylated receptors have an increased affinity for β-arrestin and this binding leads to the breakdown of the GPCR-$G_{\beta\gamma}$ complex interaction and therefore terminates signaling. Following β-arrestin recruitment, most GPCRs are internalized by CME into vesicle with higher acidic environment causing in most cases receptor/ligand separation. Receptors are either recycling to the plasma membrane or targeted to the lysosomal degradation pathway (14, 15). However, the universality of this model has been challenged by examples of sustained signaling by a GPCR-$G_{\beta\gamma}$ protein-β-arrestin supercomplex after internalization (45).

As previously mentioned, the presence of an amyloid in a cell inhibits clathrin mediated endocytosis of transferrin receptor and AMPA receptor (11). However, it is unknown whether this effect would remain valid for very low expressed proteins such as GPCRs (46). Considering what is known about GPCR regulation, inhibition of the CME should lead to the accumulation of densitized receptors on the plasma membrane and lead to a progressive breakdown of signal transduction. Vice versa, if the receptor sustains signaling upon internalization, an increase of activity may also be observed.
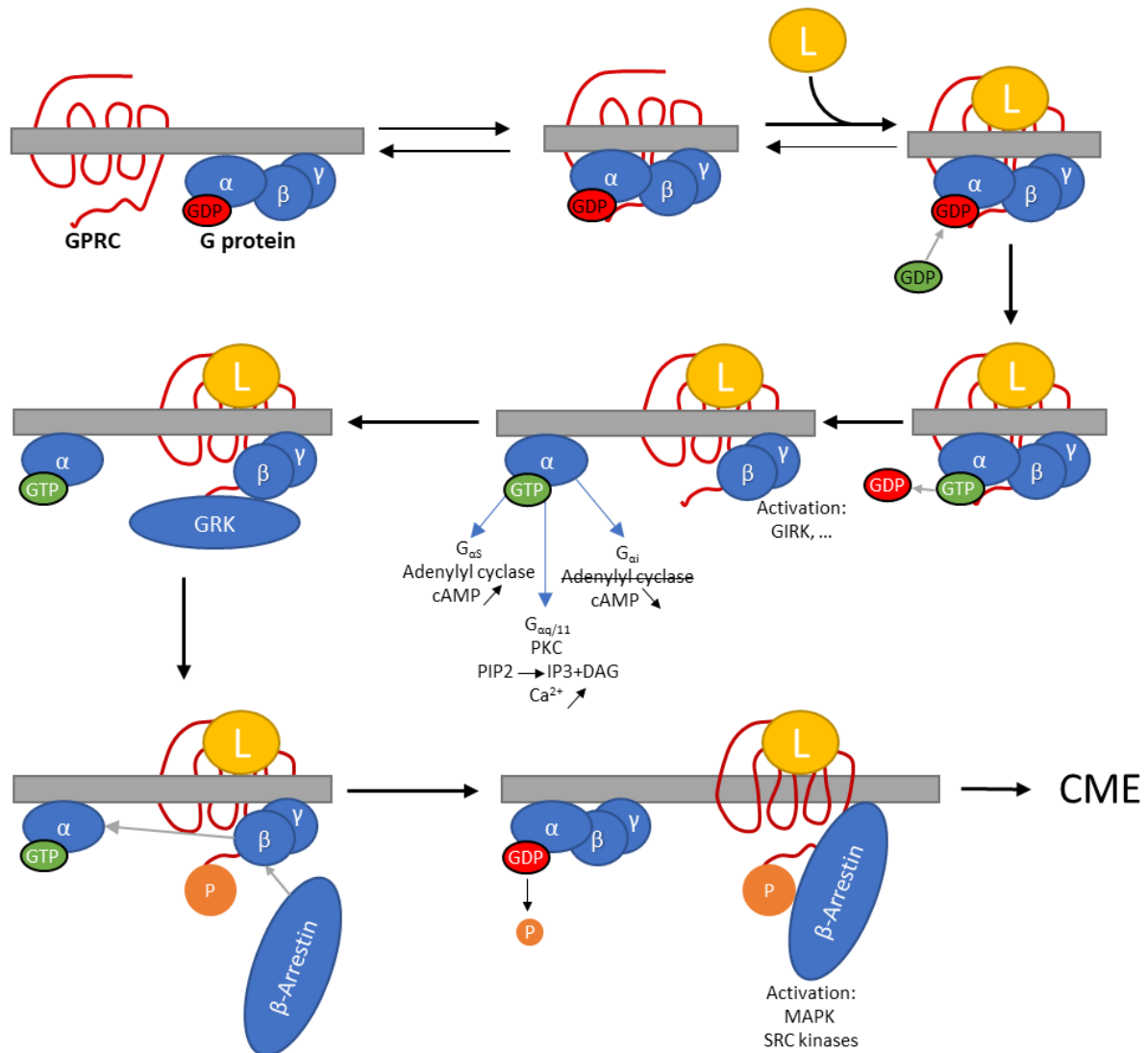
Figure 2. Signal transduction mediated by GPCRs. Receptors regulate multiple intracellular signaling cascades including G-protein-dependent and G-protein-independent pathways. Coupling of heterotrimeric G proteins to the activated receptor triggers nucleotide exchange followed by dissociation of the G protein into the G_α and $G_{\beta\gamma}$ subunits. Both subunits can regulate different downstream effector proteins. G-protein-mediated signaling is terminated by hydrolysis of GTP and reassociation of Gα with Gβγ to the inactive heterotrimer. Activation of the receptor causes phosphorylation by GRKs and subsequent coupling to arrestin. Arrestin coupling triggers desensitization and arrestin-mediated activation of downstream effector proteins such as mitogen-activated protein kinases (MAPKs) or SRC kinases. Arrestin activation also promotes the internalization of the receptor into endosomes followed by degradation or recycling to the plasma membrane.

If amyloid aggregates do have an effect on trafficking and signaling of GPCRs, this would shed light on the causes of previously unexplained symptoms and comorbidity of neurodegenerative disorders. It was one of the aims of this work to analyze an influence. As far as the development of depression episodes in prodromal disease states is concerned, it is also interesting to analyze the influence of amyloids aggregates on the SERT transporters directly. This transporter is the major target for anti-depressant drugs and inhibition of internalization and thus increase of membrane levels may favor depressive events.

2. Serotonin Transporter

The serotonin transporter (SERT) is a neurotransmitter transporter belonging to the solute carrier 6 gene family. It is a twelve transmembrane domain protein of 40kb and its main function is to facilitate serotonin (5-HT) transport across the plasma membrane (47). This protein is located in lipid rafts, both C and N termini are intracellular and many protein-protein interaction are insuring SERT structure, function, and localization (48). SERT contains two sites of N-linked glycosylation (49). 5-HT is a monovalent cation which is transported together with one Cl^- and one Na^+ ion. Transports is driven by the Na^+ gradient across the plasma membrane maintained by the Na/K ATPase. It is electroneutral due to the efflux of K^+ (50, 51). Interestingly SERT has also been shown to create currents, therefore it is possible that other stoichiometries exist (52).

In addition to depression, other disorders have been associated with 5-HT regulation defects such as, autism spectrum disorders, anxiety (53) or obsessive compulsive disorders (54, 55). Therefore, a lot of research has been performed in order to understand 5-HT homeostasis as well as to identify drugs that effects the regulation of its transport and function. The main strategies include maintaining or increasing the levels of 5-HT in the synapse directly or more generally in the area around the serotonergic neurons. 5-HT as a neurotransmitter has an unusual release pattern. It is not only released by the presynaptic button but also at extrasynaptic sites such as the soma (56, 57) and the neuritic varicosities (58). Various types of compounds have been developed targeting SERT, such as tricyclic inhibitors with the lead compound imipramine which was the first antidepressant drug available in 1958. Modern antidepressant drugs targeting SERT include the selective serotonin reuptake inhibitors (SSRI; e.g. paroxetine or fluoxetine). Transport reversal drugs are usually psychostimulants (e.g. amphetamine, MDMA) (59). Altogether, 70 identified compounds have been found to target this transporter either directly or indirectly (DrugBank (26, 27)).

However, tricyclic compounds and SSRI have a 3 weeks delay for the positive effects to appear (60) and 33% of patient are all together unresponsive to treatment (61, 62). Therefore, despite the large amount of work done with SERT, there is still a lot of unknowns concerning its regulation.

Multiple papers have connected overall SERT activity to its expression in the plasma membrane (63–65). Many factors have been shown to influence SERT's expression and therefore its activity. SERT polymorphisms (66–70) could also be associated with disorders such as depression (71), anxiety (53) or obsessive compulsive disorder (47, 72).

The transcription of SERT is cAMP dependent as its promoter contains a cAMP response element-like motif (CRE) (73). Therefore, connection to cAMP signaling indicates that SERT expression can potentially be influenced by GPCR signaling.

The membrane level of SERT is not only related to its transcription, translation and trafficking. Cholesterol levels have been shown to positively influence the number of SERT molecules (74) and SERT was located on lipid rafts (75). This localization is important to maintain proper folding of SERT increasing its 5-HT transport function as well as stabilizing its membrane expression (76). Furthermore, PIP2 level of the ER positively influences SERT membrane expression. SERT binding to PIP2 facilitates SERT homodimerization in the ER and thereby its trafficking through the secretory pathway to the plasma membrane. Uptake of 5-HT is consequently increased (77).

SERT membrane expression is controlled by several other factors. Protein kinase C (PKC) together with the LIM domain adaptor protein Hic-5 promotes SERT internalization (78). PKG as well at the Akt/PKB protein kinase enhance SERT membrane level potentially by directly phosphorylating SERT (79, 80). Ca^{2+}-activated protein phosphatase calcineurin also has an influence on the number of SERT molecules in the plasma membrane, but it was also shown to directly interact with SERT and to reverse the 5-HT uptake inhibition usually caused by PKC phosphorylation (81, 82). Some small molecules, such as SSRI have also been found to affect SERT membrane levels (83–85).

SERT activity is regulated by many cross-talking factors. The 5-HT$_{2B}$ receptor (5-HT$_{2B}$R) has been found to regulate SERT activity as well Na/K ATPase (86). 5-HT$_{2B}$R is controlling the SERT phosphorylation performed by PCK. An excess of 5-HT leads to 5-HT$_{2B}$R IP3/PKC activation increasing SERT and Na/K ATPase phosphorylation, thereby

inhibiting the activity of both transporters. 5-HT residence time in the synaptic space is thereby increased (47). It is also worth noting that hyperphosphorylated SERT molecules have a reduced SSRI affinity which might, at least in part, explain resistances to antidepressant drugs (47).

SERT functions has also been associated with neurodegenerative disorders. It has been shown that soluble α-synuclein directly binds to SERT and induces its internalization in turn leading to reduced 5-HT uptake (25, 87). It is then expected that in Parkinson's disease, when the availability of α-synuclein is reduced because of its accumulation in aggregates, membrane expression of SERT is increased which could explain the early onset of depression that most Parkinson's patients experience (23, 24).

Surprisingly little is known about the fate of SERT following internalization. It has been shown that SERT is constitutively internalized and directed to late endosomes and eventually to lysosomes (88) suggesting that SERT undergoes either clathrin-mediated endocytosis (CME) or pinocytosis (89). If SERT indeed uses the clathrin pathway for its internalization, it is conceivable that the internalization is also affected by amyloid aggregates. In this case, CME inhibition by the amyloid aggregates would lead to plasma membrane accumulation of SERT and thereby to an increased presynaptic uptake of 5-HT which could also be a factor for understanding early onset of depression in neurodegenerative diseases.

3. Clathrin-mediated endocytosis

CME is a complex process involving more than 50 different proteins. During CME, plasma membrane and extracellular proteins and molecules are transported into the cell cytoplasm by vesicle formation (90). Vesicles are coated by a protein lattice of clathrin molecules. A clathrin molecule itself is a triskelion-shaped protein formed by three heavy chains (190 kDa) and three light chains (25 kDa). The three heavy chains form a complex *via* their N-terminal domains. Each heavy chain has a light chain subunit attached to it. CME is regulated by a wide variety of processes including nutrient uptake, cell adhesion, developmental regulation through morphogens and most importantly cell signaling. Such ligand-induced internalization also involves multiple steps.

First, proteins to be internalized start by clustering on the plasma membrane and interact with intracellular proteins such as AP2 or β-arrestin (90). This initializes the formation of the coat by forming an inner bend of the membrane also known as a clathrin coated pit

(CCP). This is believed to be the main regulator of the internalization efficiency. Of note, this process can still be reverted (91, 92).

Multiple types of adaptor proteins exist in CME. The ubiquitous adaptor is the heterotrimeric AP2 heterotrimer acting sometimes together with more specific monomeric adaptor proteins. In the case of GPCRs for example, β-arrestin first binds to the receptor and then recruits the adaptor protein AP2. AP2 and most adaptor proteins directly interact with the plasma membrane at specific lipids such as phosphatidylinositol 4,5-bisphosphate (PI(4,5)P2). Once the recruited adaptor protein starts to bind clathrin, the bend of the plasma membrane increases and this invagination forms the CCP. The bend of the membrane is not only promoted by the recruitment of the coat components as actin also plays a role, in particular in the later stages of the internalization process. Microscopic studies showed that actin filaments act directly at the rim of the clathrin coat and inhibitors of the actin filament polymerization were shown to cause the stop of CME when invaginations have a U shape.

The location for the formation of CCPs is not always random. In highly differentiated cells such as neurons for example, CME occurs at very specific subcellular locations which are related to membrane composition. CCP formation is driven by local concentration of membrane proteins to be endocytosed which is achieved either by localized delivery or localized ligand interaction (93). High concentration of PI(4,5)P2 which interacts directly with many adaptor proteins and causes their recruitment to the plasma membrane is also a strong influencer of CCP localization (94, 95).

CCP are cut out of the membrane by actin filament nucleation, myosin motor proteins and dynamin. CCPs then become clathrin coated vesicles (CCVs). The next critical step of this process is the removal of the clathrin coat recycling the machinery components for a novel round of internalization. This step is performed by chaperones, protein kinases and lipid phosphatases. PI(4,5)P2 was demonstrated to be converted into phosphoinositol (4)-phosphate (PI4P) and to cause the disassembly of the clathrin coat. This step is performed by synaptojanin 1 in neurons (96) and inositol polyphosphate 5-phosphatase OCRL1 in other tissues (97). The constitutively expressed HSC70, which is recruited to the vesicle by its co-chaperone, the J protein auxilin, has a key role in this process. Based on structural studies, auxilin was shown to directly interact with the lattice. Together with HSC70 it causes a steric effect loosening clathrin-clathrin interactions and helping in the solubilization of the clathrin coat (98, 99).

Chaperone functions in the clathrin coat disassembly could be disrupted by presence of amyloid aggregates in cells (11). These aggregates can recruit HSC70 complexes to a much higher degree than CCVs leading to a depletion of free HSC70 and consequently an inhibition of the CME. In this work, it was explored whether ligand-induced CME of GPCRs is also inhibited by amyloid aggregates and whether this causes changes in the signaling patterns of the receptor.

4. Amyloid aggregates

Amyloid aggregates also known as Amyloid fibrils are protein aggregates but unlike amorphous aggregates, they are formed of mainly one protein in an organized structure. Under stress conditions, these proteins start interacting with themselves and aggregate into insoluble amyloid fibers (100, 101). Even though there are many types of amyloids aggregates formed by different proteins, they share some fundamental properties. Amyloid fibrils are made of cross-β structures (101, 102) which are rigid and they are unaffected by thermal treatments (102), chemical denaturation or degradation (103). Even though these aggregates are formed primarily by one specific protein, it has been shown that they may co-aggregate with proteins of the proteostasis system, in particular with members of the chaperone family (104).

The presence of amyloid aggregates has been linked to many neurodegenerative diseases. Aggregate formation depends on ageing and/or mutations in specific genes. Such diseases are called amyloidosis (100, 101). Interestingly, the location of amyloid deposition can differ from their production site, in this case they are referred to as systemic amyloidosis as opposed to localized amyloidosis (105).

The process of amyloid formation involves several defined stages. First, the primary nucleation happens, where monomers start forming small, still soluble aggregates also known as oligomers. Then the elongation takes place and the fibril grows by the addition of more and more monomers. After that, the secondary nucleation takes place, the secondary nucleation is catalyzed by the presence of the pre-existing fibrils and causes the formation of new small soluble aggregates. In the final fragmentation stage, fibrils break apart increasing their overall number (106).

Oligomers are believed to be highly toxic and they play an important role in the tissue toxicity observed in neurodegenerative diseases (107–110). These toxic species have been demonstrated to cause synapse loss in Alzheimer's disease by overstimulation of glutamatergic synaptic transmission (111). The oligomers can interact with the cell

membrane (111) and were shown to cause altered calcium homeostasis (112, 113), oxydative stress (114), mitochondrial dysfunction (114) and inflammation (114). The toxicity in systemic diseases seems to be related to both insoluble fibrils and oligomers (114). It was also shown that fibrils could cause extracellular mechanical stress and organ failure (105). In inherited neurodegenerative diseases, fibril formation is promoted by mutant proteins that do normally not form aggregates (115, 116).

This work focused mainly on the effect of the Huntington's disease-causing Huntingtin protein (HTT). It was also tried to establish detection assays for Parkinson's disease related α-Synuclein and the ALS related SOD in order to expand on the results found using HTT.

4.1. Huntingtin

Huntingin (HTT) is the causative agent of Huntington's Disease (HD), an incurable neurodegenerative disorder which typically begins between 30 and 50 years of age (20–22). This disorder affects around 5-10 per 100 000 individuals (19). The neuropathology of HD is characterized by neuronal death caused by the formation of huntingtin amyloid aggregates. The cortical projections to the striatum and the neurons of the striatum itself are mainly affected during disease progression.

Symptoms of the disease are a loss of coordination, shaking, dementia and a loss of mental abilities (19). In affected patients, autosomal dominant inherited mutations in the first exon of the HTT gene aberrantly expand the protein with a poly-glutamine stretch. Amyloid fibrils are forming when the number of glutamine is beyond a critical ~35-37 repeats threshold (19, 22).

The earliest signs of this disease are cognitive and can be detected up to 10 years before the development of the motor symptoms. Psychiatric symptoms are also highly prevalent, in particular depression is strongly associated with the disease and while it is more prevalent during the disease itself it is also present during the prodrome of HD (16). This suggests that the amyloid effects are not limited to cytotoxicity but may also affect cell regulation and signaling in early HD stages.

In this study exon 1-encoded HTT expanded by a 74 residues poly glutamine stretch (HttExon1Q74) was used as a model for an amyloid forming protein. As a negative control, exon 1-encoded HTT expanded by only a 23 residues poly glutamine stretch (HttExon1Q23) was used.

4.2. α-Synuclein

α-Synuclein (α-Syn) is an abundant protein in the brain residing mainly in presynaptic nerve endings. This protein is the major component of Lewy bodies which are amyloid aggregates found in some forms of Parkinsons disease (PD)(117). PD is one of the major age-related neurodegenerative diseases with about 1% of the population above 60 being affected (118). Symptoms are tremor, muscular rigidity, bradykinesia, and postural instability. At later stages dementia occurs. Life expectancy is decreased because of lung infections favored by bradykinesia and contingency in bed (119). Depression is also a common trait of PD patients and is usually preceding the motor symptoms of the disease (23, 24). As HD, this disease is characterized by premature neuronal cell death.

While the exact triggers are unknown, cell death is usually associated with the presence of Lewy bodies but whether these are the causes or consequences of the disease processes remain to be defined. Neuronal cell death lead to a decrease of the neurotransmitter dopamine in the substantia nigra. The exact physiological functions of α-Syn remain undetermined but lipid binding properties of its N-terminal repeats have been identified (120, 121). It can also induce SERT internalization (25, 87). Missense mutation of α-Syn (A53T E46K, or A30P) has been identified in late onset familial forms of PD suggesting the importance of α-Syn in the pathogenesis of PD in these cases (117). Interestingly, while A53T and E46K were found to increase the number of cells with aggregates, cells transfected with A30P showed fewer inclusions compared to the wild-type (122). In addition, subcellular distribution of all mutants was also modified. Of note, familial cases of PD could also be linked to the duplication or triplication of the SNCA gene resulting in high cellular α-Syn concentration (123). Therefore, α-Syn stability as well as protein concentration may play a role.

The study of α-Syn is challenging, because the fluorescent tags which are normally used to localize proteins within the cell cause problems. In a previous study, it was shown that the green fluorescent protein was cleaved off from a fusion with α-Syn prior aggregation (124). As a result, the aggregates of α-Syn and its mutant could be observed only by immunodetection and not by their fluorescence These findings suggest that C-terminal destabilization might enhance α-Syn aggregation (124). A second difficulty arises from the tag itself. α-Syn is a small protein (15 kDa) while the GFP is almost double the size (27 kDa). It was hence proposed that GFP might sterically hinder the aggregation and toxicity of α-Syn (125). Using antibody staining, the aggregation of α-Syn was studied in SH-SY5Y neuroblastoma cells. While only 6% of cells transfected with WT α-Syn

contained inclusions, the mutant α-Syn-A53T lead to an increase to 12%, α-Syn-E46K and α-Syn-E46KΔG showed inclusions in 18% or 40% of transfected cells, respectively (126).

Similar as for Htt, it was studied in this work whether α-Syn could be used to analyze the influence of aggregates on GPCR signaling and trafficking.

4.3.   Superoxide Dismutase 1

Like PD, ALS occurs as a sporadic and familial form. ALS is a neuromuscular disease-causing progressive motor deficits. It is characterized in most cases by the formation of inclusion bodies which induce neuronal cell death. Whereas the risk of developing Alzheimer's disease or PD increases with age, the highest risk of developing ALS is at ages 50-75 (126). About 85-95% of ALS cases are sporadic but twin studies revealed a genetic contribution (127, 128). Similar to HD and PD, ALS is also associated with depression (129). In familial cases of ALS, mutations have been found in genes encoding C9orf72 (40%), SOD1 (20%), FUS (1-5%) and TARBDP (1-5%) (130, 131). The etiology of the remaining 40 to 20% of familial forms is still not known.

Overall, more than 30 proteins are associated with ALS. The function of these proteins can be grouped in three categories depending on the pathway in which they are involved: RNA biology, protein turnover and axonal transport (131). Similar to the situation with other neurodegenerative diseases, therapy options are very limited for ALS. However, the compound riluzole has been shown to increase life span of affected patients, although the mechanism is not clear as of yet (132). Riluzole is known to decrease the release of glutamate thereby inhibiting AMPA postsynaptic receptor activation. It is discussed that riluzole thereby inhibits excitotoxicity (calcium cell poisoning after activation) (131). AMPA CME was shown to be inhibited *in vitro* by the presence of SOD1A4V aggregates leading to an increase of the plasma membrane expression of AMPA (11). One could postulate that, this increase in AMPA membrane receptor expression upon aggregate formation may explain the mechanism of action of riluzole.

Of note, the protein composition of the inclusion bodies is different whether the disease is sporadic or familial. In sporadic ALS, the major component of these inclusions is the TDP-43 RNA interacting protein while in familial forms, the main component of the inclusions is the mutated protein itself (131). To date, cellular models of ALS aggregation are based on the identified familial mutants; the TDP-43 aggregation is difficult to trigger without inducing major cell stress (133–135). In this work, it was analyzed whether the

mutant SOD1A4V of SOD could be used to analyze the influence of aggregates on GPCR trafficking and signaling.

In the case of the SOD1 gene, over 150 mutations have been discovered but only a few could be associated with the disease (126, 131). Like α-Syn, SOD1 has a relatively low molecular weight (16 kDa), and fusion of fluorescent tags could potentially alter its aggregation properties. Indeed, the SOD1G93A mutant lost its property to form fibrils when tagged with GFP (136). On the other hand, aggregation of GFP-tagged SOD1A4V has been observed in human PC3 prostate adenocarcinoma cells using fluorescence microscopy and it was shown to inhibit CME (11).

5. Pulse Shape analysis

In order to quantify amyloids as well as to measure their influence on GPCR trafficking, a novel flow cytometry technique named Pulse Shape analysis (PulSa) can be used. A flow cytometer functions by measuring fluorescence over time. When a fluorescent object passes in front of the laser, the signal measured by the detector raises above the baseline and when the object leaves, the signal returns back. Considering that the flow rate inside the FACS is constant, the time of exit minus the time of entry allows the calculation for the pulse width (W parameter). During this gate window, the maximum fluorescence of the pulse is also measured giving the pulse height (H parameter). Usually these two parameters are combined to form a fitted gaussian curve; the area under the curve representing the measure of this pulse (A parameter). In the PulSa technique, the
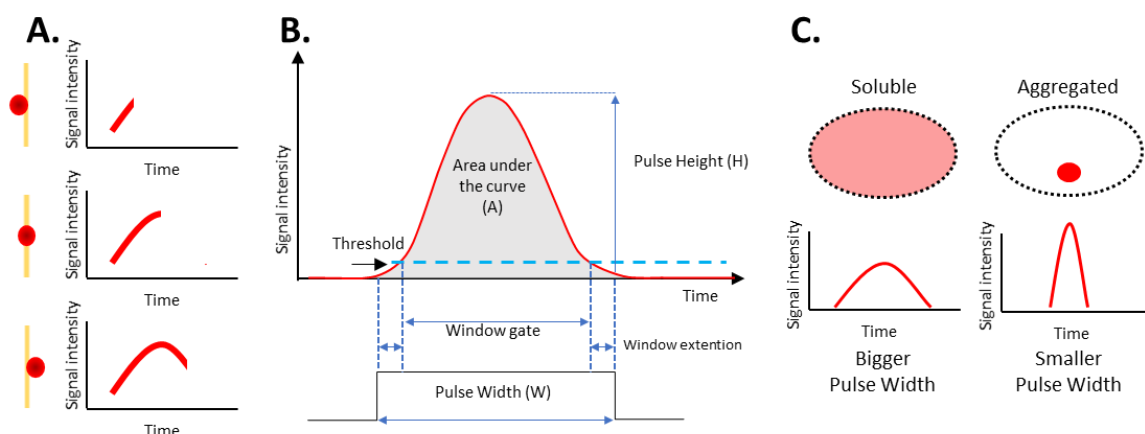
Figure 3. Underlying principles of PulSa analysis. A. A flow cytometer measures fluorescence over time. When a fluorescent object passes in front of the laser, a gausian shaped signal is detected. **B.** Representation of the parameters estimated out of over time recording of detector voltage. Pulse Height parameter (H) is the maximum fluorescence recorded. Pulse width (W) is the window gate plus two times the window extension. The area under the curve (A) is estimated using both H and W parameters. **C.** Principle behind PulSA. The fluorescence width of a protein diffused in the cytoplasm of a cell is bigger than the one of an aggregated protein.

pulse width and the pulse height are plotted against each other allowing a separation and independent gating of pulse groups of different sizes (137, 138).

This technique is very powerful to study the effects of huntingtin and other aggregates as it allows independent cell analyses within a mixed population depending on whether a cell contains aggregated or soluble proteins. Huntingtin in its soluble form is expressed diffusely throughout the whole cytoplasm, aggregates in contrast form much brighter structures inside the cell and occupy a much smaller area. Therefore, at equivalent fluorescent A fluorescence, the H and W parameters will be different (lower H and higher W for soluble HTT, higher H and lower W for aggregated HTT). This gating then allows the independent analysis of other fluorescent parameters. Here, PulSa was used in order to analyze the influence of HttExon1Q23 and soluble and aggregated HttExon1Q74 on the trafficking of various GPCRs (V1aR, V2R, UTS2R and CRF1R). Of note, PulSa is suitable to differentiate cells containing amyloid aggregates from cells containing still soluble forms within a mixed cell population.

6. Detection of Amorphous aggregates

In this study, it should also be studied whether amorphous aggregates have the same effect on CME as amyloid aggregates. The first requirement to examine the effect of amorphous aggregates is to quantify the amount of aggregation. Historically, mutants of the firefly luciferase (Fluc) were generated for this purpose. Variants such as FlucDM (139) have a decreased stability and form amorphous aggregates. Native folding and luminescence depend on chaperone activity and decreased luminescence is consequently a measure for amorphous aggregate formation. Modern techniques use chemical fluorescent sensors to study the formation of amorphous aggregates. The tetraphenylethene maleimide (TPE-MI)(140) has been proposed to represent such a tool when using CLSM. When proteins are misfolded, TPE-MI fluorescence is activated by forming disulfide bonds with free cysteine thiols, normally buried in the core of proteins that are exposed upon unfolding. The immobilization of the phenyl rotamer is amplifying further this fluorescence (140). TPE-MI fluorescence is consequently a measure for amorphous aggregate formation

7. Aim of the study

The aims of this study are not only relevant for the field of neurodegenerative disorders, but also for the biology of the whole GPCR protein family, since no studies addressed

the influence of protein aggregation (amyloidic or amorphous) and cell ageing on trafficking and signaling of these receptors so far.

Specifically, it was intended here to analyze whether the previously described defects of CME observed in the presence of amyloid aggregates are also detectable in the case of such lowly–expressed membrane proteins as GPCRs or whether residual, non-sequestered HSC70 could still drive CME and signal transduction.

Furthermore, it was intended to study the effect of amyloids aggregates on the membrane levels of SERT since it is conceivable that this transporter might undergo constitutive CME. SERT is very interesting in this respect due to its drugability and significance for disease.

II. Results

1. Cells expressing mCherry-HttExon1Q74 represent a mixed cell population of soluble, aggregation-prone proteins and insoluble aggregates.

To study the influence of HTT aggregates on GPCR trafficking and signaling, the exon 1 of HTT N-terminally was fused with mCherry and C-terminally with a 74 repetition polyglutamine stretch exceeding the critical ~35-37 repetition threshold required for aggregation (construct mCherry-HttExon1Q74). An equivalent construct containing only a 23-repetition stretch was used as a non-aggregating control. Non fluorescent, C-terminally HA-tagged versions of these constructs were also generated to perform immune-fluorescence studies. A scheme of the respective constructs mCherry-HttExon1Q23, mCherry-HttExon1Q74, HttExon1Q23-HA and HttExon1Q74-HA is shown in Fig. 4.
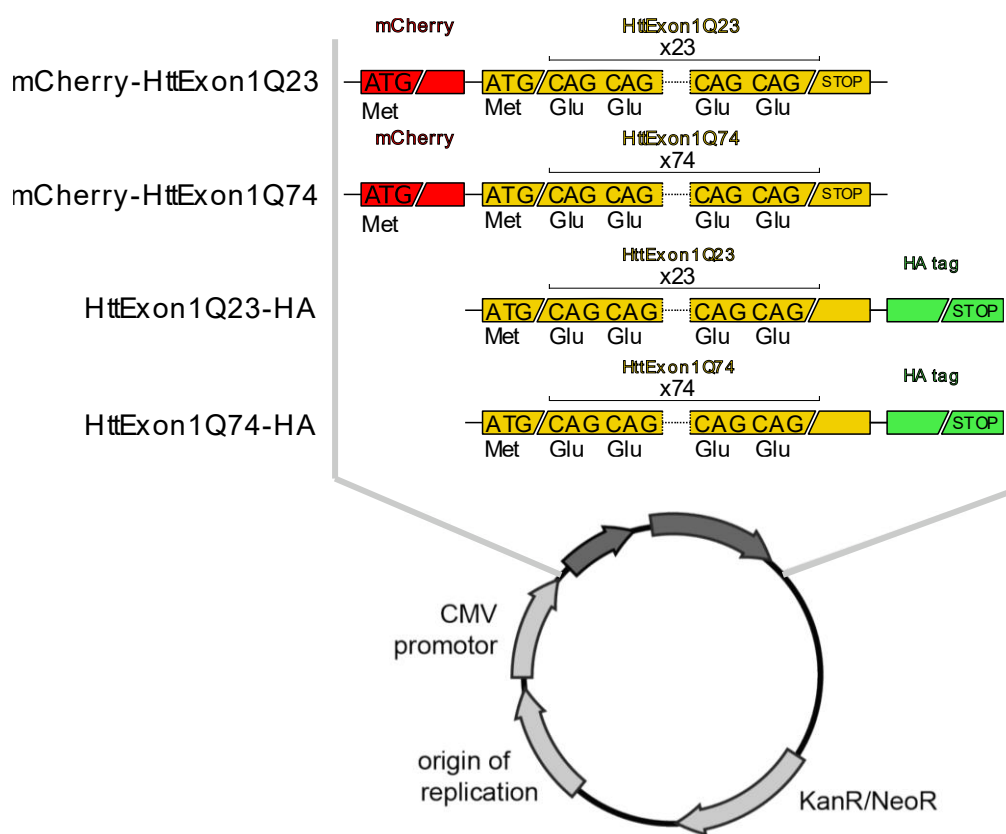
Figure 4: Map of HttExon1 plasmids generated and used in this study. The backbone of all plasmids contained an origin of replication for plasmid amplification in *E. coli* and genes encoding kanamycin and neomycin resistance which were used as a selectable markers. The human cytomegalovirus (CMV) promotor allows expression of the constructs in mammalian cells. DNA sections that differ between the plasmids are shown in more detail.

To confirm that mCherry-HttExon1Q74 forms aggregates while mCherry-HttExon1Q23 remains soluble, the constructs were transiently expressed in HEK 293 cells. Visualization by CLSM revealed that the control construct mCherry-HttExon1Q23 is indeed expressed only in its soluble form diffusely in the cytosol of the cells (Fig. 5 A). In contrast, mCherry-HttExon1Q74 was expressed in two distinct forms. Most of the cells expressed the aggregation-prone protein in its diffuse, soluble form, other cells clearly showed inclusion bodies indicating protein aggregation (Fig. 5 B). The fact that cells expressing mCherry-HttExon1Q74 showed a mixed cell population was experimentally challenging, limiting our analyses to single cell method. On the other hand, it offered the opportunity to represent an internal control for each of the experiments.

In order to confirm that the microscopically detectable large inclusions for mCherry-HttExon1Q74 (Fig. 5 B, white arrow) are indeed aggregates, protein diffusion using fluorescence recovery after photobleaching (FRAP) was measured (Fig. 5C). The fluorescence recovery of the mCherry-HttExon1Q23 control was almost complete (Fig. 5 C, red curve). The recovery of the still soluble mCherry-HttExon1Q74 (blue curve) was very similar to that of mCherry-HttExon1Q23. In contrast, when the ROI was set to the inclusion bodies in cells expressing mCherry-HttExon1Q74 (green curve), no such recovery was detected demonstrating that these proteins are unable to diffuse and thus form non-soluble, immobile aggregates.
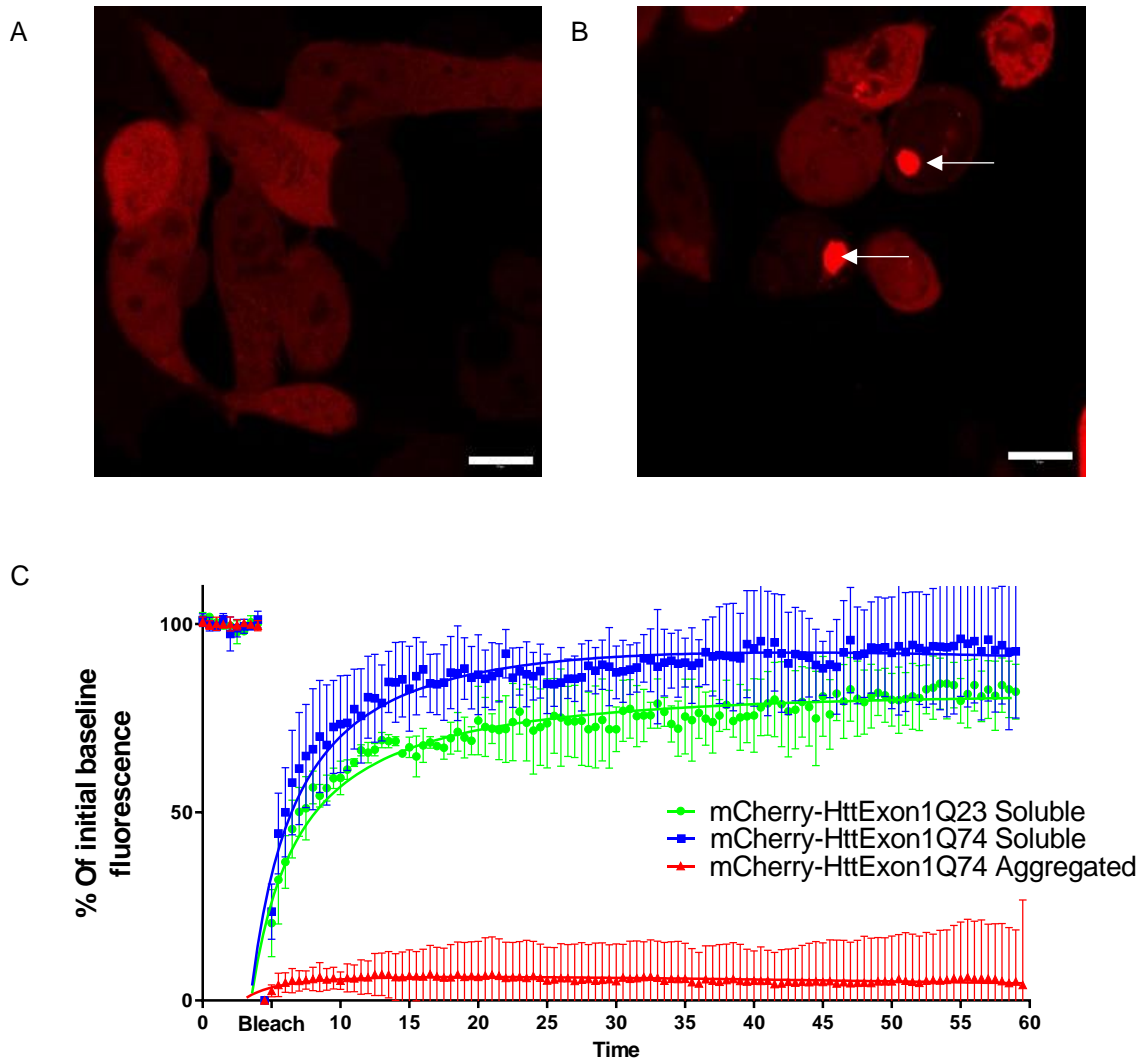
Figure 5: FRAP measurements using mCherry-HttExon1Q23 and mCherry-HttExon1Q74 in its soluble and aggregated form. Prior to the experiment, HEK293 cells were transiently transfected with mCherry-HttExon1Q23 (A) and mCherry-HttExon1Q74 (B) and incubated for 72 h. Cells were then analyzed by CLSM. Cells containing mCherry-HttExon1Q23 expressed the mCherry fluorescence diffusely in the cytoplasm and nucleus (see A). Cells expressing mCherry-HttExon1Q74 were found in two different states, either the mCherry fluorescence was expressed in the cytoplasm and nucleus (as with the mCherry-HttExon1Q23) or the fluorescence was concentrated in inclusion bodies (see B; white arrows). Pictures show xy scans of representative cells of three independent experiments. Scale bar = 10 μm. (C) FRAP measurements of the constructs. ROIs were selected in the cytoplasm for cells expressing soluble mCherry-HttExon1Q23 or mCherry-HttExon1Q74 or in the center of the aggregates for cells containing mCherry-HttExon1Q74 inclusion bodies. Initial fluorescence was measured for 10 cycles of 0.5 seconds; ROI bleaching was performed and the mean of ROI fluorescence was measured every 0.5 seconds for an additional 50 seconds. Cells having cytoplasmic fluorescence showed an almost full recovery of fluorescence indicating that HttExon1Q23 and HttExon1Q74 are present in their soluble form in these cells. No significant fluorescence recovery could be measured in the inclusion bodies, indicating that these fluorophores are trapped as non-soluble aggregates. Data points show mean values of three independent experiments ±SD (soluble mCherry-HttExon1Q23 and mCherry-HttExon1Q74) and mean values of 7 independent experiments ±SD (aggregated mCherry-HttExon1Q74).

2. HSC70 is sequestered by the mCherry-HttExon1Q74 aggregates.

As described in recent literature, other amyloid aggregates sequester the HSC70 chaperone causing a loss of function in CME (11, 141–143). To confirm that this also happens with the HttExon1Q74 constructs, HttExon1Q23 and HttExon1Q74 were fused with C-terminal HA tags and transiently transfected them in HEK293 cells. Labeled HA tags were used because the fluorescence of aggregates containing mCherry in the condition of the experiment was extremely intense leading to fluorescent bleed-through in all other measured channels rendering colocalisation studies very difficult.
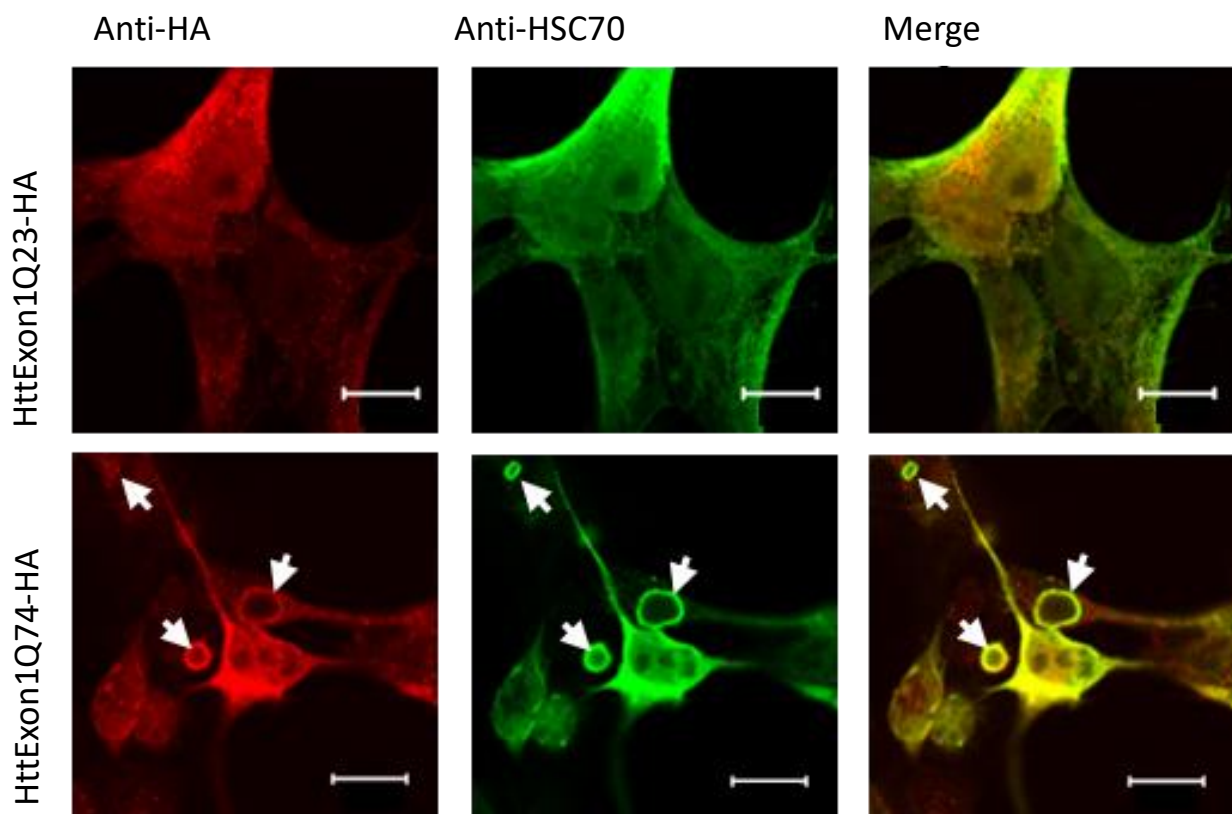
Figure 6: Recruitment of HSC70 by HttExon1Q74 amyloid aggregates. HEK293 cells were transiently transfected with HttExon1Q23-HA (upper panel) and HttExon1Q74-HA (lower panel) and incubated for 3 days. Cells were fixed with PFA (4%) and permeabilized with Triton-X100. Huntingtin constructs were labeled using mouse anti-HA and goat anti-mouse Alexa Fluor™ 647 antibodies (red, left panel). HSC70 was labeled using rabbit anti-HSC70 antibodies and CY3-conjugated goat anti-rabbit antibodies (green, central panel). Yellow color in the overlay (right panel) indicates co-localization. Cells containing amyloid aggregates showed a difference in subcellular HSC70 distribution. When HttExon1Q74-HA is aggregated, HSC70 is recruited almost completely to the amyloid aggregates (white arrows) and the cytoplasmic pool is depleted. In contrast, in cells expressing soluble HttExon1Q23-HA or HttExonQ74-HA, HSC70 remains diffusely in the cytoplasm. Pictures show xy scans of representative cells of three independent experiments. Scale bar = 10 µm.

As previously observed, cells expressing HttExon1Q23-HA did not form aggregates (Fig. 6). For cells expressing HttExon1Q74-HA, again cells with aggregates or soluble proteins were detected. In the latter case, aggregates appeared as rings because the center of

the aggregates is not accessible for antibodies. In cells containing HttExon1Q23-HA or HttExon1Q74-HA in its soluble form (red fluorescence), HSC70 (green fluorescence) is located mainly throughout the cytosol and in the nucleus. In cells possessing HttExon1Q74-HA aggregates (white arrows), however, HSC70 is almost completely recruited to the aggregates and only barely detectable amounts could be seen in the cytoplasm or the nucleus. These results confirm that HttExon1Q74 aggregates completely sequester HSC70 from its cytosolic location as previously shown for other amyloid aggregates (11).

3. mCherry-HttExon1Q74 aggregates impair ligand-induced CME of GPCRs

To address the question whether the sequestration of HSC70 by HttExon1Q74 aggregates influence ligand-induced CME of GPCRs, stably transfected HEK293 cells expressing FLAG-CRF1R-GFP and FLAG-V2R-GFP that were transiently transfected with mCherry-HttExon1Q23 or mCherry-HttExon1Q74 were used. Two other GPCRs, namely FLAG-V1aR-GFP and FLAG-UTS2R-GFP were transiently co-transfected with mCherry-HttExon1Q23 or mCherry-HttExon1Q74.

First, a microscopic analysis was performed. Cells were stimulated with agonists for the respective receptors in order to trigger ligand-induced CME. CLSM pictures were taken before and after 30 minutes of stimulation (Fig. 7 shows exemplary results for FlagV1aR-GFP; Supplementary Fig. 1 shows the other receptors). In cells expressing mCherry-HttExon1Q23 or mCherry-HttExon1Q74 in its soluble form, receptors were internalized in a comparable manner. The number of intracellular vesicles containing receptor GFP fluorescence signals increased substantially (Fig. 7 A & B cells without arrow) while the GFP signals in the plasma membrane decreased concomitantly. In contrast, in cells expressing mCherry-HttExon1Q74 in its aggregated form (Fig. 7 B, cell indicated with white arrow), the number of formed vesicles containing receptor GFP fluorescence signals was significantly reduced, and the plasma membrane GFP signals of the receptors were detectable in substantial amounts. These results indicate that the presence of amyloid aggregates indeed affect ligand-induced CME of GPCRs.

mCherry-HttExon1Q23

mCherry-HttExon1Q74
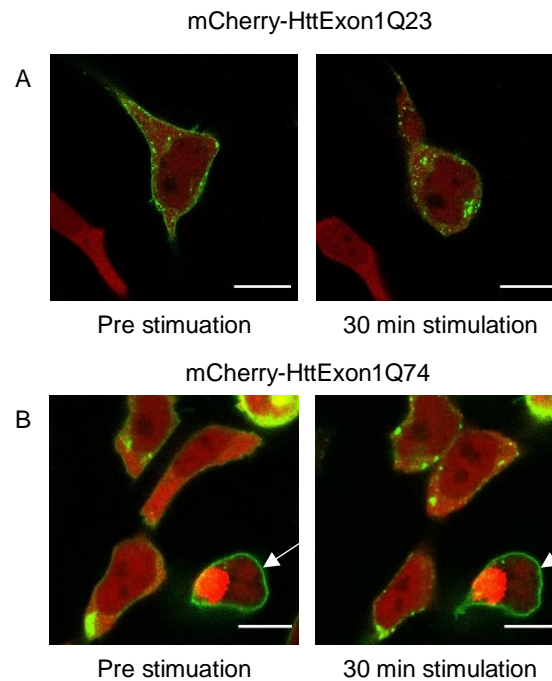
Figure 7: Ligand-induced internalization of Flag-V1aR-GFP in presence of mCherry-HttExon1Q23 and mCherry-HttExon1Q74. HEK293 cells expressing Flag-V1aR-GFP (green) were co-transfected with mCherry-HttExon1Q23 (A) or with mCherry-HttExon1Q74 (B red), incubated for three days and analyzed by CLSM. Pictures were recorded before and after 30 minutes of V1aR stimulation using the ligand AVP (100 nM). In the absence of amyloid aggregates (cells containing mCherry-HttExon1Q23 (A) or still soluble mCherry-HttExon1Q74 (B, cells without arrow), vesicles were detectable inside the cells and the membrane level of the receptor was significantly reduced. However, the presence of aggregated mCherry-HttExon1Q74 (B, cell with white arrow) not only reduced the number of formed vesicles but also kept the membrane expression level of the receptor constant indicating that ligand-induced CME is inhibited. Pictures show xy scans of representative cells of three independent experiments. Scale bar = 10 µm.

Microscopy can be easily done at a single cell level but statistical analyses are notoriously difficult to obtain. On the other hand, quantifying the effect of aggregates on ligand-induced CME in a mixed cell population is experimentally very challenging.

First, among the cells expressing mCherry-HttExon1Q74, the percentage of cells developing aggregates was determined. To this end, the relatively novel FACS-based technique, namely Pulse Shape analysis (PulSA) was used (137, 138). A flow cytometer measures two parameters per channel: the height (maximum fluorescence) and the width (size) of the pulse which are usually combined into the area under the curve which is used to quantify fluorescence levels. However, the PulSA technique takes into account that the area occupied by the fluorescence of an aggregate is smaller and brighter in comparison to its soluble form. Therefore, when measuring HEK293 cells expressing the soluble mCherry-HttExon1Q23 following transient transfection, only one peak could be detected in the pulse width mCherry channel (Fig. 8 B). In contrast, two peaks could be detected in cells expressing mCherry-HttExon1Q74, one representing the soluble form

and the other with smaller size representing the aggregates (Fig. 8 C). By plotting the width against the height of each pulse, cells containing mCherry-HttExon1Q74 aggregates could be differentiated from cells containing the still soluble form in these heterogeneous samples. The PulSA technique was used to quantify the number of cells containing mCherry-HttExon1Q74 aggregates in the same GPCR expressing cells (N-terminally FLAG and C-terminally GFP-tagged) as in the previous experiment. The percentage of cells containing amyloid aggregates was similar for the different receptors and were in the range from 22% (FLAG-V2R-GFP) to 35% (FLAG-V1aR-GFP) (Fig. 9 A).
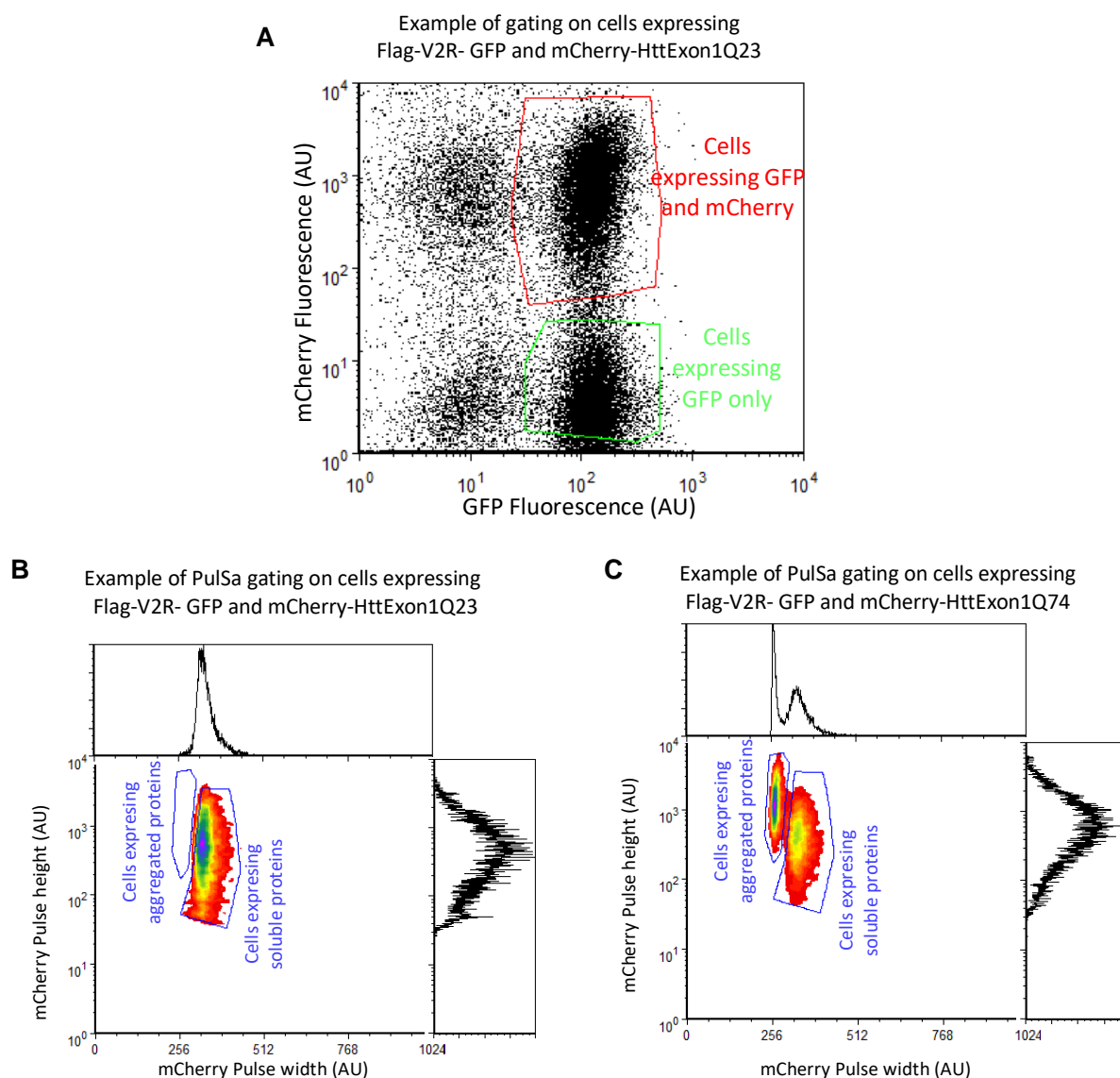
Figure 8: Example gating of a PulSa analysis of stably transfected HEK293 cells expressing mCherry-HttExon1Q23 or mCherry-HttExon1Q74 (A) Example gating for cells expressing both Flag-V2R-GFP and HttExonQ23. (B) Example PulSa gating for cells expressing mCherry-HttExon1Q23 and (C) mCherry-HttExon1Q74 (C)

In order to quantify the effect of the amyloid aggregates on ligand-induced CME of GPCRs, the same cells were used as in the two previous experiments. Plasma membrane expression levels of the receptors were quantified 3 days after transfection and following 1 hour of stimulation with 100 nM of the corresponding ligands. Due to the transient co-transfection of stable cell lines, multiple cell populations were observed in the same sample, which could all be distinguished by the PulSA technique: cells expressing the receptor alone, cells expressing the receptor and soluble mCherry-HttExon1Q23 or mCherry-HttExon1Q74 and cells expressing aggregated mCherry-HttExon1Q74.

The membrane level of each receptor was defined as the ratio of anti-FlagM2 antibody labeling of the membrane receptors and GFP fluorescence labeling of the entire receptor pool. Data were normalized to the ratio of non-stimulated receptor-expressed alone values for each condition.

The results of these analyses showed a robust ligand-induced CME for Flag-V1aR-GFP, Flag-V2R-GFP and Flag-UTS2R-GFP when the receptors were expressed alone, co-expressed with mCherry-HttExon1Q23 or still soluble mCherry-HttExon1Q74 (Fig. 9 B). While Flag-CRF1R-GFP internalization is less effective in comparison to the other receptors, no statistical difference could be measured between the internalization efficiencies in these cases.

However, when the receptors were expressed in cells containing aggregates of mCherry-HttExon1Q74, the internalization of Flag-V1aR-GFP, Flag-V2R-GFP and Flag-UTS2R-GFP was significantly reduced. The inhibition of internalization was incomplete. This can be explained by the fact that cells contain a pool of clathrin which is still available to perform some internalization as long as the cells did not encounter a ligand (ligand-naïve cells). Therefore, and because the amount of available clathrin should be limited, a second or multiple rounds of internalization should deplete the pool of available clathrin to a point where no further CME is possible. For Flag-CRF1R-GFP, the internalization inhibition in presence of aggregated mCherry-HttExon1Q74 was complete as no significant change in membrane expression could be measured upon ligand biding. With all studied receptors, the membrane should consequently be flooded with desensitized receptors upon multiple rounds of activation.

Figure 9: PulSa analysis of stably transfected HEK293 cells co-expressing mCherry-HttExon1Q74 and Flag-V1aR-GFP or Flag-V2R-GFP or Flag-UtS2R-GFP or Flag-CRF1R-GFP. (A) Number of cells possessing mCherry-HttExon1Q74 aggregates in the mixed cell population in % for the respective receptors. Columns represent mean values of 10 independent experiments ±SD. (B) Number of cells possessing mCherry-HttExon1Q74 aggregates in the mixed cell population in % for the respective receptors. Columns represent mean values of 10 independent experiments ±SD. (D) Ligand-induced CME of the respective GPCRs upon co-expression of mCherry-HttExon1Q23 or soluble or aggregated mCherry-HttExon1Q74. Cells were stimulated for 1 h with 100 nM of the respective agonist. The membrane to total receptor expression ratio is shown. Data obtained for soluble or aggregated mCherry-HttExon1Q74 were obtained by PulSa analysis from the same sample of cells. Columns represent mean values of 3 independent experiments each performed in duplicates ±SD. p value < 0,05 were considered to be significant (*), p value < 0,01 (**), p value < 0,001 (***) and p value < 0,0001 (****).

4. mCherry-HttExon1Q74 aggregates impair the receptor activation cycle of GPCRs.

Inhibition of CME by amyloid aggregates should lead to an increase of desensitized receptors in the plasma membrane upon multiple rounds of activation, which should in turn also impair G protein-coupling and signaling. However, the fact that only part of the cells formed amyloid aggregates limits signaling experiments to the single cell level. Consequently, the Gq-coupled V1aR (144) and the Gs-coupled CRF1R were selected to study the influence of amyloid aggregates on the signaling of two receptors with different G protein coupling selectivity. Both receptors were described to recycle to the plasma membrane following ligand-induced CME (145).

4.1. mCherry-HttExonQ74 aggregates impairs the receptor activation cycle of the V1AR.

The V1AR is a predominantly Gq-coupled GPCR (146). To asses for V1AR Gq-coupling upon the presence of amyloid aggregates, HEK293 cells were co-transfected with the constructs Flag-V1aR-BFP and either the control construct mCherry-HttExon1Q23 or mCherry-HttExon1Q74. Cells expressing soluble or aggregated mCherry-HttExon1Q23 or mCherry-HttExon1Q74 constructs were identified by CLSM. For the signaling experiments, a two-step activation protocol was carried out. The receptor was stimulated first with a low concentration of AVP (1 nM) and the resulting intracellular Ca^{2+} concentration was measured using the fluorescence of the Ca^{2+} sensor Fluo8 (Fig. 10, left panel). After a 30 min incubation allowing internalization/recycling of the V1AR, a second activation was carried out using a higher concentration of AVP (10 nM) and Fluo8 fluorescence was measured again (Fig. 10, right panel). Thereafter, cells were treated with the detergent digitonin allowing influx of extracellular Ca^{2+} to get the maximal Fluo8
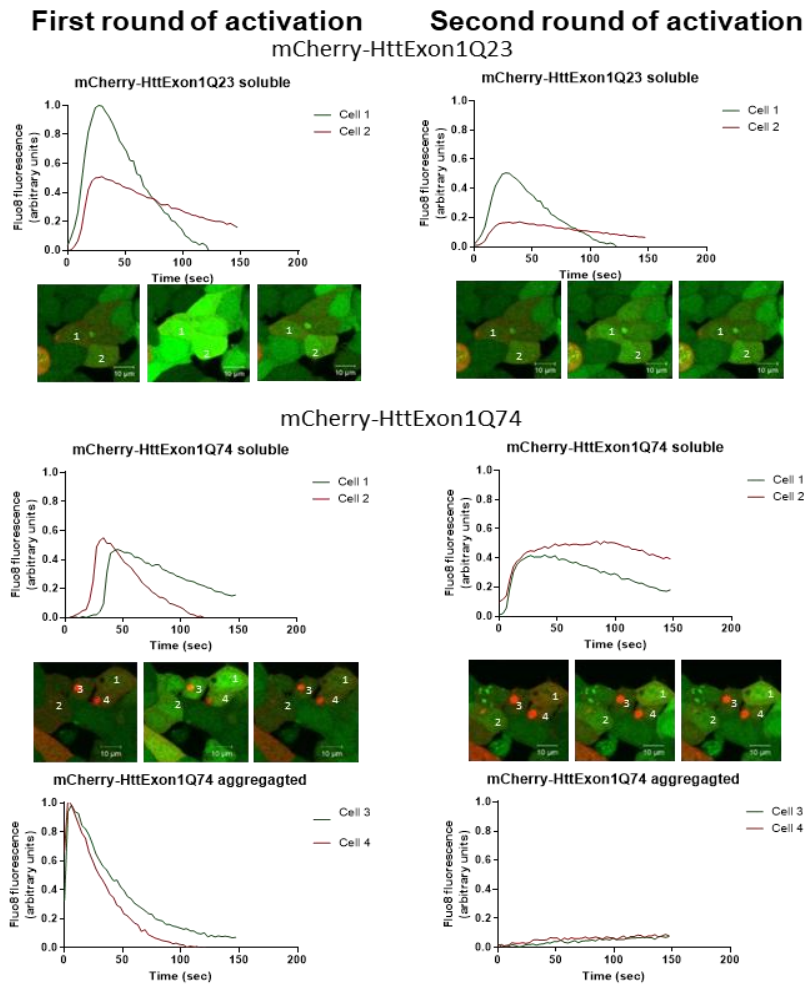
Figure 10: The presence of mCherry-HttExonQ74 aggregates impair the receptor activation cycle of the V1AR. Left panel. First round of activation. Right panel. Second round of activation. Upper panels. Ca^{2+} accumulation curves following 1st and 2nd activation of FLAG-V1aR-BFP by AVP. HEK293 cells were transiently transfected with Flag-V1aR-BFP and either the control construct mCherry-HttExon1Q23 or mCherry-HttExon1Q74, the latter remaining soluble or forming amyloid aggregates. The Gq-mediated Ca^{2+} accumulation following receptor activation was monitored using the calcium sensor Fluo8 (green fluorescence) under the indicated conditions in representative cells (curves of 2 cells are shown). The curves are representative of three independent experiments. Lower panels. CLSM analysis under the same conditions. mCherry-HttExon1Q23 or mCherry-HttExon1Q74 signals are depicted in red, Fluo8 Ca2+ signals in green. Pictures show xy scans of representative cells of three independent experiments. Scale bar = 10 μm.

fluorescence for normalization. To quantify the results following the first activation, the highest recorded fluorescence value of Fluo8 after V1AR stimulation was divided by the highest fluorescence value measured following digitonin treatment. No significant difference could be detected under these conditions (Fig. 11A). The ratios of the Fluo8 maxima of the second activation to that of the first activation for each measured cell was compared (Fig. 11B). For cells expressing the control construct mCherry-HttExon1Q23 or still soluble mCherry-HttExon1Q74, again no significant difference could be observed. However, in cells expressing aggregated mCherry-HttExon1Q74, the ratio of receptor reactivation was significantly reduced. These results are consistent with the view that the

inhibition of CME by amyloid aggregates inhibits recycling of active receptors to the plasma membrane and consequently causes a growing number of desensitized receptors at the cell surface and finally a breakdown of receptor signaling.

4.2.   Inhibition of the CME impairs the receptor activation cycle of the CRF1R.
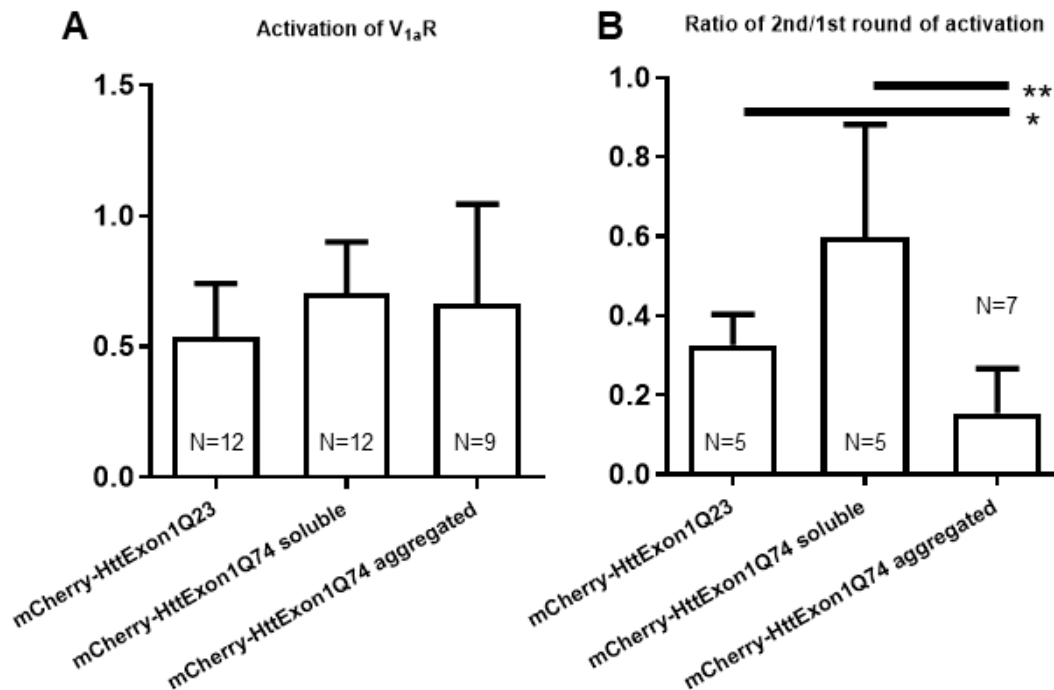
Figure 11: Quantification of the results shown in Figure 10. (A) Data following first V1AR activation. The maximum of fluorescence of Fluo8 after V1AR stimulation was divided by the maximum fluorescence measured following digitonin treatment. Fluo8 fluorescence signals were normalized to 0 using 10 reference measurements before AVP stimulation. Columns represent mean values ±SD of 9 different cells expressing aggregated mCherry-HttExon1Q74 and 12 different cells expressing soluble mCherry-HttExon1Q74 or the control construct mCherry-HttExon1Q23. **(B)** Quantification of the results following V1AR re-activation. The ratios of the Fluo8 maxima of the second activation and the first activation were compared for each measured cell depicted in (A). Columns represent mean values ±SD of N cells (N indicated in each column) p value < 0,05 were considered to be significant (*), p value < 0,01 (**).

In the case of the predominantly Gs-coupled CRF1R, a different strategy was used to study the influence of CME defects on receptor signaling. Single cell experiments for cAMP accumulation in cells containing aggregates were very difficult. An Epac-based assay, for example, would in this case lead to an experimental set up with 4 different fluorophores that would reduce substantially the FRET readout efficiency and require a triple transfection. After testing this system, the efforts proved to be not successful (data not shown). To mimic the effect of aggregate-induced CME inhibition, the inhibitor Pitstop 2 which selectively blocks endocytotic ligand association with the clathrin terminal domain and thereby CME (147) was used. As a model GPCR, the predominantly Gs-coupled CRF1R was used. As previously shown that Pitstop 2 does not inhibit activation

of the ligand-naive CRF1R (148). It was also shown that the CRF1R is a recycling GPCR (145). Pitstop 2 treatment should consequently simulate the effects of amyloids aggregates on CRF1R signaling over time.

To control such an effect of Pitstop 2, an internalization assay was performed using CRF1R-GFP and V1aR-GFP in stably transfected in HEK293 cells. Cells were pre-treated with solvent or Pitstop 2. Following ligand activation, CME was monitored over time using the receptor's GFP fluorescence signals and CLSM (Fig. 12, the first and last pictures are shown). Without Pitstop 2, CRF1R-GFP and V1aR-GFP internalization was clearly detectable by vesicle formation. Addition of Pitstop 2, however, completely abolished ligand-induced CME of these receptors demonstrating effectiveness of Pitstop 2.
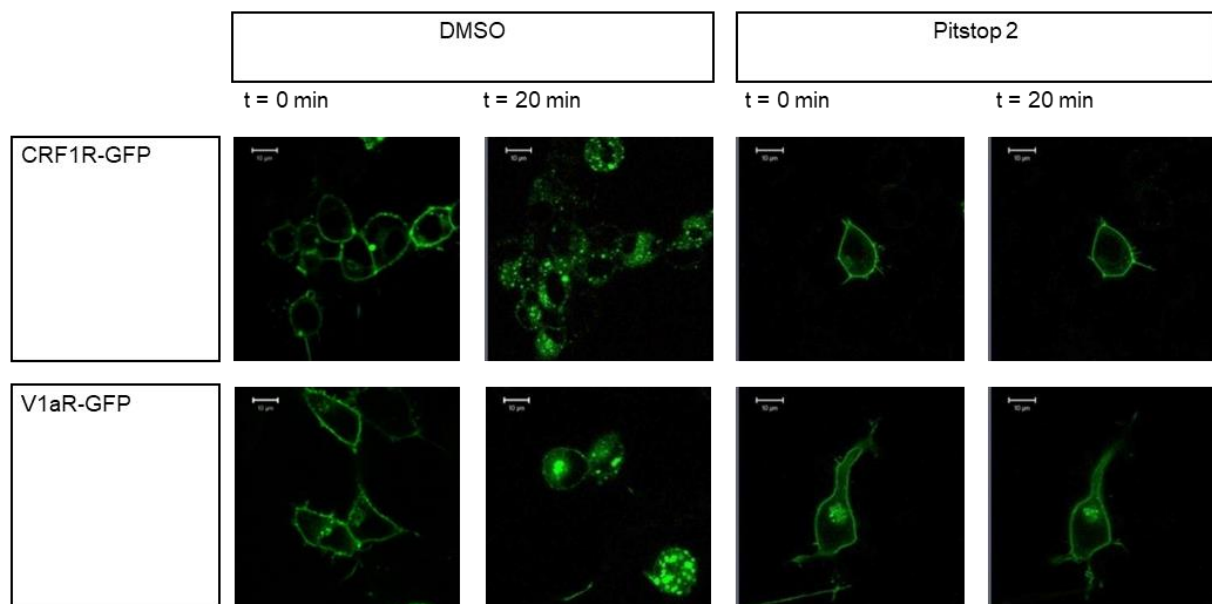
Figure 12: CLSM internalization assay using transiently transfected HEK293 cells expressing Flag-CRF1R-GFP and Flag-V1aR-GFP (upper and lower panels respectively, GFP signals in green). Cells were pretreated for 20 min with DMSO solvent or Pitstop 2 (30 µM). The agonists (100 nM Sauvagine for Flag-CRF1R-GFP; 100 nM AVP for Flag-V1aR-GFP) were added at t_0 and pictures were recorded in a time series, one picture every 2 minutes. Pictures show xy scans of representative cells of five independent experiments. Scale bar = 10 µm.

A time-resolved cAMP accumulation assay (cAMP radio immuno-assay) was conducted with Pitstop 2 or DMSO pre-treated stably transfected HEK293 cells expressing the CRF1R. Receptor activation was triggered using the agonist Sauvagine (Fig. 13). After 15 minutes of activation, cells in both conditions showed no difference in cAMP accumulation. This result is consistent with these calcium measurements for V1AR.GFP (Fig. 10 and 11) and suggests once more that the inhibition of CME does not affect the first round of activation of ligand-naïve receptors. After this time point, however, the

cAMP accumulation curves were substantially different. The cells treated with Pitstop 2 were unable to produce more cAMP over time (Fig. 13, red curve). In the control cells however, cAMP formation continues but it was not as fast as during the first activation cycle (Fig. 13, blue curve). These results could be readily explained by a defect of receptor internalization and recycling and by the resulting accumulation of desensitized receptors in the plasma membrane. Similar results should be obtained when the aggregates are present instead of Pitstop 2 treatment. However, as discussed above this is very difficult to address experimentally.
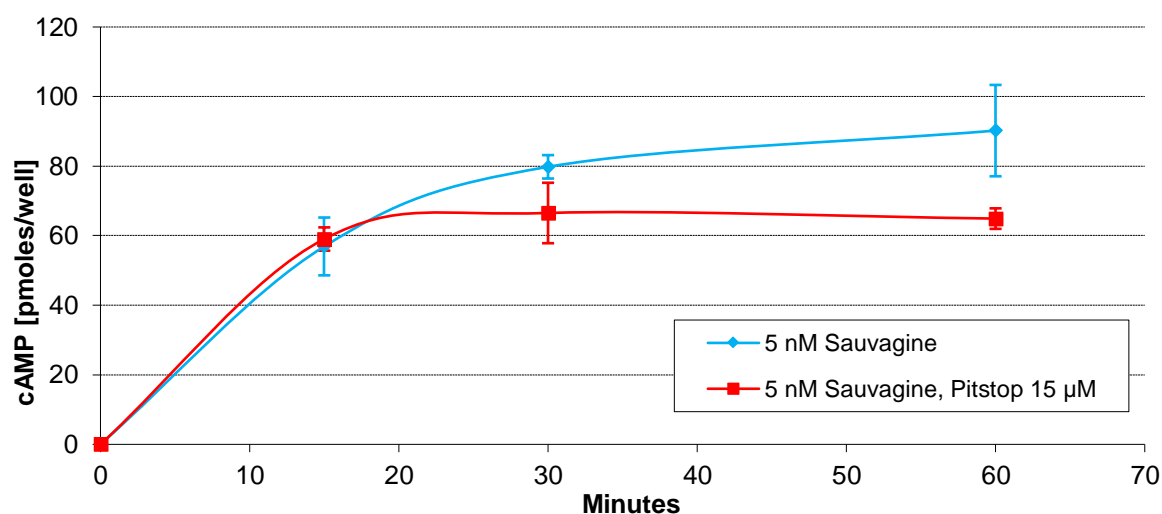
Figure 13: cAMP accumulation assay in stably transfected HEK293 cells expressing CRF1R.GFP. Cells were treated with Pitstop 2 (15 µM) or DSMO solvent and IBMX. Sauvagine (5 nM) was added at t0, cells were lysed at 0, 15, 30 and 60 minutes, and accumulation of the second messenger was measured using a cAMP-RIA. Data points represent mean values of two independent experiments each performed in triplicates ±SEM

5. Effect of amorphous aggregates on the ligand-induced CME of GPCRs

These observations that amyloid aggregates impair ligand-induced CME of GPCRs by HSC70 sequestration and consequently lead to a breakdown of GPCR signaling, raise the question if this is also true when amorphous protein aggregates are present. To address this question, it was first checked whether amorphous aggregates recruit HSC70 in a similar manner as amyloid aggregates. Induction of amorphous protein aggregation in HEK293 cells was done using the proteasomal inhibitor MG132 (149, 150) (20 µM) and immuno-labeled HSC70 as described above. Visualization the amorphous aggregates was performed using the fluorescent tetraphenylethene maleimide (TPE-MI) (140) (Fig. 14, left panels, blue fluorescence). The fluorescence of this compound is activated by binding to free cysteine thiols which are normally buried in the hydrophobic core of soluble proteins but get exposed upon protein aggregation. Upon inducing

aggregation with MG132, the vast majority of the cells contained an aggregate, thus removing the need for single cell experiments. CLSM immuno-fluorescence showed that the amorphous aggregates did only partially sequester HSC70 (Fig. 14, lower right panel white arrow) in contrast to what was seen for amyloid aggregates. A portion of HSC70 seems to be recruited to a nuclear location as described previously (151). Most importantly, cells retain a substantial cytosolic HSC70 level which could be enough to maintain CME processes of GPCRs in contrast to what was seen for amyloid aggregates.

To address this question, induction of amorphous protein aggregation as again performed using MG132 in cells stably expressing Flag-V2R-GFP. Flag-V2R-GFP was used for this experiment because it was the best internalizing receptor in the previous experiments. Thereafter, cells were stimulated with 100 nM of AVP. The receptor membrane expression level was analyzed before and after ligand treatment using flow cytometry. The treatment with MG132 did not affect the membrane level of the receptor
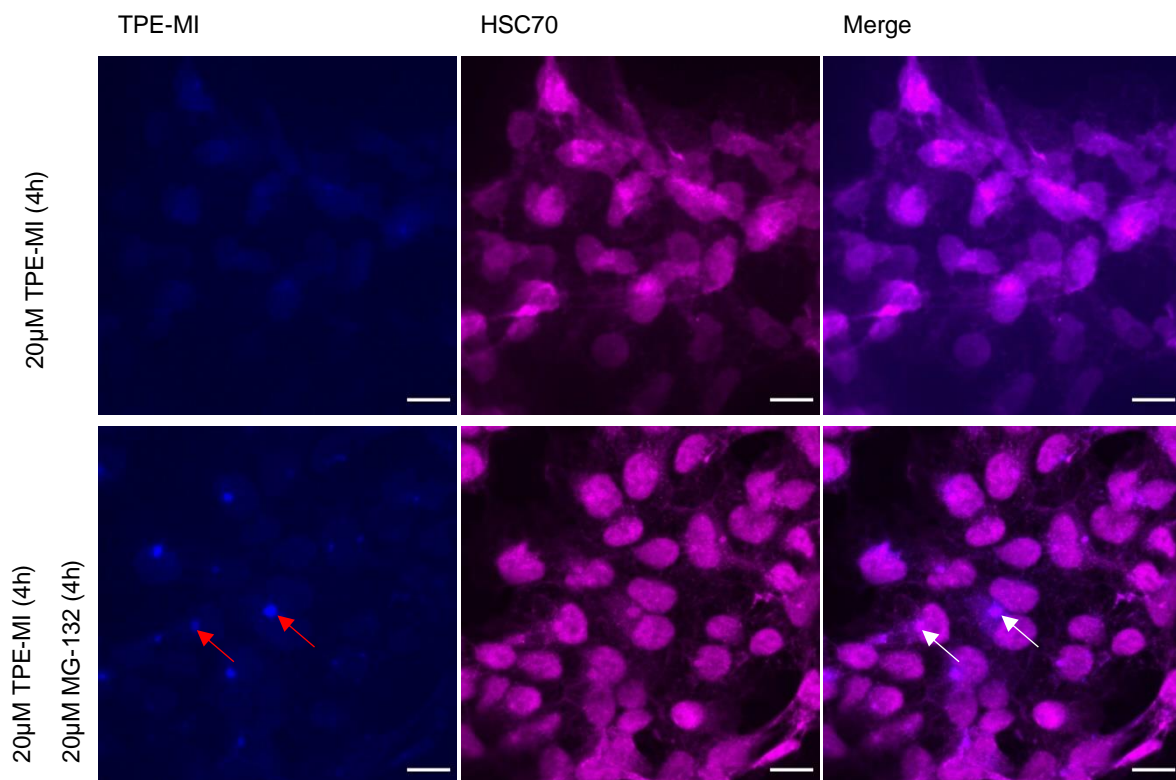
Figure 14: Recruitment of HSC70 by amorphous aggregates measured by immunofluorescence and CLSM. Formation of amorphous aggregates was induced by a 4 h MG132 treatment. Cells were labeled with the amorphous aggregate indicator TPE-MI, fixed and labeled with anti-HS70 antibodies. Fluorescence of TPE-MI was visualized (left panel, blue) demonstrating the formation of amorphous aggregates under these conditions (lower left panel, red arrows). HSC70 was visualized using rabbit anti-HSC70 antibodies and CY3-conjugated goat anti-rabbit antibodies (central panel, purple). Under these conditions HSC70 seems to be partially recruited to the nuclei but remains also cytosolic. Only an incomplete co-localization with aggregates was visible in the overlay (right panel, white arrows). Pictures show xy scans of representative cells of three independent experiments. Scale bar = 20 μm.

before activation. Similarly, CME efficiency did not differ significantly in MG132 treated or non-treated cells (Figure 15). These results indicate that amorphous aggregates do not have the same effect on CME inhibition of the V2R and most likely other GPCRs as amyloid aggregates.
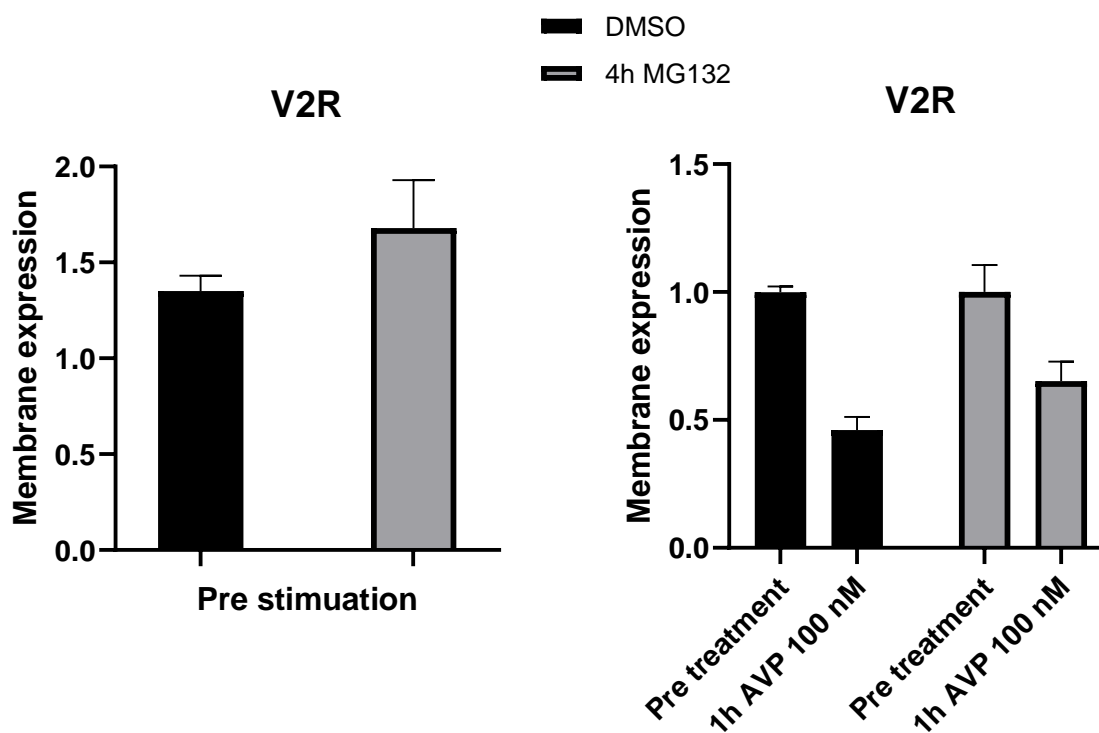
Figure 15: Ligand-induced CME of FLAG-V2R-GFP in the presence of amorphous aggregates.
Stably transfected HEK293 cells were pre-treated with MG132 or solvent and cells were stimulated with 100 nM of AVP. The expression level of the receptor in the membrane was analyzed before and after 1 hour AVP treatment by flow cytometry measurements. Columns represent mean values ±SD of two experiments in triplicates.

6. Influence of the activation of CRF1R and V2R on the aggregation of HttExon1Q74

It could be shown here that HttExon1Q74 amyloid aggregates inhibit ligand-induced internalization of GPCRs. Another question is whether GPCR activation has in turn also an influence on aggregate formation. Using PulSa experiments, also this question was addressed. To this end, stably transfected HEK293 cells expressing either Flag-CRF1R-GFP or Flag-V2R-GFP were used and co-transfected transiently with mCherry-HttExon1Q74. 72h after transfection, a PulSa measurement of the ratio of cells containing an aggregate was performed. Cells expressing Flag-CRF1R-GFP were treated using sauvagine (100nM) and AVP was used to treat cells expressing Flag-V2R-GFP. Treatment was as follows: One sample was treated 48h prior measurement, a second sample was treated 28h prior measure and a third one was treated at both time

points. Cells were then suspended and loaded into an LSRFortessa flow cytometer to perform PulSa analysis as previously described.

The proportion of cells expressing HttExon1Q74 aggregates was indeed found to be increased by activation of either receptor. This increase was larger for cells expressing Flag-V2R-GFP (maximum of ~3-fold increase) than for cells expressing Flag-CRF1R-GFP (maximum of ~1.7-fold increase) (Fig. 16.)

In addition, the time of stimulation has an influence on the aggregation rate. The percentage of cells containing aggregates was higher in the sample stimulated 48h before quantification than in the sample stimulated 28h prior measurement. There was only a small additive effect in the increase of aggregation when stimulating the cells twice at 28h and 48h before quantification.

Both the V2R and the CRF1R are activating adenylate cyclase which causes a production of cAMP from the hydrolysis of ATP. Previous studies showed that GPCR-mediated concentration of cAMP influences the survival of HttExon1Q97 expressing cells as well as the proportion of cells containing an aggregate. The activation of the cannabinoid B1 receptor causes an inhibition of adenylate cyclase and was found to provide a small increase in cell survival. On the other hand, artificial increase of cAMP concentrations using small molecules promoted cell death (152). Taken together, these data and the results mentioned above indicate that increased cAMP levels promote aggregate formation.

It was already described in this work that differences in the aggregation ratios in samples depending on the GPCR co-expressed with HttExon1Q74 (Fig. 9 A) could be quantified. Assuming that the aggregation of HttExon1Q74 can be modulated by cellular cAMP concentration, it may be speculated that these differences could be due to a basal G_s activity of these receptors.
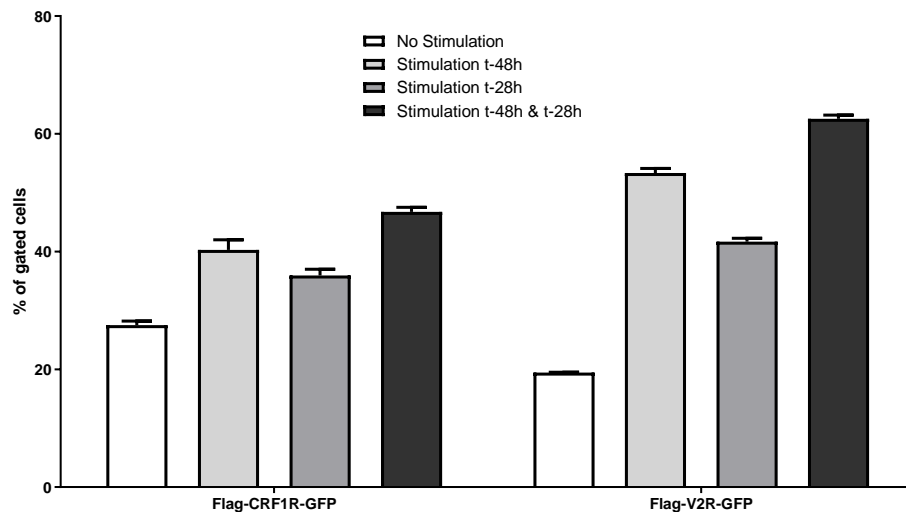
Figure 16: Aggregation of mCherry-HttExon1Q74 following Flag-CRF1R-GFP and Flag-V2R-GFP activation at multiple time points. HEK293 cells were stably expressing Flag-CRF1R-GFP or Flag-V2R-GFP were co-transfected with mCherry-HttExon1Q74 72h prior PulSa analysis. Samples were stimulated either 28h, 48h or 48h and 28h prior analyzing the percentage of cells containing HttExon1Q74 aggregates using PulSa. Cells expressing Flag-CRF1R-GFP were stimulated using Sauvagine (100 nM) and cells expressing Flag-V2R-GFP were stimulated using AVP (100 nM). Data points show mean values of a representative experiment performed in duplicates±SD.

7. The presence of mCherry-HttExon1Q74 increases the membrane expression of SERT.

GPCRs are not the only pharmacologically relevant membrane proteins for which a decrease in CME would have a major impact on their function. Another prominent example is SERT. SERT has been found to be constitutively endocytosed and targeted to lysosomes strongly suggesting that it uses a clathrin-dependent pathway (88), although this has not been addressed formally. Thus, analysis of whether SERT internalization may be influenced in the presence of HttExon1Q74 was investigated. If such effects could be detected, two conclusions may be drawn. First, this would indicate that CME disruption influences SERT membrane expression and that therefore the constitutive internalization of SERT is a clathrin-dependent process. Second, this could be a hint to explain why in early stages of Huntington's disease depressive episodes occur frequently: amyloid aggregates would increase the number of SERT molecules at the plasma membrane and increase the presynaptic re-uptake of serotonin. The synaptic serotonin pool should thereby be depleted which is associated with depression.

In order to study the influence of mCherry-HttExon1Q74 aggregation on the membrane level of SERT, a PulSA analysis was used to analyze the membrane level of SERT in cells with or without aggregates. Because both the C and N terminus of SERT are

intracellular, the previously described functional chimeric protein Flag-Tac-SERT was used in order to have an extracellular epitope for the following experiments (88, 153). This chimera contains the interleukin 2 receptor, α subunit (Tac) fused to the N terminus of SERT and an N-terminal Flag epitope fused to the extracellular domain of Tac (Fig. 17 A). Three days after transient co-transfection of HEK293 cells with Flag-Tac-SERT and either mCherry-HttExon1Q23 or mCherry-HttExon1Q74, cells were suspended and membrane-bound Flag-Tac-SERT was labelled with mouse anti-Flag M2 and anti-mouse Alexa647 antibodies. A PulSA analysis was performed and the florescence level of Alexa647 was compared for cells expressing mCherry-HttExon1Q23, and soluble or aggregated mCherry-HttExon1Q74. The results of this experiment indicate that the membrane expression level of SERT is increased 2-fold in cells expressing aggregates of mCherry-HttExon1Q74 in comparison to cells from the same sample expressing still soluble mCherry-HttExon1Q74. Surface expression of SERT was comparable upon co-expression of either soluble mCherry-HttExon1Q74 or the control construct mCherry-HttExon1Q23 (Figure 17 B).

These results show that the formation of an HTT amyloid can indeed cause an increase of the membrane level of SERT. This it at least consistent with the frequent occurrence of depressive episodes in prodromal states of Huntington's disease. Moreover, these data indicate that the already described constitutive internalization of SERT (153) seems to be clathrin dependent. It would be interesting to see whether the increased number of SERT molecules in the plasma membrane upon the presence of aggregates is indeed associated with an increased 5-HT uptake. To date, unfortunately, no single cell experiment allows the measure of 5-HT uptake. The effects of amyloids aggregates on constitutive SERT internalization were simulated using Pitstop 2. However, in contrast to ligand-induced internalization in the case of the CRF1R, this experiment was not successful since a much longer compound treatment is necessary to monitor constitutive internalization. Cells did not survive a 12 h Pitstop 2 incubation period due to the toxicity of the substance.

To overcome this experimental obstacle in the future, other amyloid aggregate forming proteins were studied, too, in order to find an aggregate/cell system which is more homogenous or where at least most of the cells contain aggregates.

A

B
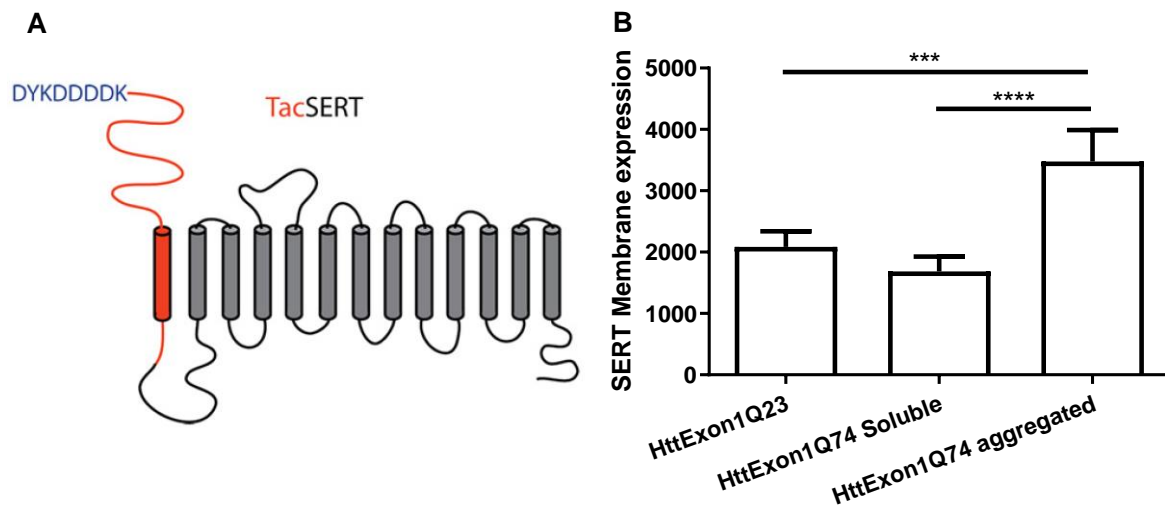
Figure 17: Membrane expression level of Flag-Tac-SERT in the presence of mCherry-HttExon1Q23 and soluble or aggregated mCherry-HttExon1Q74 measured with PulSa. **(A)** topology diagram of Flag-Tac-SERT, a chimeric protein of the interleukin 2 receptor subunit (Tac) fused to the N terminus of SERT. An N-terminal FLAG epitope was added to the extracellular domain of Tac. **(B)** PulSa analysis. HEK 293 cells were transiently co-transfected with Flag-Tac-SERT and mCherry-HttExon1Q23 or mCherry-HttExon1Q74 and incubated for 72h. Cells were labeled with mouse anti-Flag M2 and Goat anti-mouse Alexa647 antibodies and analysed by flow cytometry. The cells expressing mCherry fluorescence were gated and a PulSa analysis was used to separate cells expressing mCherry-HttExon1Q74 in its soluble or aggregated form. The fluorescence of the Alexa 647 antibody was used in each case to quantify plasma membrane expression of Flag-Tac-SERT. The Flag-Tac-SERT membrane expression level in the presence of mCherry-HttExon1Q23 and soluble mCherry-HttExon1Q74 was not significantly different. However, the cell population containing aggregated mCherry-HttExon1Q74 showed a significantly higher membrane expression of Flag-Tac-SERT. p value < 0,05 were significant (*), p value < 0,01 (**), p value < 0,001 (***) and p value < 0,0001 (****) were considered very significant.

8. Fluorescence microscopy does not allow the detection aggregates of α-Syn-mCherry or its mutants.

In an effort to expand on this study, CLSM was used to investigate the expression and cellular distribution of α-Syn and its mutants containing point mutations linked to familial form of PD. To assess for the suitability of α-Syn, HEK293 cells stably expressing Flag-CRF1R-GFP were transiently co-transfected with α-Syn-mCherry. Point mutations were induced in order to obtain the previously described PD linked mutants, E53T (124, 126), E46K (122) and E46KΔG (126). In previous studies, it has been shown that no aggregate of GFP tagged wild type α-Syn and its mutants could be detected using direct excitation of the fluorescent tag (126) indicating that the GFP tag might prevent aggregation. In the same report, inclusion could be detected only using immunofluorescence. This technique is, however, incompatible with live cell measurement of signaling as cell fixation is required. mCherry tagged constructs of α-Syn and its mutants were used to look whether this fluorescence tag is better suited than GFP. mCherry was selected as it was a successfully used in the previous aggregation studies with HTT. As controls, mCherry alone and untransfected HEK293 cells were used. The distribution of α-Syn WT and

mutants looked very similar in comparison to the mCherry control (Fig. 18). In all cases, the fluorescence was distributed diffusely across the cytoplasm of the cells. In some cases, some brighter puncta could be detected in cells expressing mCherry as well as all α-Syn variations showing that they are not related to α-Syn expression (Fig. 18). No clear difference between cells expressing mCherry control and cells expressing the α-Syn fusion protein variants was observed. Most likely, the relatively large mCherry moiety prevents α-Syn aggregation. Surprisingly, inclusions were observed in the transmission channel of cells expressing the α-Syn mutants but not in untransfected cells (Supplemental fig. 2). The frequency of inclusions even if a lot higher in α-Syn samples, was also significantly higher than the untransfected control (Supplemental fig. 3), therefore these inclusions were considered to be mCherry artefacts.

In summary, these results demonstrate that mCherry is not suitable to monitor α-Syn aggregation similar to what was shown for GFP fusions before by the other groups (see above).

9. Investigation in whether SOD1 could be used in this model

ALS is a neurodegenerative disease that is characterized by the formation of amyloid aggregates. The sporadic form of the disease represents 90% and in most of these cases the major component of these aggregates is the DNA interacting protein TDP43. The remaining 10% of ALS cases are familial and 20% of these are caused by mutations of SOD1. To address the question whether SOD1 and its mutants is better suited to get homogenous cell populations possessing aggregates, the wild type form of SOD1 as well as the A4V mutant of this protein was C-terminally tagged with mCherry (constructs SOD1-mCherry and SOD1A4V-mCherry, respectively).

9.1. mCherry is not suited to study SOD1 aggregation.

The next question to be addressed was whether cells expressing SOD1 aggregates are more suitable in terms of a homogeneous cell population. To this end, HEK293 cells were incubated for three days following transfection with SOD1-mCherry or SOD1A4V-mCherry. However, these investigations clearly showed that the subcellular distribution of neither SOD1-mCherry nor SOD1A4V-mCherry was different from that of the mCherry control alone (Fig. 19). These results imply that mCherry might prevent aggregation of SOD variants, similar to what was described for α-Syn (see above). An increase in solubility of the fusion partner specifically by mCherry has been already described by others (154). In addition, GFP-tagged SOD1A4V was shown to aggregate spontaneously

(11). Taking the latter publication into account, the analysis was also performed with GFP-tagged SOD variants.
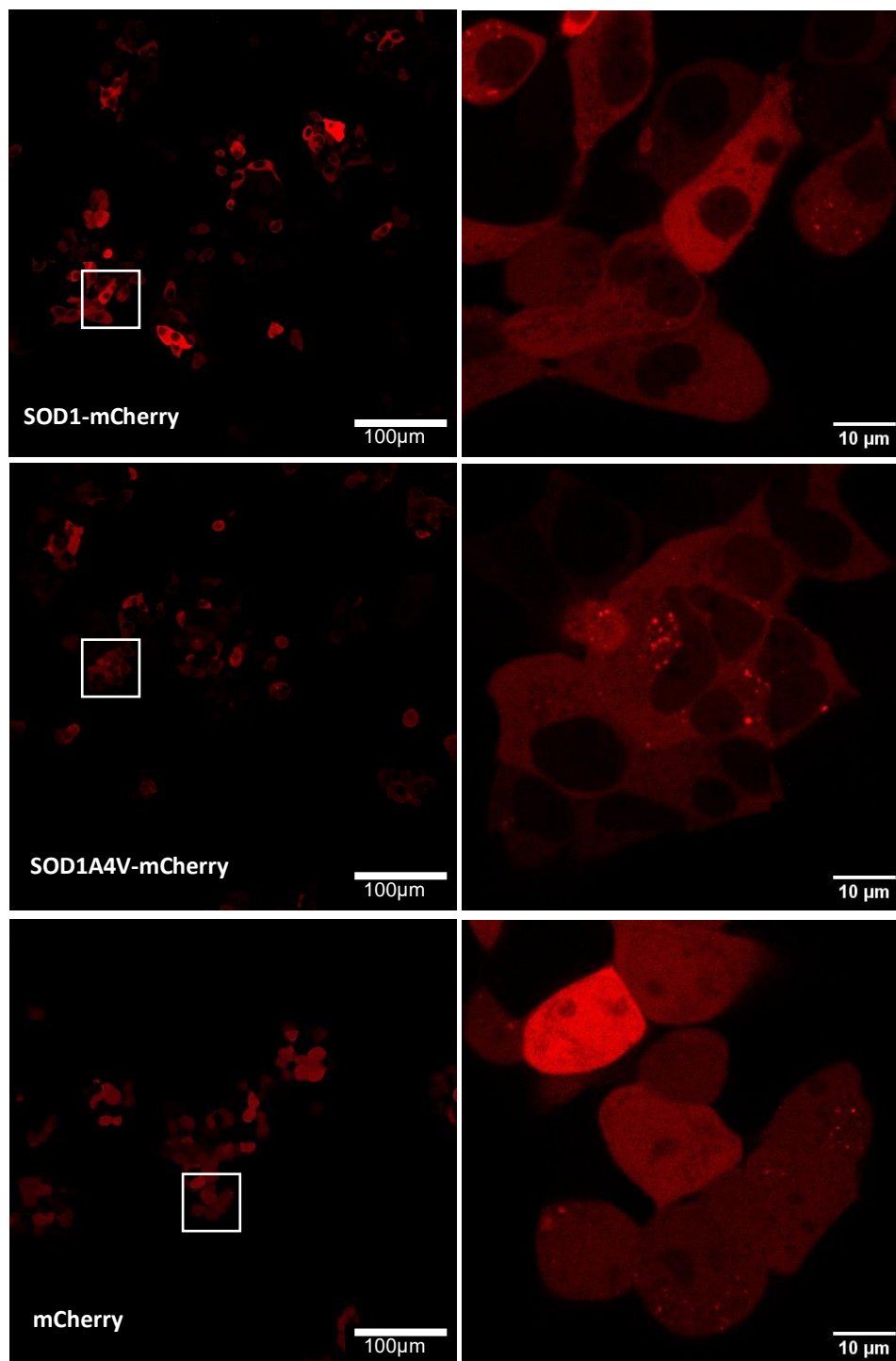
Figure 18: Subcellular distribution of mCherry-tagged SOD1 variants HEK 293 cells were transiently transfected with SOD1-mCherry, SOD1A4V-mcherry and mCherry alone. Images were taken 3 days after transfection. On the left panel, overview scans are shown. Details are shown on the right panel. No significant difference could be detected between the three different conditions. Pictures show xy scans of representative cells of three independent experiments. Scale bar = 10 µm.

9.2. GFP may be suited to study SOD1 aggregation

HEK293 cells were incubated for three days following transfection with SOD1-GFP or SOD1A4V-GFP. Cells were analyzed using CLSM to monitor if cells form amyloid aggregates and represent a homogeneous cell population (Fig. 20).
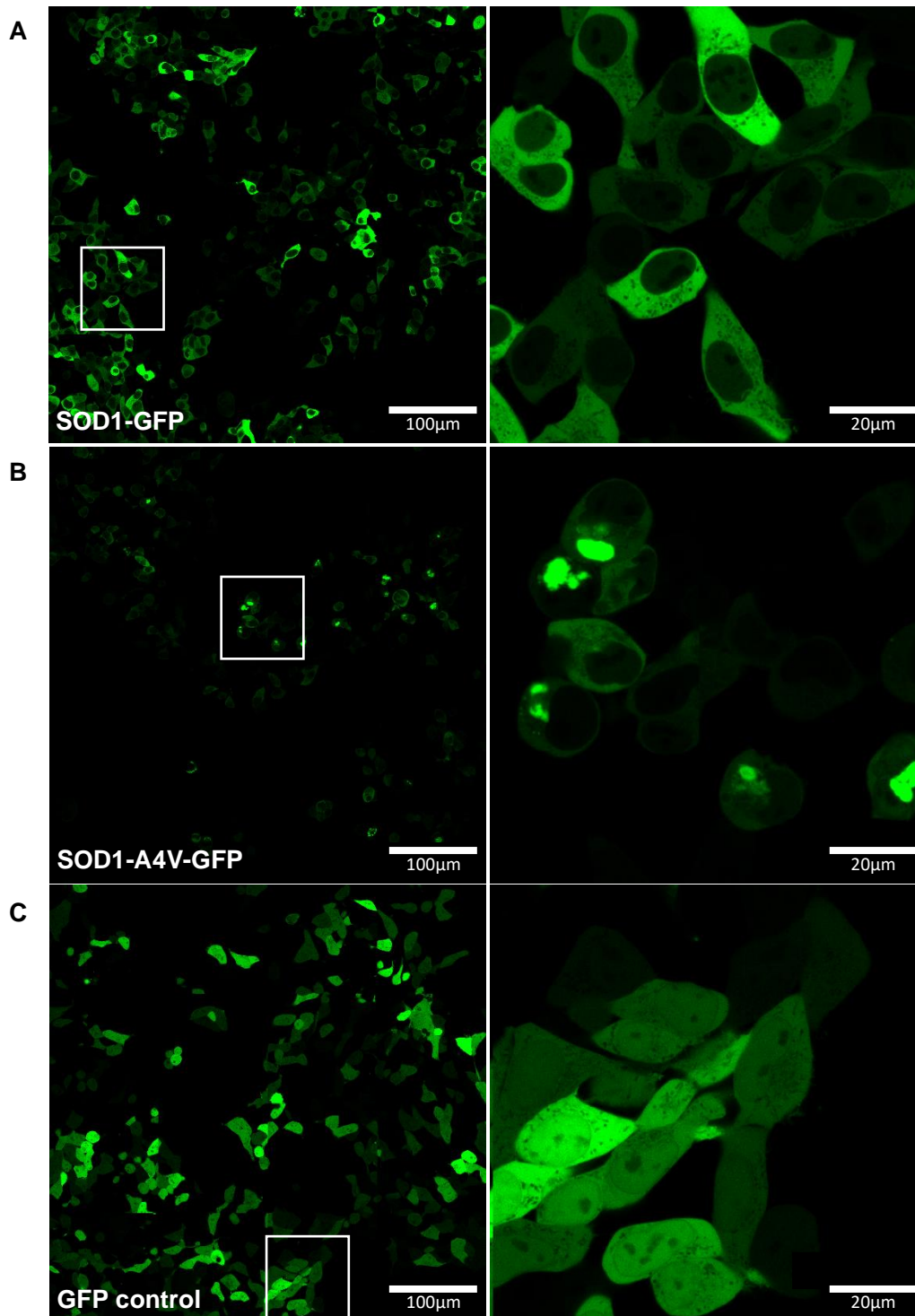
Figure 19. Subcellular distribution of GFP-tagged SOD1 variants. HEK 293 cells were transiently transfected with SOD1-GFP, SOD1A4V-GFP and GFP alone. Images were taken 3 days after transfection. On the left panel, overview scans are shown. Details (selected ROIs) are shown on the right panel. Only in the case of the SOD1A4V-GFP mutant, putative aggregates could be detected in 13.5% of the cells expressing GFP fluorescence. Pictures show xy scans of representative cells of three independent experiments.

In all cells expressing GFP alone, a diffuse green fluorescence was observed throughout the cytoplasm and nucleus (Figure 19C; it has been shown previously, that GFP may shuttle between the nucleus and the cytoplasm (155)). In all cells expressing WT SOD1-GFP variants, a diffuse fluorescence was observed in the cytoplasm confirming that WT SOD1 does not aggregate (Fig. 20 A). In some cells transfected with mutant SOD1A4V-GFP, large fluorescent puncta were observed in the cytosol which most likely represent the amyloid aggregates. To quantify how many cells of the heterogeneous cell population possess these aggregates, 4 independent experiments were performed and >150 cells expressing SOD1A4V-GFP were counted each time. 13.7 % (SD = 1.9) of the cells were found to show these distinct fluorescent inclusions.

Next, PulSa experiments using the same cells were performed. The resulting dot plots of SOD1-GFP and SOD1A4V-GFP showed obvious differences. As with mCherry-HttExon1Q74, a second group of cells with a smaller width is present in the sample expressing the aggregating SOD1A4V-GFP which was not visible in the sample of SOD1-GFP (Fig. 21). The fluorescence of soluble SOD1A4V-GFP is lower than the fluorescence of SOD1-GFP, suggesting that the aggregation of SOD1A4V is concentration dependent. Above a defined concentration threshold, the protein starts to aggregate (Fig. 21) and can thus not be present at a higher level of fluorescence in this group. More importantly, cells expressing aggregated and soluble SOD1A4V-GFP are not as well separated as were the cells expressing mCherry-HttExon1Q74 (see Figure 8. C). Using the PulSa technique, the amount of cells with SOD1A4V-GFP aggregates (4.96% (SD=0.60) was less in comparison to CLSM quantifications (13.7% (SD=1.9)).

In summary, PulSA measurement of SOD1-GFP and SOD1A4V-GFP yielded a less reliable discrimination between soluble and aggregated protein expressions than HTT and no real improvement in the homogeneity of the samples was observed. These results show that GFP-tagged SOD1 does unfortunately not represent a real progress in comparison to mCherry-tagged HTT.
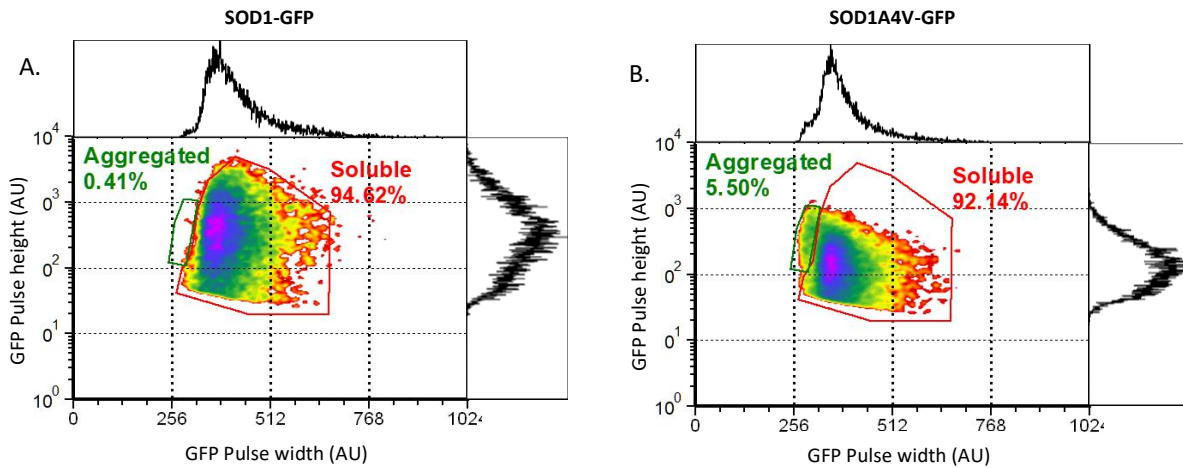
Figure 20. PulSa analysis of the aggregation of SOD1A4V-GFP. HEK293 cells were transfected with SOD1-GFP and SOD1A4V-GFP 3 days before the analysis. PulSa analysis shows that the fluorescence height of SOD1-GFP (A.) is higher than that of SOD1A4V (B.). A second group of cells can be detected in the height versus width density plot of SOD1A4V-GFP which was not present in the SOD1-GFP analysis. However, this group is very close to the main group of cells rendering the discrimination between cells containing aggregated or soluble proteins unreliable.

III. Discussion

1. Background

As the world population is getting older especially in developed countries, ageing has become the focus of many studies. Cellular ageing can be related to multiple changes, one of them is the formation of protein aggregates. Preventing the formation of these aggregates is an important task as their formation is associated with many diseases (156–160). Of these aggregates, one type plays a major role for most of the age-related diseases the so-called amyloid aggregates which are formed of one specific type of protein that becomes insoluble and forms highly stable and toxic cross-β structures. These amyloid aggregates are found in many neurodegenerative diseases (5, 6) such as Huntington's disease (HD) (7), Alzheimer's disease (8), Parkinson's disease (8) and amyotrophic lateral sclerosis (ALS) (9, 10). The symptoms of these diseases as well as their comorbidities are highly variable, which is often incompletely understood. This suggests that the significance of amyloid aggregates is not solely related to their cell cytotoxicity, they may also influence cellular signal transduction in particular in the beginning of the diseases or even when the amyloid-forming proteins are still soluble. To get a deeper insight into these early processes was the main inspiration for this study. Among the mentioned comorbidities, neuropsychiatric syndromes and in particular episodes of major depression have been found to be associated with the onset of diseases and often precede the development of neurodegenerative symptoms (16, 19, 23, 24, 129, 161, 162).

HSC70 is the main constitutively expressed heat shock protein. It has a critical role in protein homeostasis and performs housekeeping functions by ensuring proper protein folding. Using ATP and associated J proteins (163), HSC70 targets damaged proteins to their respective degradation processes (164). Neurodegenerative diseases are strongly associated with HSC70 functions and neuronal HSC70 expression levels are correlated to the frequency of Parkinson's disease and Alzheimer's disease cellular markers in animal models (165). It has been shown that HSC70 plays a major role in CME as it is responsible for the clathrin lattice disassembly allowing to maintain the pool of free clathrin and thereby CME (90, 166–170). It has been shown for multiple amyloids that the aggregates can recruit HSC70 to such an extent that it leads to a depletion of the cytoplasmic HSC70 pool which consequently impairs CME (11).

The interest and motivation for this work was to find out whether the presence of amyloid aggregates also affects the functions of membrane proteins involved in signal transduction, in particular of those which are thought to be involved in depression. GPCR regulation relies on CME, therefore suggesting that amyloid aggregates could influence GPCR trafficking and as a consequence also signal transduction. GPCRs are involved in the development of depressive disorders e.g. in the serotonergic system, the hypothalamic pituitary adrenal (HPA) stress axis and the endocannabinoid system (17, 171, 172).

Another aim was to study the influence of amyloid aggregates on the trafficking of the structurally unrelated SERT protein as it has the largest influence on serotonin signaling by enabling the presynaptic transport of this neurotransmitter. More than 70 pharmaceutical drugs are known to improve depressive symptoms by targeting this transporter and by increasing serotonin concentrations in the synaptic cleft. A huge amount of research has been made to explain how both GPCRs and SERT function. Surprisingly, virtually no study has been focused on investigating the effect of amyloid aggregates on either GPCR or SERT function. Finally, it was also addressed whether effects are only observed when amyloid aggregates are present or whether a first influence may be observed when amyloid-forming proteins are still soluble.

To date, no description of the effect of CME defects on GPRCs nor SERT have been proposed (14, 173, 174).

As the focus on GPCRs and amyloid aggregates was novel, many technical limitations had to be overcome. Most importantly, only a minority of the cells expressing an aggregation-prone protein do indeed form amyloid aggregates at a reasonable time point in cell culture. While most studies of the signaling of GPCRs and SERT are performed at a sample level, tools enabling single cell signaling measurements in mixed cell populations are lacking and had to be established here. Additionally, the study of amyloid aggregates has been focused on their formation and degradation as well as identifying interaction partners. The tools and techniques to study amyloid aggregates are thus heavily relying on immunofluorescence or *in-vitro* measurements both of which are incompatible with live cell studies required here. As a result of all these experimental obstacles, only a very limited number of GPCRs and amyloid aggregates could be studied here. Taking the huge GPCR protein family and the growing number of proteins which may form amyloid aggregates into account, conclusions of this work should not be

generalized at this stage of the study. In the next sections, the results of this work will be discussed and placed in the context of the current knowledge and literature.

2. Detection of amyloid aggregates

In the beginning, the focus was on establishing a set of tools and techniques enabling detection of amyloid aggregates in a reliable and efficient manner. To this end, multiple microscopical techniques were used such as CLSM, FRAP and immuno-fluorescence as well as a special type of flow cytometry analysis, namely PulSa.

2.1. Huntingtin protein

The first protein which was analyzed was Huntingin, the aggregation of which causes Huntington's Disease. HD is an incurable genetic dominant neurodegenerative disorder (20–22). The neuropathology of HD is characterized by neuronal death because of huntingtin aggregation. It has been shown that the truncated first exon of huntingtin contains a poly glutamine stretch and that sequences exceeding a critical 35~37 repetition threshold initiate the formation of aggregates (175, 176). Therefore, aggregating HttExon1Q74 and the non-aggregating HttExonQ23 constructs were used for the experiments.

The first approach was to simply express the protein in HEK293 cells and observe the cellular distribution of the N-terminally mCherry tagged HttExon1Q74 and HttExon1Q23 (EXP Figure 1A & B). For mCherry-HttExon1Q74, two distinct expression forms could be detected. Either cells were expressing mCherry fluorescence in a diffuse, cytoplasmic pattern or cells contained inclusion body-like structures. In cells expressing mCherry-HttExon1Q23, the fluorescence was instead exclusively found in the cytosol. FRAP analyses confirmed that the inclusion bodies were formed by insoluble mCherry-HttExon1Q74 (Figure 1C). Two conclusions could thus be drawn: First, mCherry tags are suitable to monitor aggregation of HttExon1Q74 like the previously described GFP tags. This is an important conclusion since aggregation of other amyloid-forming proteins may be prevented by mCherry (see below). The second conclusion is that the mCherry-HttExon1Q74 remains soluble in most cells and only a minor part indeed develops amyloid aggregates. This meant that the following study of mCherry-HttExon1Q74 was limited to single cells experiments. Attempts to increase the amount of cell containing aggregates (e.g. by inhibiting proteasomal degradation or by heat shock) are of doubtful advantage since other processes influencing signal transduction may be affected.

In order to increase the amount of cells that can be processed in an experiment as well as a way to increase reproducibility of the results, a flow cytometry analysis named PulSa (137, 138) was used. During these PulSA studies, it could be shown receptor expression can have an influence on the percentage of cells containing an aggregate (Fig. 9 A). This can be due to the different basal activities of these receptors. Indeed, it has been shown that modulation of cAMP levels directly activates the CRE promoter and CREB ablation resulting in Huntington-like phenotypes in mice (177). Furthermore, previous research demonstrated that the G_i-coupled Cannabinoid Receptor B1 has a cell death protective effect in huntingtin models and that HTT aggregation is promoted by an elevation of cAMP concentrations (18, 152). Consistent with these studies, experiments in this work also indicated that activation of the G_s-coupled V2R and CRF1R induce an increase in mCherry-HttExon1Q74 aggregation (Fig. 16). Whether or not second messenger levels have an influence on the number of cells expressing amyloid aggregates was not investigated in more detail here since the influence of amyloid aggregates on GPCR trafficking and signal transduction was in the focus of this study.

2.2. α-Synuclein

In order to get a broader view of the effects of amyloid aggregates, it was also intended to use α-Syn as a model. α-Syn is associated with Parkinson's disease which affects about one percent of the population above 60 years of age (178). Three C-terminally mCherry-tagged point mutations associated with familial forms of Parkinson's disease were used here: E53T (124, 126), E46K (122) and E46KΔG (126). The choice to use mCherry was motivated by previous studies showing that the GFP tag was unsuitable for the detection of α-Syn aggregation (124). It was argued that GFP may prevent α-Syn aggregation or be cleaved-off proteolytically thereby leading also to cytosolic fluorescence (124). The latter case was supported by the fact that Lewy bodies could be observed using immunofluorescence with antibodies recognizing α-Syn itself in this study (124). As immunofluorescence requires fixation, this approach was not suitable to study protein trafficking or signaling which requires live cells. It was therefore attempted here to replace GFP by mCherry in the case of α-Syn since mCherry was successful in the study of HTT aggregation (see above).

Only soluble mCherry fluorescence signals could be detected in these experiments for all α-Syn constructs similar to what was previously described for the GFP-tagged variants. Considering the previous literature indicating that α-Syn aggregates have most

likely only been formed following cleavage of the GFP tag, it was suspected that the same could have happened here with mCherry, making aggregates invisible using fluorescence microscopy. Indeed, putative aggregates could be observed using transmission microscopy, but also in the case of the mCherry protein alone indicating that these structures are not α-Syn related (Supplemental Fig. 2 & 3). In any case, these data show that mCherry tags are not suitable to study α-Syn aggregation in live cells.

2.3. SOD1

Since the attempt with α-Syn aggregates was not successful, it was tried to detect another protein for which aggregation was proven to cause a breakdown of CME, namely a mutant of SOD1 (11). Mutations of this gene are responsible for about 20% of the familial forms of ALS. Amyotrophic lateral sclerosis is a neurodegenerative disease characterized by stiff muscle, muscle twitching and a progressive loss of muscle mass due to the loss of motor neurons in the brain and the spinal cord. No cure is available and the average survival expectancy is from two to three years with only 10% of patients surviving more than 10 years (131). Similar to the previously mentioned neurodegenerative diseases, ALS is associated with a high prevalence of depression (129). The main marker of ALS is the presence of inclusion bodies in motor neurons. In most cases of ALS, these amyloid aggregates are composed of the DNA binding TDP-43 protein. Familial forms (5-15% of ALS cases) (179–181) are caused by mutations in TDP-43 or in various other genes. Interestingly, most of these mutations are not located in the gene of TDP-43. Among these are mutations of the genes encoding for C9orf72 (40%), SOD1 (20%), FUS (1-5%) and TARBDP (1-5%) (130). In the case of SOD1 and FUS mutations, the aggregating protein is not TDP-43 but SOD1 and FUS themselves. About 150 mutants of the SOD1 protein have been identified so far. In this study, the SOD1A4V mutant was used which was described in the previous study addressing the influence of amyloid aggregation on CME (11). The mutant is associated with most cases of familial ALS in the USA (182).

To keep the conditions in comparison to HttExon1Q74 as consistent as possible, mCherry-tagged SOD1A4V and wild type SOD1 were used in this study. However, similar to what was seen for α-Syn (see above), mCherry most likely prevented aggregation of the proteins (Fig. 19). The fact that SOD mutant solubility may be influenced by fused fluorescent tags have already been reported in the case of the SOD1G93A mutant fused with GFP; here the mutant protein loses its fibrillation ability

(136). When using a GFP tag here with mutant SOD1A4V, CLSM analyses revealed that approximately 14% of cells expressing the SOD1A4V-GFP mutant contained an aggregate, which was in the range of what was detected before for mCherry-HttExon1Q74. Unfortunately, when performing PulSa measurements, the discrimination between cells expressing an aggregate and cells expressing the soluble form of SOD1A4V-GFP was not as good as with mCherry-HttExon1Q74 (Fig. 9 & 21). The PulSa technique detected only 7% of cells with aggregates which was half of that found in the CLSM study. This may be caused by the higher fluorescence background of SOD1A4V-GFP in comparison to mCherry-HttExon1Q74, which could provoke a higher size-shifted W parameter measured in PulSa. This in turn could lead to a less efficient group separation of cells.

In summary, neither mCherry nor GFP-tagged SOD1A4V brought an improvement in sample homogeneity or detectability of amyloid aggregates. The same was true for mCherry tagged α-Syn mutants (see above). Only construct mCherry-HttExon1Q74 yielded promising results and was thus used throughout the rest of this study as a model for amyloid aggregates.

3. mCherry-HttExon1Q74 amyloid aggregate lead to HSC70 sequestration

It was first analyzed whether mCherry-HttExon1Q74 aggregates recruit HSC70 in a similar manner as described for other amyloid aggregate constructs in a previous study (11). Using immuno-fluorescence, it could be shown that HSC70 is indeed almost completely recruited by mCherry-HttExon1Q74 aggregates (Fig. 6) in HEK293 cells. The soluble form of mCherry-HttExon1Q74 as well as the control construct HttExon1Q23 did not show such a HSC70 recruitment.

It is important to make a distinction between amorphous aggregates and amyloid aggregates. As it was not clear whether amorphous aggregates have a similar effect on HSC70 recruitment and CME as amyloid aggregates, we decided to address also this question. To this end, the small molecule proteasome inhibitor MG132 was used to trigger the formation of amorphous aggregates (124, 150). To detect aggregate formation, the newly discovered TPE-MI substance was utilized (140, 183), which is a molecular tool that becomes fluorescent by covalent binding to free thiol groups. Such groups are usually buried in correctly folded protein but become exposed upon protein misfolding. Following disulfide bond formation, the fluorescence of this molecule becomes activated (184). These experiments in HEK293 cells revealed that amorphous

aggregates could only partially recruit HSC70 (Fig 14). After MG132 treatment for 4h, the localization of HSC70 became mainly in the nucleus, as described in previous works (185), and a minor fraction remained in the cytoplasm.

In summary, HttExon1Q74 aggregates caused indeed an almost complete recruitment of HSC70 as previously reported in the literature. Amorphous aggregates, however, only partially sequestered HSC70, leaving a significant fraction of HSC70 both in the cytoplasm and nucleus.

4. HTT amyloid aggregate effects on GPCR trafficking and signaling

After establishing that the HTT amyloid aggregates recruited HSC70 also under the conditions of our lab, the main scientific questions of this work have been addressed:

- Does the sequestration of HSC70 by the HTT aggregates also affect CME of such lowly expressed proteins as GPCRs?
- Do amyloid aggregates thereby affect signal transduction of the receptors?

The previous research used transferrin receptor and the AMPA receptor as models to study the CME breakdown (11). These proteins are, however, very different in comparison to GPCRs in multiple respects. First, GPCRs are very low expressed proteins compared to the AMPA and the transferrin receptor (46). Therefore, the remaining pool of HSC70 in the presence of HTT aggregates may be enough to maintain the internalization of GPRCs. Second, for both transferrin and the AMPA receptor, CME is part of the signaling and primary functions of these receptors (186–188). In contrast, GPCRs signaling is first carried out by G Protein activation while the CME is then part of the functional regulation of the receptors (14).

To study the influence of HTT amyloid aggregates on CME of GPCRs, the previously described PulSa technique was used (137, 138) and it could be demonstrated that the ligand-induced CME of all studied GPCRs was affected in the presence of mCherry-HttExon1Q74 aggregates. No such effect could be detected in the same sample in cells expressing soluble mCherry-HttExon1Q74 or in cells expressing the mCherry-HttExon1Q23 control. It is important to note that CME inhibition was incomplete. This suggests that despite HSC70 being recruited to the aggregates, a pool of free clathrin still allows the partial internalization of the activated GPCRs. Only when this pool is also depleted, the effects on CME should become more and more apparent. It was demonstrated by previous studies showing that the clathrin pool is not affected by the

presence of amyloid aggregates (11) as HTT amyloid aggregates with 82 glutamine residues (189) did not significantly recruit neither clathrin nor the adaptor protein complex AP-2. The controls showed that the internalization efficiency of GPCRs in cells expressing soluble HttExon1Q74 or soluble HttExon1Q23 is not different in comparison to cells expressing the receptor alone. It was also shown that the inhibition of CME is specific to amyloid aggregates since no such effect could be measured in the case of amorphous aggregates (Fig. 15).

Taking these results into account, a delayed effect of amyloid aggregate on GPCR signaling could be postulated. The activation of ligand naïve receptors should be possible without restrictions. However, following rounds of activation should be more and more impaired as receptor resensitization is prohibited due to CME inhibition. This should flood the membrane with desensitized GPCRs. This theory revealed to be true for the two studied receptors. When measuring calcium release after activation of the $G_{q/11}$ coupling V1AR, no significant difference could be measured in the case of ligand-naïve receptors (1st activation) for cells expressing either soluble or aggregated mCherry-HttExon1Q74 or mCherry-HttExon1Q23. After a resting period of 30 minutes, however, cells containing either HttExon1Q23 or soluble HttExon1Q74 could be activated again (2nd activation) while cells expressing aggregated HttExon1Q74 could not (Fig. 10 & 11).

In the case of G_s-coupled receptors, single cell experiments with a mixture of cells containing aggregates or not are challenging. However, the effect of aggregates on CME could be mimicked by treating the cells with the CME inhibitor pitstop 2 (Fig. 12)(147). Following stimulation of the Gs-coupled CRF1R in the presence of pitstop 2, an effect of over time cAMP in comparison to the control was not detectable within the first 15 min of the experiment (Fig. 13). Thereafter, cAMP accumulation continues in control samples while succumbing in pitstop 2-treated samples.

5. HTT amyloid aggregate effects on SERT

SERT is a protein having a central functional role in serotonergic neurotransmission. It also plays a central role in the treatment of depression and most of the available anti-depressant drugs target SERT (47, 52). The protein mediates 5-HT re-uptake following presynaptic release. Maintaining high concentration of 5-HT by affecting SERT activity was discovered to be an effective strategy in the treatment of depressive syndromes (47, 52, 54). The influence of neurodegenerative diseases on SERT has been established. α-Syn has been shown to directly interact with SERT and induce its internalization. In

Parkinson's disease, as a result of a decrease of α-Syn availability, SERT membrane expression is then increased. An increased SERT membrane expression decreases synaptic 5-HT and may consequently be one of the factors for developing PD-associated depression (23, 24).

SERT has been shown to be constitutively internalized (88), but the mechanism by which this protein is internalized remained unclear. As SERT is transported to lysosomes, it is however very likely that the transporter's endocytosis is clathrin-dependent (88). If this holds true, the membrane expression of SERT could be affected by the presence of amyloid aggregates. Since amyloid aggregates inhibit CME by HSC70 sequestration, SERT may accumulate in the plasma membrane under these conditions.

In order to test this hypothesis, a similar approach as with the measure of the influence of HTT aggregates on GPCR trafficking was used. The construct Flag-tac-SERT was used in this study. It represents a chimeric protein which was designed to provide an extracellular Flag epitope to facilitate trafficking studies of SERT (88, 153, 190). Upon co-expression of Flag-Tac-SERT and mCherry-HttExon1Q74, cells expressing aggregated or soluble HttExon1Q74 could be differentiated by PulSa and the membrane expression level of SERT could be determined. Amyloid aggregates indeed caused a significant increase of the membrane level of SERT (Fig. 17). Thus, its internalization is obviously clathrin dependent. The result that SERT plasma membrane expression increases upon the presence of amyloid aggregates may be a hint to explain the early onset of depressive episodes in Huntington's disease.

6. Future Experiments

6.1. α-Synuclein

α-Synuclein is associated with Parkinson's disease which is a very frequent neurodegenerative disorder. While α-Syn is found to be aggregated and its expression is elevated in PD, the factors triggering the disease as well as the mechanism remain unclear. It is therefore essential to get better insights in the effects of α-Syn to clarify etiology of the disease at the molecular level.

Late onset of PD has been linked to multiple mutations in three different genes, SNCA (encoding for α-Syn), LRRK2 and EIF4G1 (123). The genetic causes of PD revealed that SNCA gene duplication or triplication leading to an increase in α-Syn protein expression correlated with the onset of the disease (7th decade with two copies of SNCA, 4th decade with three) its progression and comorbidities (191–193). Loss of neurons and the

aggregation of α-Syn in Lewy bodies happens in the latest stage of the disease, namely the development of dementia with Lewy Bodies (DLB) (119).

Despite the high interest in studying the genetic sources of PD and the function of its mutants, familial forms of the the disease represent only 10% of the cases. The remaining 90% sporadic cases of idiopathic PD indicate that PD is a highly complex disorder and α-Syn holds a central role. PD onset has in this case mainly be linked to high concentration in regions where, in physiological condition, α-Syn concentration usually decreases with age (194–196).

In addition, neuronal death is not necessarily occurring in cells containing bigger Lewy bodies and it has been shown that most of the apoptotic cells even do not contain Lewy bodies at all (197, 198). Moreover, in PD, neurons in the subtantia nigra present dendritic abnormalities and biochemical changes that are not related to Lewy body presence (198, 199). This indicates that the toxicity of α-Syn is most probably due to the transformation of the native α-Syn into a prion-like structure. This hypothesis is further supported by the similarities of α-Syn with the characteristic prion protein cell to cell transmission and its highly dynamic structure allowing soluble to insoluble transitions. Finally, it also has seeding properties, in which the insoluble form of the protein induces the aggregation of soluble proteins (200). Histological studies of the dementia with Lewy Bodies stages showed that 90% or more of the aggregates are not located in the bigger somatic aggregates but in the form of very small deposits located in the presynaptic domain suggesting even more that the toxic effects of α-Syn are associated with synaptic dysfunctions (198, 199) where the CME plays an absolutely critical role (170, 201).

Live cells studies would bring an important insight into the toxic effect of small α-Syn aggregates. It would be of great interest to study the effects of these smaller structures on both GPRCs and SERT expression and function. However, this would require the development of new molecular tools allowing their detection in live cells.

6.2. GPCRs

Although this study provides first insights into the effects of amyloid aggregates on the trafficking and signaling of GPCRs, many questions remain unanswered. In order to fully validate the mechanism of the CME inhibition, it would be valuable to perform studies of clathrin distribution before and after stimulation in presence or absence of amyloid aggregates. Using this approach, it could be directly shown whether the pool of clathrin is indeed depleted and if the internalized vesicles are still coated with clathrin. It would

also be interesting to confirm the nature of the signaling inhibition by measuring the phosphorylation state as well as the β-arrestin recruitment of these GPRCs. It could be predicted, for example, that the number of desensitized and phosphorylated receptors in the plasma membrane increases over time.

It is important to consider that these signaling experiments were performed for only a few members of the very large GPCR protein family and only with recycling receptors (145). Because of the various desensitization/resensitization mechanisms involved in the regulation of GPCRs, it is impossible to generalize the results of this study for the GPCR family at the moment. A substantial amount of GPCRs are directed to the lysosomal degradation pathway following internalization rather than being recycled (202). Cell reactivity to the ligand on a second round of activation would then depend on novel receptor synthesis instead of recycling. In this case, receptor signaling may not be affected by the CME disruption. Of note, some of these non-recycling receptors behave in a different way. In the case of the V2R, for example, dissociation between the GPCR and the G protein complex does not happen after receptor activation and the signaling is intracellularly maintained until the complex is degraded by lysosomes (13, 45, 203). In combination with an inhibition of CME, this could eventually even lead to an abnormally sustained signaling. For some other GPCRs, the dephosphorylation necessary for receptor re-sensitization is a very fast process that takes place directly on the plasma membrane without the need for CME (204). It is conceivable that such receptors would not be affected dramatically by the presence of amyloid aggregates. These hypotheses would need to be confirmed with further experiments. Additionally, clarification on the regulation of the GPCRs in presence of amyloid aggregates could be further investigated. To fully confirm this model, investigation of the phosphorylation state of the receptors as well as the binding dynamics of β-arrestin to the receptors should have priority.

6.3. SERT

Concerning the study of the trafficking of SERT, it would be interesting to measure whether the amyloid aggregate-induced increase of membrane expression is connected to a difference in 5-HT uptake. To date, however, there is no 5-HT reporter allowing uptake experiments at a single cell level. Pitstop 2 was used to simulate the effect of amyloids on CME in this study. However, Pitstop 2 could not be used for the longer time period needed in this experiment because its general inhibition of CME is toxic for the cells. This raises the need for new techniques to be developed.

6.4. Technical developments

Taking the results of this study with the different fluorescent proteins and amyloid aggregates into account and to streamline the study of neurodegenerative diseases, it would be very interesting to perform a more general survey to identify which of the available fluorescent proteins is best suited to analyze the effects of these aggregates. Effects of the fluorescent fusion proteins on the aggregation efficiency have been measured in this study and also by several other groups (136, 154). Such effects are not surprising considering that the size of some amyloid forming proteins such as SOD1 or α-Syn (~15kDa) is small in comparison to the fluorescent fusion partners such as GFP or mCherry (~27kDa). It may also be possible in the future to avoid fluorescent protein fusions by using small molecule reporters of aggregation. TPE-MI is a first step towards this direction. However due to its dependence on free thiol groups, it is not suitable to monitor the aggregation of all aggregating proteins. For example, α-Syn does not contain cysteine residues. Alternatively, it has been shown that, fluorescence lifetime imaging microscopy could be used as a way to detect HTT and α-syn aggregation at a single cell level (205, 206). This technique exploits the fluorescent absorbing capabilities of amyloid aggregates reducing the fluorescence lifetime of a nearby fluorophore. This allows the detection of oligomers before the formation of inclusions. The use of this technique, however, requires specific hardware (high frequency pulsing LED laser, nanosecond range highly sensitive light sensor) (207) and is, of course, still dependent on fluororescent protein fusions.

The fact that the expression of amyloid forming proteins result in the production of heterogenous cell samples represent a major experimental obstacle. This limits the study mainly to single cell analysis. Strategies allowing to generate more homogenous samples would facilitate greatly the study of such effects. However, it is also very important to limit the stress for the cells which may cause unwanted effects influencing the results. Stress induction (oxidative stress, heat shock etc.) or temporary inhibition of proteasome of the autophagy would, for example, lead to multiple side effects such as an increased chaperones synthesis or the formation of amorphous aggregates.

Surprisingly, promising results in this direction were obtained when measuring the influence of activating G_s-coupled receptors on aggregate formation (Fig. 16). Upon stimulation of the receptors, the aggregation of mCherry-HttExon1Q74 was substantially increased. Previous studies also came to interesting and consistent conclusions for GPCR activation and amyloid formation. The activation of the cannabinoid receptor 1

(CB1), a G_i-coupled GPCR, provided a small protective effect on cell death induced by the aggregation of HttExon1Q97 (152). This protection could be reverted by increasing cAMP using pertussis toxin. More interestingly, both cAMP increase and activation of CB1 lead to an increase of the aggregation of construct HttExon1Q97. Therefore, artificially increasing the cytoplasmic cAMP concentrations using small molecules like forskolin, which directly activates adenylyl cyclase, might be a promising strategy to increase the aggregation of amyloid prone proteins without directly affecting proteostasis systems. All techniques facilitating soluble to aggregate transition would be very valuable tools in science.

Considering the proteins causing neurodegenerative diseases, it is particularly important to note that most studies with aggregating proteins were done with mutant proteins associated with the familial forms of diseases. Familial forms of diseases represent only a very small portion of all the cases (5-15% for ALS, 10% for PD). It should be stressed that proteins involved in the formation of amyloid aggregates can be different between sporadic and familial cases. For example, TDP43 is aggregating in sporadic ALS and either SOD1 or FUS are aggregating in most familial cases (130, 131). In addition, in PD, familial as well as early familial forms of the disease are associated with an increase in α-Syn (191–196) but point mutations increase the penetrance of the disease only at higher ages. Results obtained for the familial cases may thus not be representative for the more frequent sporadic forms of the individual diseases.

7. Conclusion

This study contributes to the understanding of the effects of amyloid aggregates on the CME and its consequences on trafficking and signaling of membrane proteins. It could also be the starting point to clarify the mechanisms underlying the psychiatric comorbidities which are associated primarily with the early stages of these diseases. It was shown here that the presence of aggregated mCherry-HttExon1Q74 causes an inhibition of the CME of GPCRs. Using two recycling receptors, it could be measured that the CME disruption leads to an accumulation of most likely desensitized receptors on the plasma membrane and consequently blocks GPCR signal transduction over time. It is important to note that the signaling inhibition could be measured only after a first successful round of stimulation. The internal controls used in this work allow the conclusion that this effect is specific to the formation of amyloid aggregates, at least in the case of HttExon1Q74 aggregates used here, as no effect on either the internalization or the signaling of soluble HttExon1Q74 present in the same sample could be measured. Moreover, amorphous aggregates do not have the

same effect as amyloid aggregates since their effect on HSC70 recruitment differed substantially.

These results are important not only for the field of neurodegenerative diseases but may also be used as an inspiration to gain treatment options in the future. Inhibition of GPCR CME could also be used as pharmaceutical strategy as it could induce a modulation of the receptor signal after a first round of activation. This could help in some cases where the first signal is needed but where a sustained signal is a problem such as in stress or inflammation. It has also been show in the past that GPCR CME inhibition could be used as a to fight cellular viral entry (147). Thus, disrupting CME of specific receptors could also be a valid antiviral strategy.

The study of the influence of amyloid aggregates on the constitutive internalization of SERT gave hints to answer some important questions. As the internalization of SERT was disturbed by the presence of amyloid aggregates, it is very likely that this process is clathrin dependent. In addition, as the membrane expression of SERT is increased in cells expressing aggregates of HttExon1Q74, it may be postulated that this CME inhibition could be one of the underlying mechanisms causing depression in the prodromal states of Huntington's disease.

Lessons can also be learned from the attempts to detect different types of amyloids using fluorescent proteins. A technique which is suitable for one amyloid aggregate may not be directly transferred to another type. Obviously, different fluorescent proteins have varying effects on the aggregation abilities of the aggregation prone proteins. It has been shown that mCherry for example can directly prevent protein aggregation due to its high solubility (154). This could also be shown for SOD1A4V-mCherry while the aggregation of SOD1A4V-GFP was still possible. GFP which was used in many studies of protein aggregates was not suited to study the aggregation of α-Syn and some mutants of SOD1 (126, 136). All these effects can easily be explained by the size difference between the amyloid-forming protein and the fluorescent proteins which are usually larger. In the future, the use of small fluorophores such as fluorescent activated β-barrels (14 kDa) (208) could be a way to avoid such effects. Small molecules allowing the detection of amyloid aggregates in live cells may also be a good solution.

Indirect effects of amyloid aggregates on the cell physiology may also be used as reporters. The measure of such known effects could be used to develop *in-vitro* assays and thereby novel screening assays in drug development.

IV. Materials and Methods

1. Chemicals and reagents

Standard chemical reagents that were used are listed in Tab. 1.

Tab. 1 Standard chemicals and reagents

Name	Company
Agar	Carl Roth
Agarose	Serva
Bacto Peptone	BD Difco
Calcium chloride	Carl Roth
CutSmart Buffer	NEB
Deoxynucleoside triphosphates (dNTP)	New England Biolabs
DNA loading dye (6×)	Thermo Scientific
Dulbecco's Modified Eagle Medium (DMEM) + GlutaMAX™-I	Gibco
Ethylenediaminetetraacetic acid (EDTA)	Carl Roth
Ethanol	J.T.Baker
Fetal bovine serum (FBS)	Invitrogen GmbH
GeneRuler 1 kb DNA ladder	MBI Fermentas
Glucose	Carl Roth
Glycerol	Carl Roth
i-Propanol	VWR International
Kanamycin	Carl Roth
Magnesium chloride	Carl Roth
Magnesium sulfate	Carl Roth
Penicillin-streptomycin	Carl Roth
Poly-L-lysine hydrobromide mol wt ≥300,000	Sigma-Aldrich
Potassium chloride	Carl Roth
Potassium dihydrogen phosphate	Carl Roth
RedSafe nucleic acid staining solution	iNtRON Biotechnology
Sodium acetate	Carl Roth
Sodium chloride	Carl Roth
Sodium hydrogen phosphate	Carl Roth
Trypsin	Invitrogen
Tryptone	AppliChem
Yeast extract	Carl Roth

2. Buffers, solutions, and media

Buffers, solutions, and media for cell culture and culture of bacteria were prepared ac- cording to Sambrook *et al.* [40] and are listed in Tab. 2. To prepare aqueous solutions, tridistilled water was used.

Tab. 2 Buffers, solutions, and media used in bacteria and cell culture

Buffers and Solutions	Components
1×PBS (pH 7.2)	137 mM NaCl 2.7 mM KCl 10 mM Na_2HPO_4 1.8 mM KH_2PO_4
1×PBS (+)(+)	1×PBS 1 mM $CaCl_2 \cdot 2H_2O$ 0.5 mM $MgCl_2 \cdot 6H_2O$
LB Kanamycin medium	10 g/l Peptone 5 g/l Yeast extract 5 g/l NaCl 50 µg/ml Kanamycin
Poly-L-lysin solution for cell attachment	10 ml Poly-L-lysine hydrobromide mol wt ≥300,000 30 ml H_2O
LB agar	15 g Agar per 1 l LB medium
SOC medium for *E. coli*	2 % (w/v) Tryptone 0.5 % Yeast extract 8.6 mM NaCl 2.5 mM KCl 10 mM $MgCl_2$ 20 mM Glucose
DMEM for cell culture	DMEM 10 % FBS 1 % Penicillin-streptomycin antibiotic solution

3. Enzymes

*Pfu*Turbo DNA polymerase was obtained from Stratagene. All restriction enzymes were purchased from New England Biolabs.

4. Kits

The NucleoSpin® Plasmid QuickPure kit and the NucleoBond® Xtra Midi kit for plasmid preparation and purification were purchased from Macherey-Nagel.

5. Vectors

The vectors used for expression and site-directed mutagenesis were pα-Syn-mCherry as well as pSOD1-GFP and pSOD1-A4V-GFP (a gift from the group of Richard I. Morimoto, Northwestern University, Evanston).

6. Oligonucleotide primers

Custom-made oligonucleotide primers used for site-directed mutagenesis were obtained from BioTeZ Berlin-Buch GmbH and are listed in Tab. 3.

Tab. 3: Oligonucleotide primers used to generate α-Syn variants in site-directed mutagenesis PCR. Point mutations are printed in bold and the relevant codon is shaded in grey.

Name	Sequence
α-Syn A53T	sense (5'-) GCATGGTGTG**ACA**ACAGTGGC antisense (5'-) GCCACTGTT**TGT**CACACCATGC
α-Syn E46K	sense (5'-) GCTCCAAAACCAAG**A**AGGGAGTGGTGCATGGTG antisense (5'-) CACCATGCACCACTCC**CTT**CTTGGTTTTGGAGC
α-Syn E46KΔG	sense (5'-) GCTCCAAAACCAAG**A**AG---GTGGTGCATGGTG antisense (5'-) CACCATGCACCAC---**CTT**CTTGGTTTTGGAGC

7. DNA manipulations

Standard DNA manipulations were carried out according to the handbook of Sambrook and Russel (Sambrook and Russell 2001). The nucleotide sequences of the plasmid constructs were verified using the Sanger sequencing service from Source Bioscience (Berlin, Germany).

8. Cell culture and transfection

HEK-293 cells were cultured at 37°C and 5% CO_2 In Dulbecco's modified Eagle's medium containing 10%(v/v) heat- inactivated fetal calf serum, 100 units/ml penicillin and 100 µg/ml streptomycin. The transfections were performed with PEI as previously described (Longo et al. 2013). Stable cells line were generated using G418 selection

protocols described in the handbook of Sambrook and Russel (Sambrook and Russell 2001)

9. FRAP measurement of mCherry-HttExon1Q74 and mCherry-HttExon1Q23.

FRAP analyses were performed at 37 C° on the temperature-controlled stage of a Zeiss LSM780 confocal microscope (Carl Zeiss Microimaging GmbH, Jena, Germany). Fluorescence of mCherry-HttExon1Q23 or mCherry-HttExon1Q74 was recorded using the 561nm laser and detected using a 564 – 758 band pass filter. A region of interest (ROI) was selected in each studied cell, in the cytoplasm for cells without aggregates and in the center of the aggregates for cells containing aggregates. Initial reference fluorescence of the ROI was measured for 10 cycles at 0.5 seconds intervals. Bleaching of a defined ROI of an individual cell was performed using a 405 nm laser line at 100% power for 5 seconds. Recovery was monitored over 110 cycles of imaging with a 0.5-second interval between each acquisition. The mean fluorescence intensity in the ROIs was quantified using the Zeiss Zen software (Carl Zeiss Microimaging GmbH, Jena, Germany). Microscope settings: objective: Plan-Apochromat 63x/1.40 Oil DIC M27; GFP detection: argon laser λ_{exc}: 488 nm, band pass filter 490-550nm; mCherry detection: DPSS laser λ_{exc} = 561, band pass filter 564-758.

10. Immunofluorescence of HSC70 in presence of mCherry-HttExon1Q74 or mCherry-HttExon1Q23.

Transiently transfected HEK293 cells expressing HttExon1Q23-HA and mCherry-HttExon1Q74-HA were incubated three days after transfection. The cover plates were washed two times with PBS (137 mM NaCl, 2.7 mM KCl, Na_2HPO_4 10mM, KH_2PO_4 1.8mM; pH of 7.4) and then fixed for 10 minutes at room temperature with a solution of 4% PFA and 4% sucrose in PBS. After two washing steps with PBS, blocking and permeabilization was performed using goat serum dilution buffer (GSDB) (10% goat serum, 100mM NaCl, 0.3% Triton X-100, 20mM Na_2HPO_4; pH7.4). The treatment with the primary antibody was performed at room temperature. A 35 μl drop of the diluted antibody solution (rabbit anti-HSC70 polyclonal antibody 1:100 or mouse anti-HA in GSDB 1:100) was placed on a piece of parafilm® before leaving the coverslip upside down on the drops for 1h in a dark humid chamber. The cover plates were washed after this step three times with immunowashing buffer (IW) (100mM NaCl, 0.3% Triton X-100, 20mM NaH_2PO_4; pH7.4). The treatment with the secondary antibody was performed under the same condition as with the primary antibodies using a solution of

goat anti-mouse Alexa Fluor™ 647 or goat anti-rabbit antibody tagged with CY3 (1:600 in GSDB). The cover plates were washed three times with IW, one time with PBS and dipped three times in water before being mounted on microscope slides with Thermo Scientific™ Shandon™ Immu-Mount™. The microscope slides were dried overnight. Thereafter, XY-stack pictures were recorded using the confocal Carl Zeiss LSM 780 microscope and the software ZEN 2010 (Carl Zeiss Microimaging GmbH, Jena, Germany). Microscope settings: objective: Plan-Apochromat 63x/1.40 Oil DIC M27; splitter 561/633 nm; Cy3 detection: DPSS laser λ_{exc} = 561 nm, range 565-637 beam; Alexa Fluor™ 647 detection: HeNe-laser, λ_{exc} = 633, range 637-735.

11. Membrane expression measurement of GPCRs upon activation co-expressed with mCherry-HttExon1Q23 or mCherry-HttExon1Q74 using CLSM

HEK293 cells stably transfected with the N-terminally FLAG and C-terminally GFP-tagged receptors (CRF1R, V2R) were seeded on 30 mm cover slips. The next day, cells were transfected with mCherry-HttExon1Q23 or mCherry-HttExon1Q74. Cells were stimulated using 100 nM of the corresponding agonist to induce CME in PBS-BSA for 1 hour. Alternatively, HEK293 cells were seeded and the following day, Flag-V1aR-GFP and Flag-UTS2R-GFP DNA were transiently co-transfected with mCherry-HttExon1Q23 or mCherry-HttExon1Q74.

72h after transfection, cells were mounted at 37 C° on the temperature-controlled stage of the Zeiss LSM780 microscope. Ligand induced CME was stimulated using receptor agonists in PBS-BSA buffer (Flag-V1aR-GFP and Flag-V2R-GFP: 100nM AVP; Flag-CRF1R-GFP: 100nM Sauvagine; Flag-UTSR-GFP: 100nM UTS). A time series of 25 pictures in 20 minutes was recorded using a Zeiss LSM 780 confocal microscope and the Zeiss software ZEN 2010 (Carl Zeiss Microimaging GmbH, Jena, Germany). Resulting images were analyzed using FIJI (Rahbek-Clemmensen et al. 2014). Microscope settings were: objective: Plan-Apochromat 63x/1.40 Oil DIC M27; GFP detection: argon laser λ_{exc}: 488 nm, band pass filter 490-550nm; mCherry detection: DPSS laser λ_{exc} = 561, band pass filter 564-758.

12. Membrane expression measurement of GPCRs upon activation co-expressed with mCherry-HttExon1Q23 or mCherry-HttExon1Q74 using PulSa

HEK293 cells stably transfected with the N-terminally FLAG and C-terminally GFP-tagged receptors (CRF1R and V2R) were seeded on 35 mm well plates. The next day, cells were transfected with mCherry-HttExon1Q23 or mCherry-HttExon1Q74. For

Flag-V1aR-GFP and Flag-UTS2R-GFP, HEK293 cells were seeded and the following day the receptor DNA was co-transfected with mCherry-HttExon1Q23 or mCherry-HttExon1Q74.

72h after transfection, cells were stimulated using 100 nM of the corresponding agonist to induce CME in PBS-BSA for 1 hour. After stimulation, cells were cooled down to 4 °C. From this point on, cell treatment was performed on ice. Cells were detached using gentle pressure from the pipet, transferred into FACS tubes and were washed twice using PBS-BSA and collected at 500x g for 5 minutes. Cells were re-suspended into 200 µl PBS-BSA containing monoclonal mouse anti-Flag M2 antibodies (Sigma) (1:1000) and incubated on ice for 10 minutes. Cells were washed as above, re-suspended in 200 µl PBS-BSA containing anti-mouse Alexa Fluor™647 antibodies (1:100) and incubated for 10 minutes on ice. Cell were washed 3 times as described above using 1 ml PBS-BSA, re-suspended in 100 µl of PBS-BSA and then loaded into an LSRFortessa BD Bioscience (Allschwil, Switzerland) cell analyzer. GFP fluorescence data were collected using a 488 nm laser for excitation and a 530/30 nm bandpass filter (A parameter recording). mCherry fluorescence data were collected using a 561 nm laser for excitation and a 610/20 nm bandpass filter (W and H parameter recording). Alexa Fluor™647 data were collected using a 640 nm laser for excitation and a 670/30 bandpass filter (A parameter recording).

FCS 3.1 files were exported using FACSDiva and imported into FCS Express (De Novo software, Glendale, CA, USA). Cells expressing both GFP and mCherry fluorescence were gated, then a second gating was performed by plotting the mCherry pulse height against the mCherry pulse width to separate cells with and without aggregates, following the previously described PulSa protocol (Ramdzan et al. 2012; Ramdzan, Wood, and Hatters 2013). Cells expressing GFP fluorescence only were gated as a negative control for expression of the HttExon1Q variants upon internalization. Fluorescence intensity of each pulse was added to each other and normalized to 10,000 cells. Thereafter, the cumulated intensity of Alexa Fluor™647 fluorescence was divided by the cumulated intensity of GFP fluorescence in order to normalize to the receptor expression levels. This ratio was then normalized to mean of the ratio of unstimulated samples. p value < 0,05 were considered to be significant (*), p value < 0,01 (**), p value < 0,001 (***) and p value < 0,0001 (****).

13. Ca^{2+} signal response assay upon activation of Flag-V1aR-BFP in presence of mCherry-HttExon1Q74 or mCherry-HttExon1Q23.

HEK293 cells were seeded on 30 mm coverslips. The next day, cells were co-transfected with Flag-V1aR-BFP and mCherry-HttExon1Q23 or mCherry-HttExon1Q74. After three days of incubation, cells on coverslips were transferred to a Zeiss LSM 780 confocal microscope. Cells were pretreated with the Ca^{2+} sensor Fluo8-AM (4 μM) for 40 minutes in PBS-BSA and washed using PBS-BSA. Measurements were performed taking a picture every 3 seconds. In the beginning, 10 pictures were taken to record the baseline without agonist. Image recording was paused and the buffer was replaced by PBS-BSA containing 1 nM of AVP to induce ligand-mediated CME. Measurements were resumed and an additional 90 pictures were recorded. Cells were washed three times using PBS-BSA and incubated for 30 minutes to allow recycling of functional receptors to the plasma membrane. A second round of stimulation was performed as described above but using 10 nM AVP. Measurements were again paused and the agonist-containing PBS-BSA was replaced by PBS-BSA supplemented with 15 μM of digitonin. This final step was carried out to allow Ca^{2+} influx into the cells from the buffer in order to get a maximal Fluo8 fluorescence signal for normalization. Microscope settings: objective: Plan-Apochromat 63x/1.40 Oil DIC M27; BFP detection: Diode laser, λ_{exc} = 405 nm, band pass filter 415-495; Fluo8 detection: argon laser, λ_{exc} = 488 nm, band pass filter 491 – 560 nm; mCherry detection: DPSS laser λ_{exc} = 561, band pass filter 564-706; beam splitter MBS 488/561, MBS InVis 405.

The Z-stack of the cells was used to separate cells into different categories, namely cells containing mCherry-HttExon1Q23, mCherry-HttExon1Q74 soluble and mCherry-HttExon1Q74 aggregated. ROIs were selected in the cytoplasm of each measured cells using FIJI (Rahbek-Clemmensen et al. 2014) and the time series analyzer V3 plug-in (https://imagej.nih.gov/ij/plugins/time-series.html) to get the average fluorescence of the ROI at each time points. Fluo8 fluorescence measurements were normalized to 0 using the average of the first 10 measurements (without agonist) and to 1 using the maximal fluorescence signal resulting from the final digitonin treatment. The maximal Fluo8 fluorescence levels following the first activation were compared for each category of cells using a one-way ANOVA test. A ratio of the Fluo8 maxima of the second activation and the first activation was used to compare the ability of receptor

re-activation for each category of cells. These ratios were compared statistically using a one-way ANOVA test.

14. Internalization studies of Flag-CRF1R-GFP and Flag-V2R-GFP in cells treated with Pitstop 2 using CLSM.

Experiments were performed with HEK293 cells stably transfected with GFP tagged receptors (Flag-CRF1R-GFP and Flag-V1aR-GFP) at 37 C° on the temperature-controlled stage of the Zeiss LSM780 microscope. Cells were incubated for 20 minutes with Pitstop 2 (30 µM) or DMSO (1 µl/ml) in PBS containing $CaCl_2$ (1 mM) and $MgCl_2$ (0.5 mM) and 0.5% of BSA (PBS-BSA). Ligand induced CME was stimulated using receptor agonists in PBS-BSA buffer (V1aR-GFP: 100nM AVP). A time series of 25 pictures in 20 minutes was recorded using a Zeiss LSM 780 confocal microscope and the Zeiss software ZEN 2010 (Carl Zeiss Microimaging GmbH, Jena, Germany). Resulting images were analyzed using FIJI (Rahbek-Clemmensen et al. 2014). Microscope settings were: objective: Plan-Apochromat 63x/1.40 Oil DIC M27; GFP detection: argon laser λ_{exc}: 488 nm, band pass filter 490-550nm; mCherry detection: DPSS laser λ_{exc} = 561, band pass filter 564-758.

15. cAMP radioimmuno accumulation assay upon activation of Flag-CRF1R-GFP in presence of Pitstop 2.

HEK293 cells stably transfected with Flag-CRF1R-GFP were incubated for 2 days. Cells were pre-treated with Pitstop 2 (30 µM) in PBS-BSA for 20 min or DMSO solvent. Agonist-mediated CME was triggered in PBS-BSA using Sauvagine (5.0 nM) and IBMX (0.23 mM) at t_0. Thereafter, accumulating cAMP was measured at different time points (15, 30 and 60 min.) For assay termination, the stimulation medium was removed, and cells were lysed for 30 min. at 4°C with 750 µl of 0.1 % trifluoroacetic acid containing 0.005 % Triton X-100. The lysates were treated at 95°C for 10 min. and dried by a rotation vacuum concentrator (Alpha-RVC, Christ, Germany) overnight. The dried samples were resuspended in RIA buffer (100 mM sodium acetate, 0.1 % BSA, 0.1 % Triton X-100; pH 6.0) incubated for 20 min at 4°C and centrifuged at 23,000 x g for 15 min at 4° C.

After appropriate dilutions, the concentration of cAMP in the supernatant was determined by RIA. To improve sensitivity, both the samples and standards (samples of defined cAMP concentrations) had to be acetylated. The samples (30 µl) were diluted in 470 µl RIA buffer and incubated with 20 µl of a mixture of acetic anhydride

and triethylamine (1:2) under immediate vigorous shaking at room temperature. 100 µl of this acetylated sample or standard, was supplemented with 100 µl RIA buffer, 100 µl (10,000 cpm) of [125I]-cAMP-tyrosylmethylester (specific activity 81,4 TBq/mmol) and 100 µl rabbit anti-cAMP-succinimidyl-protein conjugate antiserum (final dilution 1:160,000). To set up the standard curve, the incubation mixture contained cAMP in the range of 0.2 to 146 fmol per sample. The samples were incubated for 20 hours at 4° C. To separate the free and antibody-bound fractions, 50 µl sheep anti-rabbit antibody cellulose conjugate suspension (Sac-cel, IDS-IBL) was added and the mixture was incubated for 40 minutes at 4°C. Samples were washed using 1 ml RIA buffer, centrifuged (4,200 g, 15 minutes, 4 °C) and the supernatant was aspirated. The radioactivity of the pellet (antibody-bound fraction) was quantified in a scintillation counter. The detection limit was 0.9 fmoles cAMP/sample. cAMP concentrations in a range between 4 and 100 fmoles/sample could be determined with an interassay coefficient of variation less or equal 10 %.

Statistical analysis was performed using a one-way ANOVA test as well as a Dunnett's multiple comparison test (GraphPad Prism 5, GraphPad software, Inc., La Jolla, CA, USA); p value under 0,05 (*) were considered significant, p value < 0,01 (**).

16. HSC70 localization studies after treatment with MG132 using immunofluorescence and TPE-MI as a marker for amorphous aggregation.

HEK293 cells stably expressing FlucDM were seeded on cover plates. 2 days after seeding, cells were treated for 4 hours using MG132 (20 µM) together with TPE-MI (20 µM) or TPE-MI only as control (20 µM). HSC70 was labeled using rabbit anti-HSC70 polyclonal antibody (Proteintech) (1:100) and goat anti-rabbit Alexa Fluor™ 647 (1:600 in GSDB) as described above. The microscope slides were dried overnight. Thereafter, z-stack pictures were recorded using the confocal Carl Zeiss LSM 780 microscope and the software ZEN 2010 (Carl Zeiss Microimaging GmbH, Jena, Germany). Microscope settings were: objective: Plan-Apochromat 63x/1.40 Oil DIC M27; TPE-MI detection: Diode laser, λ_{exc} = 405 nm, band pass filter 415-495, band pass filter 564-706; Alexa Fluor™ 647 detection: HeNe-laser, λ_{exc} = 633, range 637-735. Beam splitter MBS 488/561, MBS_InVis -405.

17. Membrane expression measurement of Flag-V2R-GFP upon activation in presence of amorphous protein aggregation using PulSa.

HEK293 cells stably transfected with Flag-V2R-GFP were seeded on 35 mm well plates. 48h after seeding, cells were pre-treated using 20 µM of MG132 for 4h. Cells were then stimulated using AVP (100 nM) to induce CME or with DMSO as a control in PBS-BSA for 1 h. Receptors were labelled using the same protocol as for the PulSa experiment. GFP fluorescence data were collected using a 488 nm laser for excitation and a 530/30 nm bandpass filter (A parameter recording). Alexa Fluor™647 data were collected using a 640 nm laser for excitation and a 670/30 bandpass filter (A parameter recording).

FCS 3.1 files were exported using FACSDiva and imported into FCS Express. Cells expressing GFP fluorescence signals were gated. Fluorescence intensity of each pulse was added to each other and normalized to 10,000 cells. Then the cumulated intensity of Alexa Fluor™647 fluorescence was divided by the cumulated intensity of GFP fluorescence in order to normalize to the receptor expression levels. This ratio was then normalized to mean of the ratio of unstimulated samples.

18. Measurement of the aggregation of mCherry-HttExon1Q74 upon GPCR activation

HEK293 cells stably transfected with the N-terminally FLAG and C-terminally GFP-tagged receptors (CRF1R and V2R) were seeded on 35 mm well plates. The next day, cells were transfected with mCherry-HttExon1Q74. 24h or 44h after transfection, a set of samples were incubated for 1h using 100nM of the corresponding agonist in 1mL PBS. Cells were washed with PBS and incubated with DMEM until the measurement or the second activation.

Cells were suspended and washed 3 times as described above using 1 ml PBS-BSA, re-suspended in 100 µl of PBS-BSA and then loaded into an LSRFortessa BD Bioscience (Allschwil, Switzerland) cell analyzer. GFP fluorescence data were collected using a 488 nm laser for excitation and a 530/30 nm bandpass filter (A parameter recording). mCherry fluorescence data were collected using a 561 nm laser for excitation and a 610/20 nm bandpass filter (W and H parameter recording).

FCS 3.1 files were exported using FACSDiva and imported into FCS Express (De Novo software, Glendale, CA, USA). Cells expressing both GFP and mCherry fluorescence

were gated, a second gating was performed by plotting the mCherry pulse height against the mCherry pulse width to separate cells with and without aggregates, following the previously described PulSa protocol (Ramdzan et al. 2012; Ramdzan, Wood, and Hatters 2013). The number of cells detected to contain aggregates was divided by the number of cells detected to express mCherry fluorescence.

As this experiment was performed only once, no statistical analysis took place.

19. Membrane expression measurement of SERT in presence of soluble or aggregated m-Cherry HttExon1Q74.

HEK293 cells were transiently co-transfected using the previously described Flag-Tac-SERT (Rahbek-Clemmensen et al. 2014) and mCherry-HttExon1Q74 or mCherry-HttExon1Q23. Cells were incubated for 72h, prepared and resuspended using the same PulSa protocols and antibodies as described above. mCherry fluorescence data were collected using a 561 nm laser for excitation and a 610/20 nm bandpass filter (W and H parameter recording). Alexa Fluor™647 data were collected using a 640 nm laser for excitation and a 670/30 bandpass filter (A parameter recording).

FCS 3.1 files were exported using FACSDiva and imported into FCS Express (De Novo software, Glendale, CA, USA). Cells expressing mCherry fluorescence were gated. As the SERT construct did not express any fluorophore, cells expressing mCherry were considered to also express Flag-Tac-SERT. A second gating was performed by plotting the mCherry pulse height against the mCherry pulse width to separate cells with and without aggregates, following the previously described PulSa protocol (Ramdzan et al. 2012; Ramdzan, Wood, and Hatters 2013). Alexa Fluor™ 647 fluorescence intensity means of each group of cells expressing either aggregated or soluble mCherry-HttExon1Q74 or mCherryExon1Q23 were compared. T test p value < 0,05 were considered to be significant (*), p value < 0,01 (**), p value < 0,001 (***) and p value < 0,0001 (****).

20. Quantification α-Syn and α-Syn mutants inclusions using transmission microscopy.

HEK293 stably expressing Flag-CRF1R-GFP were transiently transfected using either α-Syn-mCherry, α-Syn A53T-mCherry, α-Syn E46-mCherry, α-Syn E46KΔG-mCherry or mCherry alone. 72h after transfection, tile scan pictures of the samples were recorde3d using a Carl Zeiss LSM 780 microscope and the software ZEN 2010 (Carl

Zeiss Microimaging GmbH, Jena, Germany). The number of inclusions observed in the transmission channel in each cell was counted manually using FIJI (Schindelin et al. 2012). Cells expressing Flag-CRF1R-GFP and mCherry were detected by using the fluorescent channels. Cells expressing Flag-CRF1R-GFP were then classified according to the number of inclusions observed using Microsoft Excel. Frequency analysis of the data was performed using the Prism 8 software (GraphPad Software, Inc.). Microscope settings: objective: Plan-Apochromat 63x/1.40 Oil DIC M27; GFP detection: argon laser λ_{exc}: 488 nm, band pass filter 490-550nm; mCherry detection: DPSS laser λ_{exc} = 561, band pass filter 564-758nm, T-PMT for transmission light detection.

21. Quantification of aggregates of SOD1 and SOD1A4V using CLSM.

HEK293 cells were transiently transfected with SOD1-mCherry, SOD1A4V-mCherry, SOD1-GFP or SOD1A4V-GFP. 72h after transfection, tile scan pictures of the samples were acquired using a Carl Zeiss LSM 780 microscope and the software ZEN 2010 (Carl Zeiss Microimaging GmbH, Jena, Germany). Microscope settings: Plan-Apochromat 63x/1.40 Oil DIC M27; GFP detection: argon laser λ_{exc}: 488 nm, band pass filter 490-550nm; mCherry detection: DPSS laser λ_{exc} = 561, band pass filter 564-758nm.

Aggregate formation in cells was quantified using the corresponding mCherry or GFP fluorescent channels and FIJI (Rahbek-Clemmensen et al. 2014). The tile scans images of four independent experiments were used and the number of cells with visible aggregates among all cells expressing mCherry or GFP was determined. The mean and SD of the amount of aggregates in the samples were calculated using the Prism 8 software (GraphPad Software, Inc.).

22. SOD1 and SOD1A4V aggregation detection using PulSa.

HEK293 cells were transfected using the previously described SOD1-GFP or SOD1A4V-GFP. Cells were incubated for 72h and then washed 3 times as previously described using 1 ml PBS-BSA. Cells were re-suspended in 100 µl of PBS-BSA and loaded into an LSRFortessa BD Bioscience (Allschwil, Switzerland) cell analyzer. GFP fluorescence data were collected using a 488 nm laser for excitation and a 530/30nm bandpass filter (A, W and H parameter recording).

FCS 3.1 files were exported using FACSDiva and imported into FCS Express (De Novo software, Glendale, CA, USA). Cells expressing GFP fluorescence were gated. A second gating was performed by plotting the GFP pulse height against the GFP pulse width to separate cells with and without aggregates, following the previously described PulSa protocol (Ramdzan et al. 2012; Ramdzan, Wood, and Hatters 2013).

V. Literature

1.   Klaips CL, Jayaraj GG, Hartl FU (2018) Pathways of cellular proteostasis in aging and disease. *J Cell Biol* 217(1):51–63.

2.   Mogk A, Bukau B, Kampinga HH (2018) Cellular Handling of Protein Aggregates by Disaggregation Machines. *Mol Cell* 69(2):214–226.

3.   Nillegoda NB, Wentink AS, Bukau B (2018) Protein Disaggregation in Multicellular Organisms. *Trends Biochem Sci* 43(4):285–300.

4.   Scior A, et al. (2018) Complete suppression of Htt fibrilization and disaggregation of Htt fibrils by a trimeric chaperone complex. *EMBO J* 37(2):282–299.

5.   Soto C, Pritzkow S (2018) Protein misfolding, aggregation, and conformational strains in neurodegenerative diseases. *Nat Neurosci* 21(10):1332–1340.

6.   Jucker M, Walker LC (2018) Propagation and spread of pathogenic protein assemblies in neurodegenerative diseases. *Nat Neurosci* 21(10):1341–1349.

7.   Caterino M, et al. (2018) Huntingtin protein: A new option for fixing the Huntington's disease countdown clock. *Neuropharmacology* 135:126–138.

8.   Choi ML, Gandhi S (2018) Crucial role of protein oligomerization in the pathogenesis of Alzheimer's and Parkinson's diseases. *Febs j* 285(19):3631–3644.

9.   Maurel C, et al. (2018) Causative Genes in Amyotrophic Lateral Sclerosis and Protein Degradation Pathways: a Link to Neurodegeneration. *Mol Neurobiol* 55(8):6480–6499.

10.   Brauer S, Zimyanin V, Hermann A (2018) Prion-like properties of disease-relevant proteins in amyotrophic lateral sclerosis. *J Neural Transm* 125(4):591–613.

11.   Yu A, et al. (2014) Protein aggregation can inhibit clathrin-mediated endocytosis by chaperone competition. *Proc Natl Acad Sci* 111(15):E1481–E1490.

12.   Hauser AS, Attwood MM, Rask-Andersen M, Schiöth HB, Gloriam DE (2017) Trends in GPCR drug discovery: New agents, targets and indications. *Nat Rev Drug Discov* 16(12):829–842.

13.   Rajagopal S, Shenoy SK (2018) GPCR desensitization: Acute and prolonged phases. *Cell Signal* 41:9–16.

14. Pavlos NJ, Friedman PA (2017) GPCR Signaling and Trafficking: The Long and Short of It. *Trends Endocrinol Metab* 28(3):213–226.

15. Calebiro D, Godbole A (2018) Internalization of G-protein-coupled receptors: Implication in receptor function, physiology and diseases. *Best Pr Res Clin Endocrinol Metab* 32(2):83–91.

16. Epping EA, Paulsen JS (2011) Depression in the early stages of Huntington disease. *Neurodegener Dis Manag* 1(5):407–414.

17. Ceccarini J, et al. (2018) Behavioral symptoms in premanifest Huntington disease correlate with reduced frontal CB1R levels. *J Nucl Med*. doi:10.2967/jnumed.118.210393.

18. Basavarajappa BS, Shivakumar M, Joshi V, Subbanna S (2017) Endocannabinoid system in neurodegenerative disorders. *J Neurochem* 142(5):624–648.

19. Saudou F, Humbert S (2016) The Biology of Huntingtin. *Neuron* 89(5):910–926.

20. Arrasate M, Finkbeiner S (2012) Protein aggregates in Huntington's disease. *Exp Neurol* 238(1):1–11.

21. Tabrizi SJ, et al. (2009) Biological and clinical manifestations of Huntington's disease in the longitudinal TRACK-HD study: cross-sectional analysis of baseline data. *Lancet Neurol* 8(9):791–801.

22. Langbehn DR, Hayden MR, Paulsen JS (2010) CAG-repeat length and the age of onset in Huntington disease (HD): a review and validation study of statistical approaches. *Am J Med Genet B Neuropsychiatr Genet* 153b(2):397–408.

23. Marsh L (2013) Depression and Parkinson's disease: current knowledge. 13(12):409.

24. Bhat S, Acharya UR, Hagiwara Y, Dadmehr N, Adeli H (2018) Parkinson's disease: Cause factors, measurable indicators, and early diagnosis. *Comput Biol Med*. doi:10.1016/j.compbiomed.2018.09.008.

25. Wersinger C, Sidhu A (2009) Partial regulation of serotonin transporter function by γ-synuclein. *Neurosci Lett* 453(3):157–161.

26. Wishart DS, et al. (2018) DrugBank 5.0: a major update to the DrugBank database for 2018. *Nucleic Acids Res* 46(D1):D1074–D1082.

27. Wishart DS, et al. (2006) DrugBank: a comprehensive resource for in silico drug discovery and

exploration. *Nucleic Acids Res* 34(Database issue):D668-72.

28. Fredriksson R, Schiöth HB (2005) The Repertoire of G-Protein-Coupled Receptors in Fully Sequenced Genomes. *Mol Pharmacol* 67(5):1414–1425.

29. Hauser AS, et al. (2018) Pharmacogenomics of GPCR Drug Targets. *Cell* 172(1–2):41-54.e19.

30. Oprea TI, et al. (2018) Unexplored therapeutic opportunities in the human genome. *Nat Rev Drug Discov* 17(D1):317.

31. Terakita A (2005) The opsins. *Genome Biol* 6(3). doi:10.1186/gb-2005-6-3-213.

32. Mombaerts P (2004) Genes and ligands for odorant, vomeronasal and taste receptors. *Nat Rev Neurosci* 5(4):263–278.

33. Bjarnadóttir TK, et al. (2006) Comprehensive repertoire and phylogenetic analysis of the G protein-coupled receptors in human and mouse. *Genomics* 88(3):263–273.

34. TK A, JB F (1994) Fingerprinting G-protein-coupled Receptors. *Protein Eng* 7(2). doi:10.1093/PROTEIN/7.2.195.

35. Kolakowski LF (1994) GCRDb: A G-protein-coupled receptor database. *Recept Channels* 2(1):1–7.

36. Foord SM, et al. (2005) International Union of Pharmacology. XLVI. G protein-coupled receptor list. *Pharmacol Rev* 57(2):279–288.

37. McCudden CR, Hains MD, Kimple RJ, Siderovski DP, Willard FS (2005) G-protein signaling: Back to the future. *Cell Mol Life Sci* 62(5):551–577.

38. Rasmussen SGF, et al. (2011) Crystal Structure of the β2Adrenergic Receptor-Gs protein complex. *Nature* 477(7366):549.

39. Marcinkowski P, et al. (2019) A new highly thyrotropin receptor-selective small-molecule antagonist with potential for the treatment of graves' orbitopathy. *Thyroid* 29(1):111–123.

40. Okashah N, et al. (2019) Variable G protein determinants of GPCR coupling selectivity. *Proc Natl Acad Sci U S A* 116(24):12054–12059.

41. Qin K, Dong C, Wu G, Lambert NA (2011) Inactive-state preassembly of Gq-coupled receptors and Gq heterotrimers. *Nat Chem Biol* 7(10):740–747.

42. Clapham DE, Neer EJ (1997) G PROTEIN βγ SUBUNITS. *Annu Rev Pharmacol Toxicol* 37(1):167–203.

43. Chen-Izu Y, et al. (2000) G(i)-dependent localization of beta(2)-adrenergic receptor signaling to L-type Ca(2+) channels. *Biophys J* 79(5):2547–56.

44. Papadopoulou N, et al. (2004) Protein Kinase A-Induced Negative Regulation of the Corticotropin-Releasing Hormone R1α Receptor-Extracellularly Regulated Kinase Signal Transduction Pathway: The Critical Role of Ser [301] for Signaling Switch and Selectivity. *Mol Endocrinol* 18(3):624–639.

45. Thomsen ARBB, et al. (2016) GPCR-G Protein-β-Arrestin Super-Complex Mediates Sustained G Protein Signaling. *Cell* 166(4):907–919.

46. Sriram K, et al. (2019) Detection and Quantification of GPCR mRNA: An Assessment and Implications of Data from High-Content Methods. *ACS Omega* 4(16):17048–17059.

47. Baudry A, Pietri M, Launay J-M, Kellermann O, Schneider B (2019) Multifaceted Regulations of the Serotonin Transporter: Impact on Antidepressant Response. *Front Neurosci* 13:91.

48. Allen JA, Halverson-Tamboli RA, Rasenick MM (2007) Lipid raft microdomains and neurotransmitter signalling. *Nat Rev Neurosci* 8(2):128–140.

49. Launay JM, et al. (1992) One-step purification of the serotonin transporter located at the human platelet plasma membrane. *J Biol Chem* 267(16):11344–11351.

50. Rudnick G, Haven N (1977) Active Transport of 5-Hydroxytryptamine by Plasma Membrane Vesicles Isolated from Human Blood Plate1 . ets. *J Biol Chem* 252(7):2170–2175.

51. Rudnick G, Nelson PJ (1978) Platelet 5-hydroxytryptamine transport, an electroneutral mechanism coupled to potassium. *Biochemistry* 17(22):4739–42.

52. De Felice LJ (2016) A current view of serotonin transporters. *F1000Research* 5. doi:10.12688/f1000research.8384.1.

53. Lesch KP, et al. (1996) Association of anxiety-related traits with a polymorphism in the serotonin transporter gene regulatory region. *Science* 274(5292):1527–1531.

54. Murphy DL, Lesch K-P (2008) Targeting the murine serotonin

transporter: insights into human neurobiology. *Nat Rev Neurosci* 9(2):85–96.

55. Murphy DL, Lerner A, Rudnick G, Lesch K-P (2004) Serotonin Transporter: Gene, Genetic Disorders, and Pharmacogenetics. *Mol Interv* 4(2):109–123.

56. Trueta C, Kuffler DP, De-Miguel FF (2012) Cycling of dense core vesicles involved in somatic exocytosis of serotonin by leech neurons. *Front Physiol* 3:175.

57. Kaushalya SK, et al. (2008) Three-photon microscopy shows that somatic release can be a quantitatively significant component of serotonergic neurotransmission in the mammalian brain. *J Neurosci Res* 86(15):3469–80.

58. Törk I (1990) Anatomy of the serotonergic system. *Ann N Y Acad Sci* 600:9–34; discussion 34-5.

59. Squire LR (2008) *Fundamental neuroscience* (Elsevier/Academic Press).

60. Machado-Vieira R, et al. (2010) The Timing of Antidepressant Effects: A Comparison of Diverse Pharmacological and Somatic Treatments. *Pharmaceuticals (Basel)* 3(1):19–41.

61. Fava M (2003) Diagnosis and definition of treatment-resistant depression. *Biol Psychiatry* 53(8):649–59.

62. Fekadu A, et al. (2009) What happens to patients with treatment-resistant depression? A systematic review of medium to long term outcome studies. *J Affect Disord* 116(1–2):4–11.

63. Ali FR, et al. (2010) Combinatorial interaction between two human serotonin transporter gene variable number tandem repeats and their regulation by CTCF. *J Neurochem* 112(1):296–306.

64. Lau T, Schloss P (2012) Differential regulation of serotonin transporter cell surface expression. *Wiley Interdiscip Rev Membr Transp Signal* 1(3):259–268.

65. Carneiro AMD, Cook EH, Murphy DL, Blakely RD (2008) Interactions between integrin αIIbβ3 and the serotonin transporter regulate serotonin transport and platelet aggregation in mice and humans. *J Clin Invest* 118(4):1544–1552.

66. Prasad HC, et al. (2005) Human serotonin transporter variants display altered sensitivity to protein kinase G and p38 mitogen-activated protein

kinase. *Proc Natl Acad Sci U S A* 102(32):11545 LP – 11550.

67. Glatt CE, et al. (2001) Screening a large reference sample to identify very low frequency sequence variants: comparisons between two genes. *Nat Genet* 27(4):435–438.

68. Kilic F, Murphy DL, Rudnick G (2003) A Human Serotonin Transporter Mutation Causes Constitutive Activation of Transport Activity. *Mol Pharmacol* 64(2):440–446.

69. MacKenzie A, Quinn J (1999) A serotonin transporter gene intron 2 polymorphic region, correlated with affective disorders, has allele-dependent differential enhancer-like properties in the mouse embryo. *Proc Natl Acad Sci U S A* 96(26):15251–5.

70. Fiskerstrand CE, Lovejoy EA, Quinn JP (1999) An intronic polymorphic domain often associated with susceptibility to affective disorders has allele dependent differential enhancer activity in embryonic stem cells. *FEBS Lett* 458(2):171–4.

71. Caspi A, et al. (2003) Influence of Life Stress on Depression: Moderation by a Polymorphism in the 5-HTT Gene. *Science (80-)* 301(5631):386–389.

72. Wendland JR, et al. (2007) A novel, putative gain-of-function haplotype at SLC6A4 associates with obsessive-compulsive disorder. *Hum Mol Genet* 17(5):717–723.

73. Heils A, et al. (1998) Functional characterization of the murine serotonin transporter gene promoter in serotonergic raphe neurons. *J Neurochem* 70(3):932–9.

74. Scanlon SM, Williams DC, Schloss P (2001) Membrane cholesterol modulates serotonin transporter activity. *Biochemistry* 40(35):10507–10513.

75. Magnani F, Tate CG, Wynne S, Williams C, Haase J (2004) Partitioning of the serotonin transporter into lipid microdomains modulates transport of serotonin. *J Biol Chem* 279(37):38770–8.

76. Laursen L, et al. (2018) Cholesterol binding to a conserved site modulates the conformation, pharmacology, and transport kinetics of the human serotonin transporter. *J Biol Chem* 293(10):3510–3523.

77. Anderluh A, et al. (2017) Direct PIP2 binding mediates stable oligomer formation of the serotonin transporter. *Nat Commun* 8:14089.

78. Carneiro AMD, Blakely RD (2006) Serotonin-, protein kinase C-, and Hic-5-associated redistribution of the platelet serotonin transporter. *J Biol Chem* 281(34):24769–80.

79. Zhu C-B, Hewlett WA, Feoktistov I, Biaggioni I, Blakely RD (2004) Adenosine Receptor, Protein Kinase G, and p38 Mitogen-Activated Protein Kinase-Dependent Up-Regulation of Serotonin Transporters Involves Both Transporter Trafficking and Activation. *Mol Pharmacol* 65(6):1462 LP – 1474.

80. Ramamoorthy S, Samuvel DJ, Buck ER, Rudnick G, Jayanthi LD (2007) Phosphorylation of threonine residue 276 is required for acute regulation of serotonin transporter by cyclic GMP. *J Biol Chem* 282(16):11639–47.

81. Seimandi M, et al. (2013) Calcineurin Interacts with the Serotonin Transporter C-Terminus to Modulate Its Plasma Membrane Expression and Serotonin Uptake. *J Neurosci* 33(41):16189 LP – 16199.

82. Latty SL, et al. (2015) Referenced Single-Molecule Measurements Differentiate between GPCR Oligomerization States. *Biophys J* 109(9):1798–1806.

83. Lau T, Horschitz S, Berger S, Bartsch D, Schloss P (2008) Antidepressant-induced internalization of the serotonin transporter in serotonergic neurons. *FASEB J* 22(6):1702–1714.

84. Kittler K, Lau T, Schloss P (2010) Antagonists and substrates differentially regulate serotonin transporter cell surface expression in serotonergic neurons. *Eur J Pharmacol* 629(1–3):63–67.

85. Matthäus F, et al. (2016) The allosteric citalopram binding site differentially interferes with neuronal firing rate and SERT trafficking in serotonergic neurons. *Eur Neuropsychopharmacol* 26(11):1806–1817.

86. Launay J-M, Schneider B, Loric S, Da Prada M, Kellermann O (2006) Serotonin transport and serotonin transporter-mediated antidepressant recognition are controlled by 5-HT $_{2B}$ receptor signaling in serotonergic neuronal cells. *FASEB J* 20(11):1843–1854.

87. Wersinger C, Rusnak M, Sidhu A (2006) Modulation of the trafficking of the human serotonin transporter by human alpha-synuclein. *Eur J Neurosci* 24(1):55–64.

88. Rahbek-Clemmensen T, Bay T, Eriksen J, Gether U, Jørgensen TN (2014) The Serotonin Transporter Undergoes Constitutive Internalization and Is Primarily Sorted to Late Endosomes and Lysosomal Degradation. *J Biol Chem* 289(33):23004–19.

89. Conner SD, Schmid SL (2003) Regulated portals of entry into the cell. *Nature* 422(6927):37–44.

90. Kaksonen M, Roux A (2018) Mechanisms of clathrin-mediated endocytosis. *Nat Rev Mol Cell Biol* 19(5):313–326.

91. Ehrlich M, et al. (2004) Endocytosis by random initiation and stabilization of clathrin-coated pits. *Cell* 118(5):591–605.

92. Loerke D, et al. (2009) Cargo and dynamin regulate clathrin-coated pit maturation. *PLoS Biol* 7(3):e57.

93. Layton AT, et al. (2011) Modeling vesicle traffic reveals unexpected consequences for Cdc42p-mediated polarity establishment. *Curr Biol* 21(3):184.

94. Zoncu R, et al. (2007) Loss of endocytic clathrin-coated pits upon acute depletion of phosphatidylinositol 4,5-bisphosphate. *Proc Natl Acad Sci U S A* 104(10):3793–8.

95. Antonescu CN, Aguet F, Danuser G, Schmid SL (2011) Phosphatidylinositol-(4,5)-bisphosphate regulates clathrin-coated pit initiation, stabilization, and size. *Mol Biol Cell* 22(14):2588–600.

96. Cremona O, et al. (1999) Essential role of phosphoinositide metabolism in synaptic vesicle recycling. *Cell* 99(2):179–88.

97. Erdmann KS, et al. (2007) A role of the Lowe syndrome protein OCRL in early steps of the endocytic pathway. *Dev Cell* 13(3):377–90.

98. Fotin A, et al. (2004) Structure of an auxilin-bound clathrin coat and its implications for the mechanism of uncoating. *Nature* 432(7017):649–653.

99. Sousa R, Lafer EM (2015) The role of molecular chaperones in clathrin mediated vesicular trafficking. *Front Mol Biosci* 2:26.

100. Hartl FU (2017) Protein Misfolding Diseases. *Annu Rev Biochem* 86(1):21–26.

101. Dobson CM (2003) Protein folding and misfolding. *Nature* 426(6968):884–890.

102. Chiti F, Dobson CM (2006) Protein Misfolding, Functional Amyloid, and Human Disease. *Annu Rev Biochem* 75(1):333–366.

103.	Knauer MF, Soreghan B, Burdick D, Kosmoski J, Glabe CG (1992) Intracellular accumulation and resistance to degradation of the Alzheimer amyloid A4/beta protein. *Proc Natl Acad Sci U S A* 89(16). doi:10.1073/pnas.89.16.7437.

104.	Hartl FU, Hayer-Hartl M (2009) Converging concepts of protein folding in vitro and in vivo. *Nat Struct Mol Biol* 16(6):574–581.

105.	Blancas-Mejía LM, Ramirez-Alvarado M (2013) Systemic amyloidoses. *Annu Rev Biochem* 82:745–74.

106.	Knowles TPJ, et al. (2009) An Analytical Solution to the Kinetics of Breakable Filament Assembly. *Science (80-)* 326(5959):1533–1537.

107.	Fusco G, et al. (2017) Structural basis of membrane disruption and cellular toxicity by α-synuclein oligomers. *Science (80-)* 358(6369):1440–1443.

108.	Chen SW, et al. (2015) Structural characterization of toxic oligomers that are kinetically trapped during α-synuclein fibril formation. *Proc Natl Acad Sci* 112(16):E1994–E2003.

109.	Cremades N, et al. (2012) Direct Observation of the Interconversion of Normal and Toxic Forms of α-Synuclein. *Cell* 149(5):1048–1059.

110.	Bucciantini M, et al. (2002) Inherent toxicity of aggregates implies a common mechanism for protein misfolding diseases. *Nature* 416(6880):507–511.

111.	Shankar GM, et al. (2007) Natural Oligomers of the Alzheimer Amyloid- Protein Induce Reversible Synapse Loss by Modulating an NMDA-Type Glutamate Receptor-Dependent Signaling Pathway. *J Neurosci* 27(11):2866–2875.

112.	Ferreira IL, et al. (2012) Amyloid beta peptide 1–42 disturbs intracellular calcium homeostasis through activation of GluN2B-containing N-methyl-d-aspartate receptors in cortical cultures. *Cell Calcium* 51(2):95–106.

113.	Flagmeier P, et al. (2017) Ultrasensitive Measurement of Ca $^{2+}$ Influx into Lipid Vesicles Induced by Protein Aggregates. *Angew Chemie Int Ed* 56(27):7750–7754.

114.	Cheignon C, et al. (2018) Oxidative stress and the amyloid beta peptide in Alzheimer's disease. *Redox Biol* 14:450.

115.	Galvagnion C, et al. (2015) Lipid vesicles trigger α-synuclein aggregation

by stimulating primary nucleation. *Nat Chem Biol* 11(3):229–234.

116. Kummer MP, Heneka MT (2014) Truncated and modified amyloid-beta species. *Alzheimers Res Ther* 6(3):28.

117. Goedert M (2001) Alpha-synuclein and neurodegenerative diseases. *Nat Rev Neurosci* 2(7):492–501.

118. Reeve A, Simcox E, Turnbull D (2014) Ageing and Parkinson's disease: why is advancing age the biggest risk factor? *Ageing Res Rev* 14(100):19–30.

119. Goedert M, Spillantini MG, Del Tredici K, Braak H (2013) 100 years of Lewy pathology. *Nat Rev Neurol* 9(1):13–24.

120. Cole NB, et al. (2002) Lipid Droplet Binding and Oligomerization Properties of the Parkinson's Disease Protein α-Synuclein. *J Biol Chem* 277(8):6344–6352.

121. Jo E, McLaurin J, Yip CM, St George-Hyslop P, Fraser PE (2000) alpha-Synuclein membrane interactions and lipid specificity. *J Biol Chem* 275(44):34328–34.

122. Lázaro DF, et al. (2014) Systematic comparison of the effects of alpha-synuclein mutations on its oligomerization and aggregation. *PLoS Genet* 10(11):e1004741.

123. Obeso JA, et al. (2010) Missing pieces in the Parkinson's disease puzzle. *Nat Med* 16(6):653–661.

124. McLean PJ, Kawamata H, Hyman BT (2001) Alpha-synuclein-enhanced green fluorescent protein fusion proteins form proteasome sensitive inclusions in primary neurons. *Neuroscience* 104(3):901–12.

125. Opazo F, Krenz A, Heermann S, Schulz JB, Falkenburger BH (2008) Accumulation and clearance of -synuclein aggregates demonstrated by time-lapse imaging. *J Neurochem* 106(2):529–540.

126. Pandey N, Schmidt RE, Galvin JE (2006) The alpha-synuclein mutation E46K promotes aggregation in cultured cells. *Exp Neurol* 197(2):515–520.

127. Graham AJ, Macdonald AM, Hawkes CH (1997) British motor neuron disease twin study. *J Neurol Neurosurg Psychiatry* 62(6):562–569.

128. Al-Chalabi A, et al. (2010) An estimate of amyotrophic lateral sclerosis heritability using twin data. *J Neurol Neurosurg Psychiatry* 81(12):1324–6.

129. Roos E, et al. (2016) Depression in amyotrophic lateral sclerosis. *Neurology* 86(24):2271–2277.

130. Renton AE, Chiò A, Traynor BJ (2014) State of play in ALS genetics. *Nat Neurosci* 17(1):17–23.

131. van Es MA, et al. (2017) Amyotrophic lateral sclerosis. *Lancet* 390(10107):2084–2098.

132. Miller RG, Mitchell JD, Moore DH (2012) Riluzole for amyotrophic lateral sclerosis (ALS)/motor neuron disease (MND). *Cochrane Database Syst Rev.* doi:10.1002/14651858.cd001447.pub3 .

133. Liu-Yesucevitz L, et al. (2010) Tar DNA binding protein-43 (TDP-43) associates with stress granules: Analysis of cultured cells and pathological brain tissue. *PLoS One* 5(10). doi:10.1371/journal.pone.0013250.

134. Freibaum BD, Chitta RK, High AA, Taylor JP (2010) Global analysis of TDP-43 interacting proteins reveals strong association with RNA splicing and translation machinery. *J Proteome Res* 9(2):1104–1120.

135. Chen Y, Cohen TJ (2019) Aggregation of the nucleic acid– binding protein TDP-43 occurs via distinct routes that are coordinated with stress granule formation. *J Biol Chem* 294(10):3696–3706.

136. Stevens JC, et al. (2010) Modification of superoxide dismutase 1 (SOD1) properties by a GFP tag-- implications for research into amyotrophic lateral sclerosis (ALS). *PLoS One* 5(3):e9541.

137. Ramdzan YM, Wood R, Hatters DM (2013) Pulse shape analysis (PulSA) to track protein translocation in cells by flow cytometry: applications for polyglutamine aggregation. *Methods Mol Biol* 1017:85–93.

138. Ramdzan YM, et al. (2012) Tracking protein aggregation and mislocalization in cells with flow cytometry. *Nat Methods* 9(5):467–470.

139. Gupta R, et al. (2011) Firefly luciferase mutants as sensors of proteome stress. *Nat Methods* 8(10):879–884.

140. Chen MZ, et al. (2017) A thiol probe for measuring unfolded protein load and proteostasis in cells. *Nat Commun* 8(1):474.

141. Foord SM, et al. (2005) International Union of Pharmacology. XLVI. G Protein-Coupled Receptor List. *Pharmacol Rev* 57(2):279–288.

142. Kim YE, et al. (2016) Soluble Oligomers of PolyQ-Expanded Huntingtin Target a Multiplicity of Key

Cellular Factors. *Mol Cell* 63(6):951–964.

143. Monsellier E, Redeker V, Ruiz-Arlandis G, Bousset L, Melki R (2015) Molecular interaction between the chaperone Hsc70 and the N-terminal flank of huntingtin exon 1 modulates aggregation. *J Biol Chem* 290(5):2560–76.

144. Innamorati G, Le Gouill C, Balamotis M, Birnbaumer M (2001) The long and the short cycle. Alternative intracellular routes for trafficking of G-protein-coupled receptors. *J Biol Chem* 276(16):13096–13103.

145. Schmidt A, et al. (2009) Use of Kaede fusions to visualize recycling of G protein-coupled receptors. *Traffic* 10(1):2–15.

146. Sanchez-Fernandez G, et al. (2014) Galphaq signalling: the new and the old. *Cell Signal* 26(5):833–848.

147. von Kleist L, et al. (2011) Role of the clathrin terminal domain in regulating coated pit dynamics revealed by small molecule inhibition. *Cell* 146(3):471–484.

148. Schulein R, Gibert A, Rutz C (2017) Functional Significance of the Signal Peptides of Corticotropin-Releasing Factor Receptors. *Curr Mol Pharmacol.*

doi:10.2174/18744672106661702240 94915.

149. Saito Y, Ito H, Tsubuki S, Kawashima S, Tomioka M (2012) Differential Inhibition of Calpain and Proteasome Activities by Peptidyl Aldehydes of Di-Leucine and Tri-Leucine. *J Biochem* 119(3):572–576.

150. Pehere AD, et al. (2019) Tripeptide analogues of MG132 as protease inhibitors. *Bioorganic Med Chem* 27(2):436–441.

151. Dastoor Z, Dreyer J (2000) Nuclear translocation and aggregate formation of heat shock cognate protein 70 (Hsc70) in oxidative stress and apoptosis. *J Cell Sci* 113 (Pt 1:2845–2854.

152. Scotter EL, Goodfellow CE, Graham ES, Dragunow M, Glass M (2010) Neuroprotective potential of CB 1 receptor agonists in an in vitro model of Huntington's disease. *Br J Pharmacol* 160(3):747–761.

153. Jørgensen TN, Christensen PM, Gether U (2014) Serotonin-induced down-regulation of cell surface serotonin transporter. *Neurochem Int* 73(1):107–112.

154. Mestrom L, et al. (2019) Artificial fusion of mCherry enhances trehalose transferase solubility and stability. *Appl*

Environ Microbiol 85(8). doi:10.1128/AEM.03084-18.

155. Begitt A, Meyer T, Van Rossum M, Vinkemeier U (2000) Nucleocytoplasmic translocation of Stat1 is regulated by a leucine-rich export signal in the coiled-coil domain. *Proc Natl Acad Sci U S A* 97(19):10418–10423.

156. Vendruscolo M (2012) Proteome folding and aggregation. *Curr Opin Struct Biol* 22(2):138–143.

157. David DC (2012) Aging and the aggregating proteome. *Front Genet* 3:247.

158. Kim YE, Hipp MS, Bracher A, Hayer-Hartl M, Hartl FU (2013) Molecular chaperone functions in protein folding and proteostasis. *Annu Rev Biochem* 82:323–355.

159. Chiti F, Dobson CM (2017) Protein Misfolding, Amyloid Formation, and Human Disease: A Summary of Progress Over the Last Decade. *Annu Rev Biochem* 86:27–68.

160. Arslan MA, Csermely P, Sőti C (2006) Protein homeostasis and molecular chaperones in aging. *Biogerontology* 7(5–6):383–389.

161. Marshall J, et al. (2007) Specific psychiatric manifestations among preclinical Huntington disease mutation carriers. *Arch Neurol* 64(1):116–121.

162. Giorgetti S, Greco C, Tortora P, Aprile FA (2018) Targeting Amyloid Aggregation: An Overview of Strategies and Mechanisms. *Int J Mol Sci* 19(9). doi:10.3390/ijms19092677.

163. Kirstein J, et al. (2017) *In vivo* properties of the disaggregase function of J-proteins and Hsc70 in *Caenorhabditis elegans* stress and aging. *Aging Cell* 16(6):1414–1424.

164. Zuiderweg ERP, Hightower LE, Gestwicki JE (2017) The remarkable multivalency of the Hsp70 chaperones. *Cell Stress Chaperones* 22(2):173–189.

165. Chen S, Brown IR (2007) Neuronal expression of constitutive heat shock proteins: Implications for neurodegenerative diseases. *Cell Stress Chaperones* 12(1):51–58.

166. Lafer EM (2002) Clathrin-protein interactions. *Traffic* 3(8):513–20.

167. Chang HC, et al. (2002) Hsc70 is required for endocytosis and clathrin function in Drosophila. 159(3):477–487.

168. Böcking T, Aguet F, Harrison SC, Kirchhausen T (2011) Single-molecule analysis of a molecular disassemblase reveals the mechanism

of Hsc70-driven clathrin uncoating. *Nat Struct Mol Biol* 18(3):295–301.

169. Cho HJ, et al. (2015) Probing the effect of an inhibitor of an ATPase domain of Hsc70 on clathrin-mediated endocytosis. *Mol Biosyst* 11(10):2763–2769.

170. Mettlen M, Chen P-H, Srinivasan S, Danuser G, Schmid SL (2018) Regulation of Clathrin-Mediated Endocytosis. *Annu Rev Biochem* 87(1):871–896.

171. Szafran K, et al. (2013) Potential role of G protein-coupled receptor (GPCR) heterodimerization in neuropsychiatric disorders: A focus on depression. *Pharmacol Reports* 65(6):1498–1505.

172. Hollenstein K, et al. (2013) Structure of class B GPCR corticotropin-releasing factor receptor 1. *Nature* 499(7459):438–443.

173. Moore CA, Milano SK, Benovic JL (2007) Regulation of receptor trafficking by GRKs and arrestins. *Annu Rev Physiol* 69:451–482.

174. Drake MT, Shenoy SK, Lefkowitz RJ (2006) Trafficking of G protein-coupled receptors. *Circ Res* 99(6):570–582.

175. Wagner AS, et al. (2018) Self-assembly of Mutant Huntingtin Exon-1 Fragments into Large Complex Fibrillar Structures Involves Nucleated Branching. *J Mol Biol* 430(12):1725–1744.

176. Landles C, et al. (2010) Proteolysis of mutant huntingtin produces an exon 1 fragment that accumulates as an aggregated protein in neuronal nuclei in huntington disease. *J Biol Chem* 285(12):8808–8823.

177. Landles C, Bates GP (2004) Huntingtin and the molecular pathogenesis of Huntington's disease. *EMBO Rep* 5(10):958–963.

178. Kalia L V., Lang AE (2015) Parkinson's disease. *Lancet* 386(9996):896–912.

179. Wingo TS, Cutler DJ, Yarab N, Kelly CM, Glass JD (2011) The heritability of amyotrophic lateral sclerosis in a clinically ascertained United States research registry. *PLoS One* 6(11):e27985.

180. Byrne S, et al. (2011) Rate of familial amyotrophic lateral sclerosis: A systematic review and meta-analysis. *J Neurol Neurosurg Psychiatry* 82(6):623–627.

181. Swinnen B, Robberecht W (2014) The phenotypic variability of

amyotrophic lateral sclerosis. *Nat Rev Neurol* 10(11):661–670.

182. Rosen DR, et al. (1994) A frequent ala 4 to val superoxide dismutase-1 mutation is associated with a rapidly progressive familial amyotrophic lateral sclerosis. *Hum Mol Genet* 3(6):981–987.

183. Zhang S, et al. (2019) A Maleimide-functionalized Tetraphenylethene for Measuring and Imaging Unfolded Proteins in Cells. *Chem - An Asian J.* doi:10.1002/asia.201900150.

184. Hong Y, Lam JWY, Tang BZ (2011) Aggregation-induced emission. *Chem Soc Rev* 40(11):5361–5388.

185. Dastoor Z, Dreyer JL (2000) Nuclear translocation and aggregate formation of heat shock cognate protein 70 (Hsc70) in oxidative stress and apoptosis. *J Cell Sci* 113(16):2845–2854.

186. Shepherd JD, Huganir RL (2007) The Cell Biology of Synaptic Plasticity: AMPA Receptor Trafficking. *Annu Rev Cell Dev Biol* 23(1):613–643.

187. Anggono V, Huganir RL (2012) Regulation of AMPA receptor trafficking and synaptic plasticity. *Curr Opin Neurobiol* 22(3):461–9.

188. Mayle KM, Le AM, Kamei DT (2012) The intracellular trafficking pathway of transferrin. *Biochim Biophys Acta* 1820(3):264–281.

189. Kim S, Nollen EAA, Kitagawa K, Bindokas VP, Morimoto RI (2002) Polyglutamine protein aggregates are dynamic. *Nat Cell Biol* 4(10):826–830.

190. Müller HK, Kragballe M, Fjorback AW, Wiborg O (2014) Differential Regulation of the Serotonin Transporter by Vesicle-Associated Membrane Protein 2 in Cells of Neuronal versus Non-Neuronal Origin. *PLoS One* 9(5):e97540.

191. Book A, et al. (2018) A Meta-Analysis of α-Synuclein Multiplication in Familial Parkinsonism. *Front Neurol* 9. doi:10.3389/fneur.2018.01021.

192. Ross OA, et al. (2008) Genomic investigation of α-synuclein multiplication and parkinsonism. *Ann Neurol* 63(6):743–750.
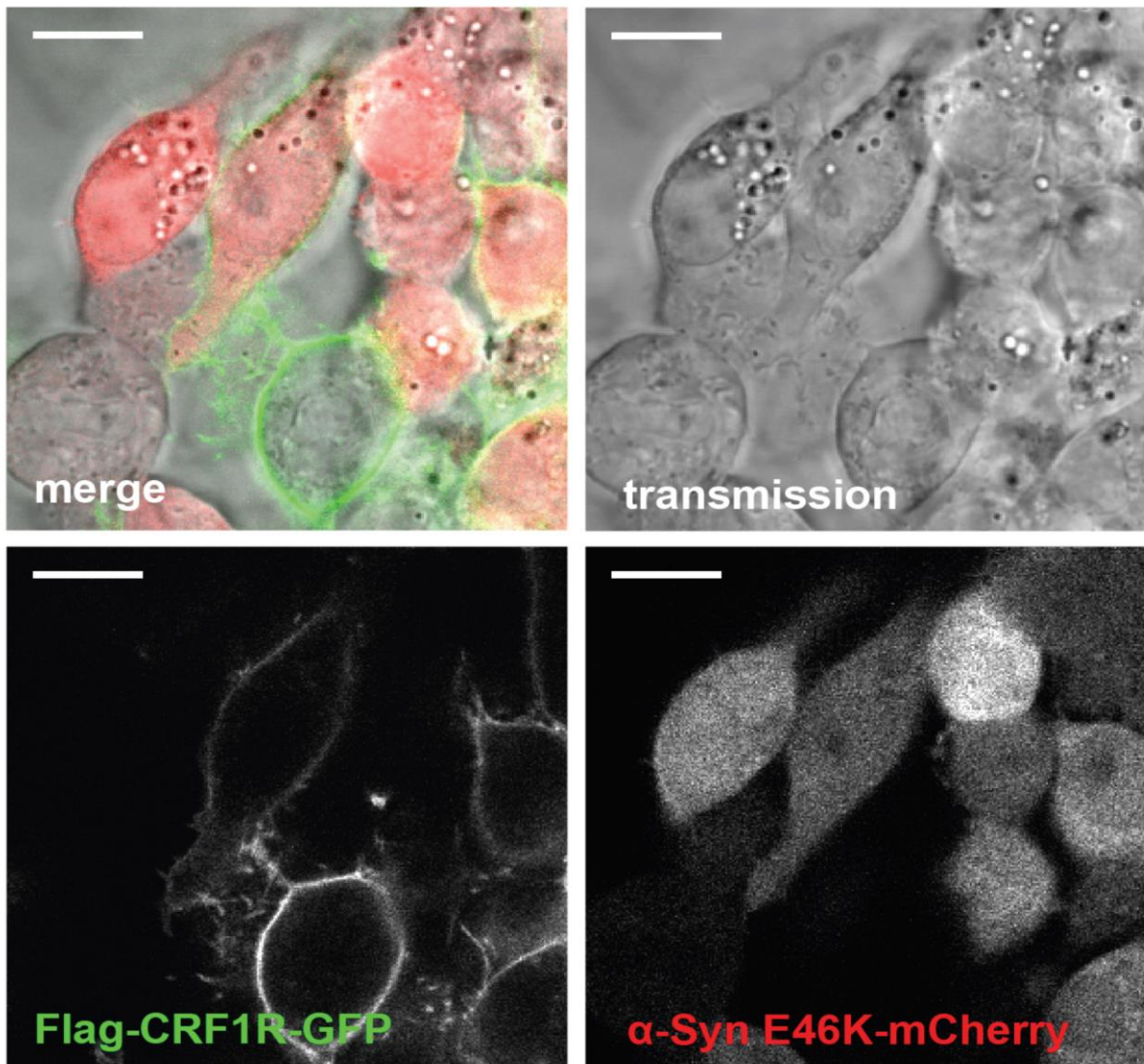
193. Singleton AB, et al. (2003) α-Synuclein Locus Triplication Causes Parkinson's Disease. *Science (80-)* 302(5646):841.

194. Xiong N, et al. (2009) Stereotaxical infusion of rotenone: A reliable rodent model for Parkinson's disease. *PLoS One* 4(11). doi:10.1371/journal.pone.0007878.

195. Xie W, et al. (2010) Proteasome inhibition modeling nigral neuron degeneration in Parkinson's disease. *J Neurochem* 115(1):188–199.

196. Tritschler HJ, Packer L, Medori R (1994) Oxidative stress and mitochondrial dysfunction in neurodegeneration. *Biochem Mol Biol Int* 34(1):169–81.

197. Tompkins MM, Hill WD (1997) Contribution of somal Lewy bodies to neuronal death. *Brain Res* 775(1–2):24–9.

198. Schulz-Schaeffer WJ (2010) The synaptic pathology of α-synuclein aggregation in dementia with Lewy bodies, Parkinson's disease and Parkinson's disease dementia. *Acta Neuropathol* 120(2):131–143.

199. Kramer ML, Behrens C, Schulz-Schaeffer WJ (2008) Selective detection, quantification, and subcellular location of α-synuclein aggregates with a protein aggregate filtration assay. *Biotechniques* 44(3):403–411.

200. Steiner JA, Quansah E, Brundin P (2018) The concept of alpha-synuclein as a prion-like protein: ten years after. *Cell Tissue Res* 373(1):161–173.

201. Kirchhausen T, Owen D, Harrison SC (2014) Molecular structure, function, and dynamics of clathrin-mediated membrane traffic. 6(5):a016725.

202. Innamorati G, Sadeghi HM, Tran NT, Birnbaumer M (1998) A serine cluster prevents recycling of the V2 vasopressin receptor. *Proc Natl Acad Sci U S A* 95(5):2222–2226.

203. Calebiro D, et al. (2009) Persistent cAMP-signals triggered by internalized G-protein-coupled receptors. *PLoS Biol* 7(8):e1000172.

204. Kliewer A, Reinscheid RK, Schulz S (2017) Emerging Paradigms of G Protein-Coupled Receptor Dephosphorylation. *Trends Pharmacol Sci* 38(7):621–636.

205. Laine R, et al. (2018) Fast fluorescence lifetime imaging reveals the aggregation processes of α-synuclein and polyglutamine in aging Caenorhabditis elegans. *bioRxiv*:414714.

206. Klucken J, Outeiro TF, Nguyen P, McLean PJ, Hyman BT (2006) Detection of novel intracellular α-synuclein oligomeric species by fluorescence lifetime imaging. *FASEB J* 20(12):2050–2057.

207. Becker W (2012) Fluorescence lifetime imaging - techniques and applications. *J Microsc* 247(2):119–136.

208. Dou J, et al. (2018) De novo design of a fluorescence-activating β-barrel. *Nature* 561(7724):485–491.

VI. Supplementary information

Supplemental figure 1: Ligand induced internalization of Flag-V2R-GFP, Flag-CRF1R-GFP and UTS2R-GFP co-expressed with mCherry-HttExonQ23 or mCherry-HttExon1Q74 measured using CLSM. HEK293 cells expressing GFP fused GPCRs (green) were co-transfected with mCherry-HttExon1Q23 or with mCherry-HttExon1Q74, incubated for three days and analyzed by CLSM. Pictures were recorded before and after 30 minutes of stimulation using the corresponding ligand (100 nM). In the absence of amyloid aggregates (cells containing mCherry-HttExon1Q23 or still soluble mCherry-HttExon1Q74, vesicles were detectable inside the cells and the membrane level of the receptor was significantly reduced. However, the presence of aggregated mCherry-HttExon1Q74 not only reduced the number of formed vesicles but also kept the membrane expression level of the receptor constant indicating that ligand-induced CME is inhibited. Pictures show xy scans of representative cells of three independent experiments. Scale bar = 10 µm.

Supplemental figure 2: LSM transmision pictures of HEK cells transiently expressing α-Syn variants. HEK 293 cells stably expressing Flag-CRF1R-GFP (shown in green) were transiently transfected with α-Syn variants fused to mCherry (shown in red), mCherry alone or left untransfected. Inclusions were observed in the transmission channel of a fluorescence confocal microscope 3 days after transfection. An exemplary section showing representative cells transfected with α-Syn E46K-mCherry fusion protein (Scale bar: 10 μm).
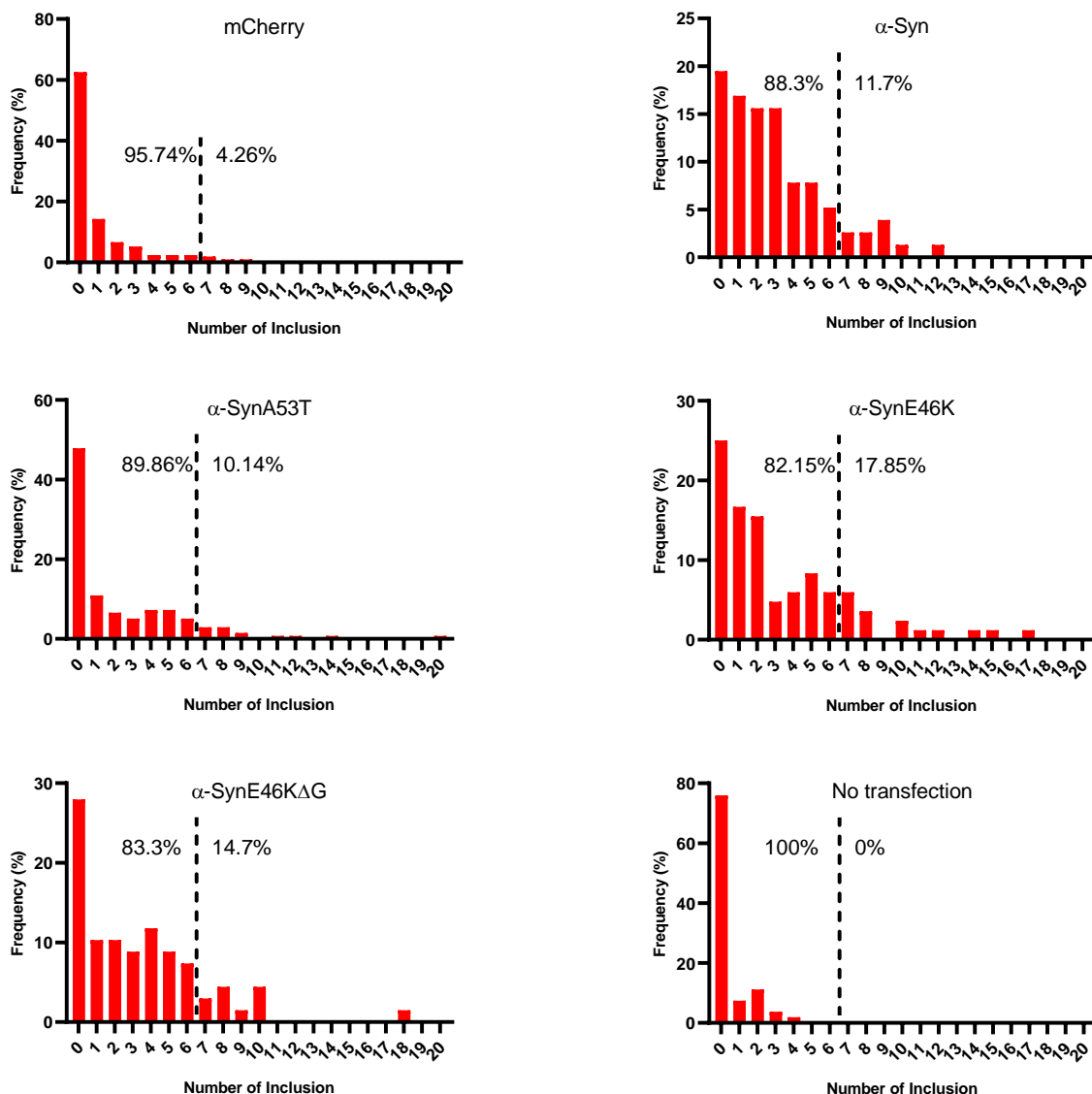
Supplemental figure 3: Frequency distribution diagrams of the inclusion number per cells in cells expressing mCherry and mCherry tagged α-Syn variants. The number of inclusion of cells expressing both Flag-CRF1R-GFP and α-Syn-mCherry fusion protein were quatified. The analysis revealed that the propotion of cells expressing α-Syn and α-Syn mutants and containing more than 6 inclusions is higher than the cells expression mCherry alone. However cells expressing solely mCherry had significantly more inclusion than cells having no mCherry expression. This show that these inclusion are probably a result of the expression of mCherry and not to the aggregation of α-syn and its mutants.